"Monitoring event-scale stream bluff erosion with repeat terrestrial laser scanning: Amity Creek, Duluth, MN"

A Thesis
SUBMITTED TO THE FACULTY OF THE GRADUATE SCHOOL
OF THE UNIVERSITY OF MINNESOTA
BY

Grant D. Neitzel

IN PARTIAL FULFILLMENT OF THE REQUIREMENTS
FOR THE DEGREE OF
MASTER OF SCIENCE

Dr. Karen Gran

April 2014

Acknowledgments

Numerous people played a role in helping me throughout this endeavor. It was a long, and sometimes rough journey, and I thank you all for the support, encouragement, guidance, and expertise that you provided.

Foremost, I would like to thank my advisor, Dr. Karen Gran, for believing in me, and providing me with the opportunity to work on such an interesting project. Thank you for the guidance throughout this thesis research, and for the support – in one form or another – during my time at UMD. I would also like to thank my committee members, Dr. John Swenson and Dr. Richard Axler for their time and expertise on various aspects of this project.

Thank you to the Geological Sciences Department at the University of Minnesota-Duluth for providing me with the graduate assistantship and the summer and travel stipends. I am also grateful for the funding that supported this research, provided by the National Center for Earth-Surface Dynamics, an NSF Science and Technology Center (EAR-0120914), and the Great Lakes Restoration Initiative (funding through the Minnesota Pollution Control Agency). Without this funding, none of this work would have been possible.

Thank you to Dr. Joe Wheaton for his patient assistance with the Geomorphic Change Detection software and for hosting an excellent workshop at Utah State University. Thank you to Ken Lyons at Faro for his willingness to help me through all the post-processing dead-ends.

I would also like to thank Marc Mayer and Daniel Johnson for all the hard hours contributed in the field; a special thank you to Tommy Tanner for his help collecting samples and the processing time spent in the lab. Thank you to Wally Lingwall at the Large Lakes Observatory for his assistance with the laser diffractometer. Thank you to Molly Wick for all the GIS help, and to Jenny Jasperson at the MPCA for all of the flow data that she provided.

Lastly, I would like to thank my family, for all of their love, support, and encouragement along the way.

Abstract

Terrestrial laser scanning (TLS) technology provides high-resolution topographic data that can be used to detect geomorphic change in natural environments. In this study, we utilize successive terrestrial laser scans to investigate the relationship between peak flow rates and stream bluff erosion in the Amity Creek watershed in Duluth, Minnesota, USA. We selected eight study bluffs to conduct terrestrial laser scans following all significant flow events over a one-year time period. The study employed a Faro Focus 3D phase-shift laser to collect TLS point cloud data. Post-processing of the TLS point cloud data sets involved: (1) digital removal of vegetation and objects other than the erosional surface of interest; (2) decimation of the point cloud in PC Tools and extraction of z_{min} values to produce a data set manageable in GIS; (3) creation of a bare earth digital elevation model (DEM) for each set of scans using ArcMap; and (4) utilization of Geomorphic Change Detection (GCD) software to generate DEMs of Difference (DoDs) from previous terrestrial laser scans. GCD data were used to calculate volumes of erosion and deposition and average retreat distances for time periods over which change was detected. Analysis of DoD color change images allowed for interpretation of the dominant processes responsible for bluff erosion. Sediment samples were collected for bulk density and grain size analyses to determine bluff characteristics and convert erosional volumes to mass; mass was then compared with Total Suspended Solids (TSS) loads from previous years. Suspended Sediment Concentration (SSC) samples were collected in areas where bluffs were located to determine spatial variation in concentrations during precipitation events.

There were four time periods from November 2011 to November 2012 in which change was measured at our study bluffs: winter and the transition into spring melt; two major precipitation events in late spring and early summer, and low base flow conditions continuing into late fall. These distinct time periods provided an opportunity to observe the impact of high flow events and other processes on bluff erosion throughout the watershed. Freeze-thaw cycling and saturated conditions in late winter and early spring were found to influence erosion of study bluffs; retreat distances averaged -0.22 m for sites measured during that time period, where negative values indicate erosion. Approximately 5 inches of intermittent rain over a six-day period from May 23-28 resulted in slumping at many bluffs and one major failure. The 500-year flood that occurred following 7.25 inches of precipitation on June 19-20 induced severe erosion; most sites experienced significant fluvial scour along the toe of the bluff. Very little change was measured in our study bluffs during the period of low base flow, spanning from early summer (post-flood) into late fall.

Change detection results and stream gage flow data were utilized to examine the effects of peak flows, total flow volume, and duration above bankfull discharge on bluff erosion. Results from our TLS analyses show a strong correlation between high flows and erosion of stream bluffs in the Amity Creek watershed. Average bluff retreat distances vary significantly over the time periods in which change was measured, ranging from -0.41 m during the June flood, to essentially no change when base flow was low.

Using our change detection measurements, we calculated an annual average retreat rate of -0.50 m/yr. By applying this rate to a watershed-scale bluff inventory, we estimated the total volume of sediment eroded from unvegetated bluffs in the watershed

between November 2011 and November 2012. Results show that bluffs are likely the primary source of fine sediment contributing to the creek's turbidity impairment. Load calculations from our bluff erosion work were compared to Minnesota Pollution Control Agency (MPCA) and Natural Resources Research Institute (NRRI) estimates from previous years, and were found to conceivably represent 100% of the total sediment load even with the 500-year event removed. Erosion during the June flood accounted for approximately 80% of the sediment load from bluff erosion between November 2011 and November 2012.

TLS results from this study show that major events are responsible for inducing considerable bluff erosion and moving the vast majority of sediment through the system. Additionally, our data demonstrate that management of turbidity-plagued watersheds along the North Shore and other regions of the state must include a focus on bluffs.

Table of Contents

List of Tables

List of Figures

1.0 INTRODUCTION

Throughout the world, increased development has placed a strain on our water resources. For many watersheds this has meant increased erosion and sediment loading in the rivers and streams that comprise them. Amity Creek, which flows into the Lester River just before reaching Lake Superior at the northeastern end of Duluth, Minnesota, has been listed on the Environmental Protection Agency's 303(d) list since 2004 as impaired for excess turbidity (SSLSWCD, 2009). As is the case with many tributaries on the North Shore of Lake Superior, Amity Creek has large clay banks and bluffs due to the underlying geology in the region (SSLSWCD, 2009; Fitzpatrick et al., 2006). Vertical features such as stream banks/bluffs are common sites of accelerated erosion, responsible for contributing excess sediment to the creek. Additionally, recent development in the watershed has led to increased stormwater runoff and amplified peak flows, resulting in higher sediment loads and potential for soil erosion (SSLSWCD, 2009). Together, the abundance of steep clay bluffs and increased development have accelerated erosion, negatively impacting water quality and aquatic habitat, and also threatening infrastructure. When managing stormwater with the intent of reducing peak flows, it is essentially assumed that increased peak flows result in higher rates of bank/bluff erosion. For this reason, slowing the erosion and reducing the fine sediment load it contributes to the creek requires an understanding of the erosional processes occurring in the watershed, and how increased peak flows affect the erosion.

Light detection and ranging (LiDAR), also known as laser scanning, is a recent innovation that has come to the forefront of surveying techniques utilized in the analysis of bank erosion (Heritage and Hetherington, 2007; Milan et al., 2007; Buckley et al.,

2008; Nasermoaddeli and Pasche, 2008; Resop and Hession, 2010; Day et al., 2012). Terrestrial Laser Scanning (TLS) allows for the creation of high-resolution digital elevation models spanning a relatively large field site in a comparatively short amount of time. Through the use of TLS, topographic features may be characterized and captured with high accuracy, resolution, and automation that was not possible a decade ago. Although the technology is not without its limitations and difficulties, these may be overcome through proper data acquisition and processing techniques. For example, TLS cannot be used to collect data during precipitation events, or when there is a high level of water vapor or dust in the air (Heritage and Hetherington, 2007). Additionally, the presence of vegetation can mask the erosional surface of interest, and must be removed during processing to ensure that an accurate model of bare earth topography can be produced (Day et al., 2012).

In order to assess the qualitative and quantitative effects that bluff erosion has on the turbidity impairment of Amity Creek, and the relationship between erosion and peak flow, we selected eight field sites that were analyzed using TLS. Study sites were selected based on characteristics such as size (surface area), location in the watershed, relative ease of access, and general lack of vegetative cover that would otherwise inhibit data collection and processing. Two of our sites were selected in order to assess the relative success of recent restoration efforts, and the effect that these efforts had on erosion rates. At each site, three to four rebar posts were set in the ground that served as permanent control points. These control points allowed us to tie data together spatially, and, in turn, calculate erosional/depositional volumes. Scans were conducted a minimum of four times per year at each study site – in the spring after snow had melted and in the

fall after deciduous cover was lost. Scanning when leaf cover was minimal allowed more points to be collected from the actual surface of interest and reduced the amount of time required for data processing. Scans were also conducted following large rain events, in order to associate volumes of erosion to a specific flow event. Multiple scans from a given site were differenced, allowing us to determine the quantity of sediment eroded/deposited, and where on the bluff face the erosion/deposition occurred. This information was combined with data related to flow conditions and soil characteristics, allowing conclusions to be drawn about the relative importance of processes governing erosion. Finally, when we apply erosion rates from our TLS work to a field inventory of un-vegetated bluffs, we are able to estimate the mass of fine sediment eroded from bluffs throughout the watershed and compare our results to sediment loads from previous years.

The goal of this study was to determine if bluff erosion rates in the Amity Creek watershed increase during high-flow events, and if bluff erosion rates vary systemically with discharge. After receiving upwards of 10 inches of rain over the course of two days in late June 2012, it became readily apparent that severe erosion had occurred in our bluffs. A study conducted by the USGS reported the event to be representative of a 500-year flood for North Shore streams in the Duluth area (Czuba et al., 2012). Certain study sites were more or less obliterated due to the extreme power of the floodwaters. The majority of rebar control posts used to tie successive scans together were bent, buried in sediment, or destroyed all together. In certain locations, the channel centerline migrated approximately five meters almost overnight. The scope of the project changed; we knew that significant bluff erosion had occurred and that it was directly related to high flows caused by the flooding in Duluth and the surrounding region. The challenge became

applying our change detection techniques to field sites that had been drastically transformed by such a rare event. Additionally, we were interested in investigating any changes in the bluffs during periods of relatively low flows – were these features stable, or was erosion occurring that was unrelated to fluvial scour during high flow events?

There has been strong regional interest in reducing sediment loads to Amity Creek in order to improve water quality and aquatic habitat. An understanding of the geomorphic environment and processes within a watershed is important because they affect the overall water quality of the stream and the plant and animal communities that surround it (Fitzpatrick et al., 2006). Through the use of TLS, highly accurate geomorphic change detection is possible. In this study, we utilize TLS in the Amity Creek watershed, allowing us to quantify the amount of sediment being eroded, and provide insight into the processes responsible for causing the erosion. Additionally, our ability to extrapolate results to the entirety of the watershed allowed us to determine the extent to which bluff erosion contributes to the turbidity impairment of Amity creek.

2.0 BACKGROUND

2.1 Terrestrial Laser Scanning

A recent innovation in spatial data acquisition that aids in the analysis and understanding of this erosion is terrestrial laser scanning (TLS), often referred to as ground-based or terrestrial LiDAR (Day et al., 2012). LiDAR utilizes a laser-based measurement system that allows for rapid collection of spatially-dense point data representing a terrain surface. In recent years, TLS instruments have become compact and robust enough to bring the technology to the forefront of surveying techniques

utilized in geomorphic change detection (Buckley et al., 2008). Detailed field measurements provide insight into the mechanisms responsible for causing bank/bluff erosion, and are valuable in any watershed restoration program aimed at rehabilitation of aquatic habitat and water quality (Nasermoaddeli and Pasche, 2008).

The advance in survey technology in the past few decades has led to a drastic increase in the amount of field data being collected. Sophisticated spatial analytical software now allows for the creation of digital elevation models (DEMs) that accurately capture variability in surface landforms. This provides an opportunity to measure and observe changes in morphology over a variety of spatial scales (Heritage and Hetherington, 2007). However, limitations are imposed upon many of these traditional survey technologies due to the necessary trade-off between spatial coverage area and resolution or morphologic detail (Figure 2.1).

Techniques such as erosion pins and terrestrial photogrammetry are typically applied to short time-scale studies. These methods present difficulties in terms of the spatial and temporal resolution captured (Nasermoaddeli and Pasche, 2008). Terrestrial photogrammetry produces accurate and dense data, but spatial extent is limited. In contrast, aerial photogrammetry increases the spatial extent covered, but suffers in its elevation accuracy (Heritage and Hetherington, 2007). Erosion pins lack in their ability to portray both spatial and temporal resolution. All methods are labor-intensive in both pre- and post-processing stages.

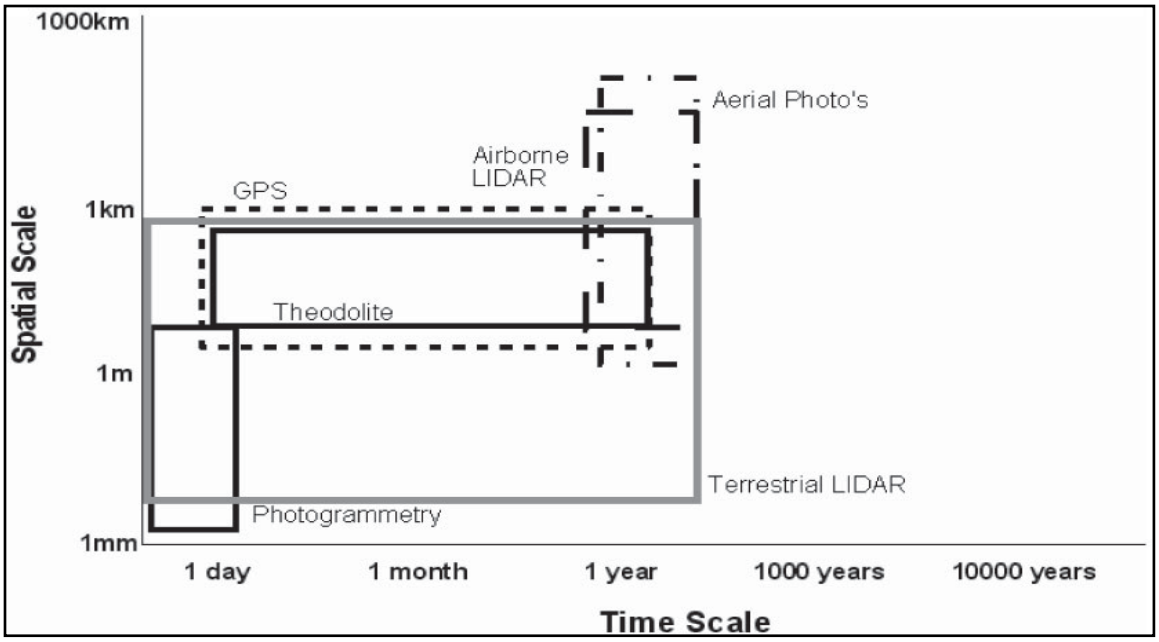

Figure 2.1: The spatial and temporal limits of conventional morphometric survey techniques (Heritage and Hetherington, 2007).

Traditional survey methods such as total station instruments and Real-Time Kinematic Global Positioning Systems (RTK-GPS) offer greater spatial coverage, but are limited in resolution. Additionally, these survey techniques are physically demanding, relatively time consuming, and have the potential for operator bias (Lawler, 1993). Depending on terrain, total stations permit collection of about 1000 points per day with a two-person team (unless robotic), while around 3000 observations per day are feasible using RTK-GPS (Milan et al., 2007). These technologies can also result in direct physical disturbance of the erosional surface of interest (Resop and Hession, 2010).

Airborne terrestrial laser mapping (ATLM), often referred to as airborne LiDAR, offers larger-scale spatial coverage than do traditional survey methods. However, due to the orientation of the aircraft with respect to near-vertical surface topography, ATLM surveys have difficulty mapping vertical features such as steep stream banks/bluffs. Multiple flight lines and proper spacing between them is a necessity if steep features are

being examined (Day et al., 2012). ATLM also requires motion compensation corrections be applied to collected data, and therefore cannot match the precision and accuracy of TLS. After post-processing has been completed, digital elevation models with precision ca. 15 cm can be produced (Charlton et al., 2003).

Many of the drawbacks associated with more traditional technologies can be overcome with TLS. The use of TLS is appropriate for time scales ranging from a few days to many years, and is applicable for spatial scales of a meter to a kilometer in size (Heritage and Hetherington, 2007). TLS produces very high spatial resolution, with precision and accuracy on the order of millimeters to centimeters (Day et al., 2012). TLS requires less data collection time than do total station and GPS methods, and all but eliminates the operator bias associated with these technologies. Additionally, direct physical disturbance of the surface of interest can be avoided with TLS. The temporal resolution attainable with TLS is much higher than its airborne counterpart, while costs associated with TLS are significantly lower (Nasermoaddeli and Pasche, 2008).

TLS does present certain challenges and limitations. Vegetation and uneven topography often result in holes in the dataset (referred to as shadows), which can sometimes be eliminated by scanning from multiple angles. In locations where this is not an option, vegetation must be removed during processing. Additionally, different materials have distinctive reflective properties, which must be taken into consideration. TLS datasets are extremely large. The product of a single scan is upwards of several million point measurements, each with a unique x,y,z coordinate and an intensity value (Buckley et al., 2008). In order to analyze the resulting point clouds, a computer capable of running specialized visualization software is necessary.

Although TLS is fairly new to the scientific arena, it has been utilized successfully in various studies of the natural environment. For example, Bitelli *et al*. (2004) used terrestrial LiDAR to examine landslide dynamics. There have also been numerous studies that utilize TLS in a fluvial setting. Resop and Hession (2010) monitored low stream bank retreat in Virginia with TLS and compared their results with those of traditional survey techniques, Milan *et al*. (2007) assessed erosional/depositional volumes in a proglacial river in Switzerland, and Day *et al*. (2012) used TLS technology to determine rates and processes of river bluff erosion in southern Minnesota. The frequency with which terrestrial LiDAR scans were conducted in these studies depended primarily on the rate at which geomorphic change was occurring, while the resolution of the instrument was selected based on the scale of the geologic feature being examined (Buckley et al., 2008).

2.2 Bank/Bluff Erosion Processes

River bank and bluff erosion is one of the most important processes in lateral channel migration, and has been identified as a major contributor to sediment loading in many watersheds, the primary cause of the declining water quality in these regions (Cancienne, et al., 2008; Nasermoaddeli and Pasche, 2008; Fox et al., 2007). Sediments derived from near-channel sources can include stream banks, bluffs, ravines, and road crossings. Bluffs differ from stream banks in that they are composed of in-situ material (as opposed to alluvial deposits) and extend beyond the height of the floodplain. For this reason, they are viewed as "hydrologically disconnected" from the present-day channel (Day, et al., 2012). However, processes occurring in the channel – such as high flow

events – still influence erosion well above the channel floodplain. For example, fluvial scour along the water's edge affects bluffs by over-steepening and/or undercutting, making them more susceptible to mass wasting.

Soil characteristics and interaction among the processes responsible for causing erosion vary both spatially and temporally within each watershed. The evolution of a channel is stochastic, and depends in a large part on the magnitude and frequency of geomorphic forces acting upon it. For this reason, any study of bank/bluff erosion incorporates short-term sampling of a long-term process (Couper and Maddock, 2001), and there is potential for wide variability in the data collected.

The main processes influencing erosion of stream banks/bluffs are near surface processes (e.g. weakening and weathering caused by freeze-thaw cycling and surface erosion), groundwater-driven processes (e.g. seepage erosion; high soil moisture content), mass failure, and fluvial entrainment/erosion (Couper and Maddock, 2001; Wynn and Mostaghimi, 2006; Resop and Hession, 2010). Near-surface processes are commonly viewed as preparatory—they weaken the surface prior to fluvial erosion, thereby increasing its efficiency (Lawler, et al., 1997). Fluvial erosion of the basal zone of a bank/bluff leads to over-steepening or undercutting, and subsequently, increases the likelihood of a mass failure event. Erosion of banks and bluffs due to flow undercutting is often modeled by an excess shear stress equation, which relates the rate of erosion to the shear stress applied once a critical shear stress is exceeded (Fox, et al., 2007). Failed bank/bluff materials may be delivered directly to the stream in the form of bed material load and/or wash load. Sediments not reaching the channel may be deposited at the base of the bank as intact blocks, or smaller aggregates. Failures that supply sediment to the

basal zone temporarily decrease bank/bluff angle and increase stability (Thorne, 1982). The rate at which fluvial erosion removes the failed material in the basal zone depends on discharge and cohesiveness of the soil.

Soil moisture content (pore water pressure) has a strong influence on the erodibility of bank/bluff materials. In general, when stream banks/bluffs are saturated, stability is decreased. In less than saturated conditions when soil pores are filled with water and air (above the water table), negative pore-water pressure develops. Negative pore-water pressure translates to positive matric suction. Matric suction is defined as the difference between the air pressure and the water pressure in the soil, and increases the shear strength (apparent cohesion) of the soil when positive (Casagli, et al., 1999; Simon, et al., 2000). Matric suction values decline in response to rain events and high flow. Excess (positive) pore-water pressures have long been associated with instability in stream banks/bluffs. Bank failures are commonly observed on the falling limb of a storm hydrograph, when positive pore-water pressures in the soil are no longer offset by the confining pressure provided by water in the channel (Simon, et al., 1999; Wilson, et al., 2007; Rinaldi et al., 2004).

Another important component of near-surface processes is freeze-thaw cycling. When water expands upon freezing, it reduces the granular interlocking between soil particles (Dietrich and Gallinatti, 1991). Soil lab experiments conducted by Asare *et al*. (1997) found that the surface shear strength of a soil decreased with an increasing number of freeze-thaw cycles, and increased with increasing bulk density. Field experiments conducted by Kok and McCool (1989) also showed a similar inverse relationship between soil shear strength and periods of freeze-thaw cycles. From these results, one

might infer that freeze-thaw cycling has the effect of decreasing soil bulk density (i.e. making it less compact), and therefore, increasingly the likelihood that erosion will occur. Wynn and Mostaghimi (2006) found a strong correlation between soil freezing and soil erosion, after noting significant removal of sediments from stream banks during bank-full flood events in late winter/early spring after freeze-thaw cycles had occurred. Additionally, their results showed that freeze-thaw cycles had lasting effects, spanning from one to three months.

Seepage erosion, also referred to as sapping, is a groundwater-driven process that contributes to stream bank/bluff erosion. Seepage erosion occurs when water infiltration rates are high – after rain events or spring melt – causing the formation of perched water tables (Cancienne, et al., 2008; Fox et al., 2007). Perched water tables develop above layers of less permeable material, or between layers having contrasting hydraulic conductivity (i.e. clay and sand). When perched water tables rise on these water-restricting layers, significant hydraulic gradients result in increased lateral subsurface flow toward channels (Fox et al., 2007, Wilson et al., 2007). This increased subsurface flow is often observed during the falling limb of a stream hydrograph, when the level of the water table is rapidly declining. Stream banks and bluffs provide an optimal point at which water can exit the soil profile, and when seepage or lateral flow is sufficient enough to entrain soil particles, erosion results (Wilson et al., 2007). As the quantity of soil particles removed increases, the bank/bluff is effectively undercut, increasing the probability for mass failure to occur (Lindow et al., 2009; Fox et al., 2007; Cancienne et al., 2008). There exists strong correlation between high water infiltration rates and the development of hydraulic gradients that drive lateral groundwater flow toward stream

channels. The increased likelihood for seepage erosion that ensues has important implications for stream restoration efforts. Lindow *et al*. (2009) have found that reconstruction/restoration of stream banks and bluffs is most effective during times of the year when lateral groundwater flow is at minimum.

Certain soil properties also influence the rate at which erosion occurs. Wynn and Mostaghimi (2006) found bulk density to be the primary factor affecting soil erosion in Southwestern Virginia. Bulk density is a measure of soil compaction, and is calculated as the dry weight of soil divided by its volume, thereby accounting for soil pore space (USDA, http://soils.usda.gov). Research conducted by Asare *et al*. (1997) showed that the shear strength of a soil increased along with increasing bulk density. Bulk density is viewed as a composite soil parameter, incorporating soil texture, root density, chemistry, and soil organic matter composition (Wynn and Mostaghimi, 2006).

Soil texture (proportion of sand/silt/clay) influences the critical shear stress, and therefore, erodibility of a soil. Smaller soil particles fill voids between the pore spaces of larger particles, effectively reducing the exposure of these larger particles to hydraulic forces. Additionally, cohesion of a soil decreases as proportions of sand increase. For this reason, the probability for erosion to occur is greater in soils having higher sand contents (Wynn and Mostaghimi, 2006), so long as the shear stress related to flow exceeds the critical force needed to transport sand.

3.0 Field Site

Amity Creek lies on the northeastern end of Duluth, Minnesota and flows in a southeasterly direction on its course to a confluence with the Lester River, just before reaching Lake Superior (Figure 3.1). The Amity Creek watershed spans approximately 43.25 square kilometers, and is comprised mostly of lowland forest (69%), in addition to portions of grassland (9%), developed land (7%), upland forest (7%), lowland shrubs (5%), and cropland (2%) (Fitzpatrick et al., 2006). These numbers make Amity Creek one of the least urbanized streams within the Duluth metropolitan area (Anderson et al., 2000).

As Amity Creek approaches the Lester River and Lake Superior, its gradient steepens and the channel incises deeply into the underlying clay-rich soils (Fitzpatrick et al., 2006). This incision results in the formation of numerous bluffs, typically lying on the outside of channel meanders. Bluff erosion is believed to be a central component of the sediment loading occurring in Amity Creek, undoubtedly contributing to the creek's turbidity impairment. Stream bluffs are locations that experience high volumes of erosion, and are ideal locations to employ TLS technology to measure any geomorphic change induced by high-flow events.

A typical drainage network transitions from a steep, erosional zone in the stream's headwaters to a low-gradient depositional zone near the mouth. However, streams on the North Shore of Lake Superior are inherently different, and reflect opposite geomorphic characteristics. For example, Amity Creek begins as a low-gradient, meandering channel and evolves into a high-gradient bedrock channel before connecting with the Lester River and Lake Superior (Figure 3.2).

The geological characteristics of the North Shore have a large influence on the erosional processes occurring within the Amity Creek watershed. The geologic history of the region dates back 1.1 billion years, when the Lake Superior Basin was created by a Midcontinent Rift system. The bedrock geology along the North Shore is dominated by stacked basalt flows and igneous intrusions formed during the rifting (Sims & Morey, 1972). These geologic units often outcrop in the lower portion of the Amity Creek watershed, and are highly resistant to erosion (Figure 3.3).

The surficial geology in the Amity Creek watershed reflects a glacial past. The Superior lobe – one of multiple late Wisconsinan lobes being part of the massive Laurentide Ice Sheet – occupied the Lake Superior Basin as recently as 10,000 yr BP (Farrand and Drexler, 1985). The Superior lobe experienced multiple episodes of advancement and retreat, with each successive advance moving a shorter distance (covering a smaller area), reaching lower elevations, and depositing finer-grained till due to the proglacial lake sediments that had become incorporated into the ice (Hobbs and Breckenridge, 2011). As the Superior lobe melted, proglacial lakes formed between the ice to the northeast and moraines to the southwest that served as dams. Glacial Lake Duluth formed in this fashion, and eventually drained via two main channels – the Portage outlet on the Minnesota side, and the Brule outlet on the Wisconsin side. However, due to differential isostatic rebound, or isostatic tilting of the Lake Superior basin as the ice sheet retreated, the Brule outlet was approximately 8-10 meters lower than the Portage outlet. For this reason, it is generally accepted that the majority of the lake was drained via the Brule outlet to the south (Carney, 1996). Differential isostatic

rebound of the basin persists today and is responsible for a drop in base level for North Shore streams, resulting in continued incision of those streams.

The Amity Creek watershed spans multiple tills laid down by successive stages (advancements) of the Superior lobe (Figure 3.3). The two formations that comprise the Amity Creek watershed are the Cromwell and Barnum Formations. The Barnum Formation can be further broken down into the Lakewood or Mahtowa (bottom), Moose Lake (middle), and Knife River (top) members (Hobbs, 2004; Hobbs and Breckenridge, 2011).

The portion of the watershed lying west of Jean-Duluth Road (no TLS sites in this portion of the watershed; Figure 3.1) is composed primarily of Cromwell Formation tills, the oldest of the glacial sediments in the Amity Creek watershed. The upper portion of the watershed falling in our study area, which is situated above the Skyline Parkway ridgeline and east of Jean-Duluth Road, is composed mostly of Lakewood and Moose Lake tills. Additionally, small regions of fine-grained lacustrine sediments deposited by glacial Lake Duluth can be found interspersed among the tills. Lakewood tills are classified as silt loams and have the largest proportion of coarse-grained sediments in the Barnum Formation, while Moose Lake tills are classified as clay loam to silty clay loams. The lower portion of the watershed, which lies below the Skyline Parkway ridgeline, is comprised mostly of bedrock and Knife River tills. Steep channel gradients in this region of the watershed have resulted in deep incision into these tills, producing an abundance of large clay bluffs. Knife River tills are classified as calcareous clays and contain few course-grained fragments or large rocks (Hobbs, 2009).

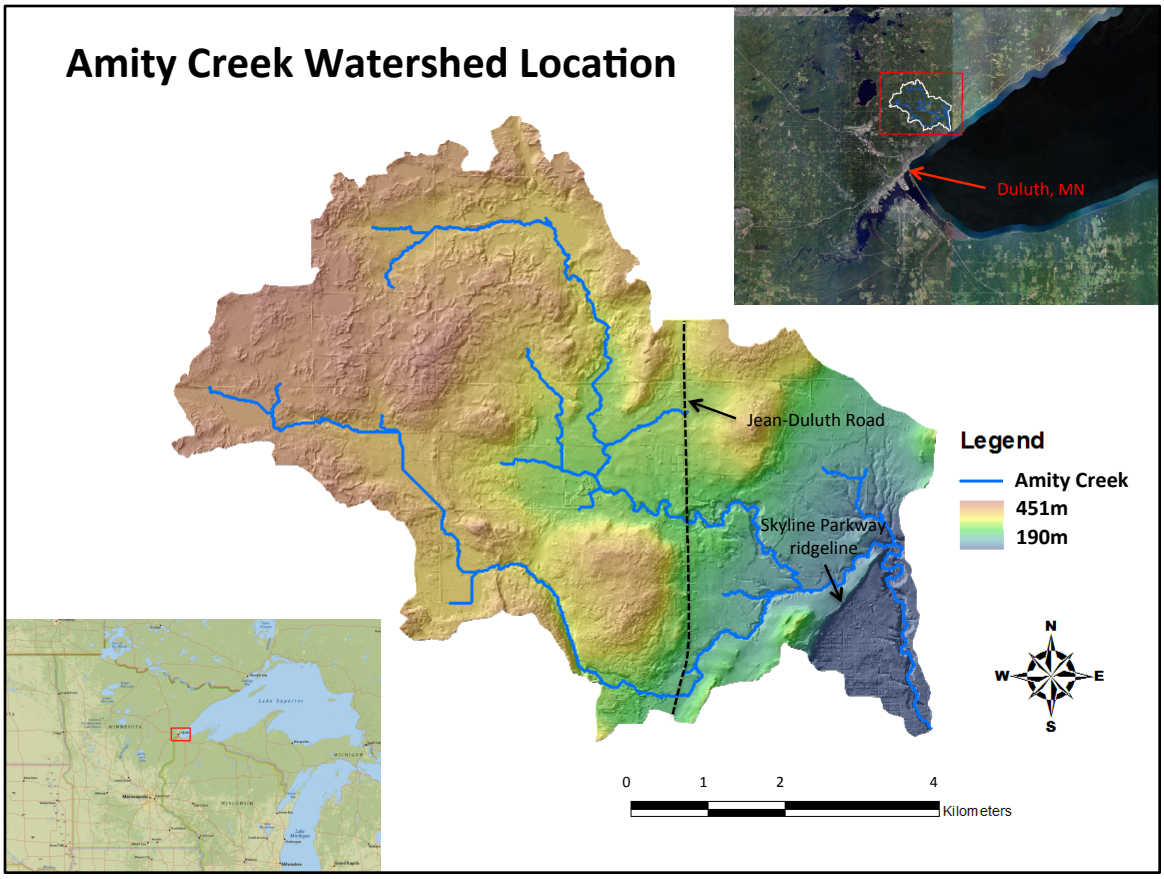

Figure 3.1: Amity Creek watershed location in Northeastern Minnesota showing the expansive, relatively flat upper watershed, and steep gradients as the stream approaches its confluence with the Lester River and then Lake Superior.

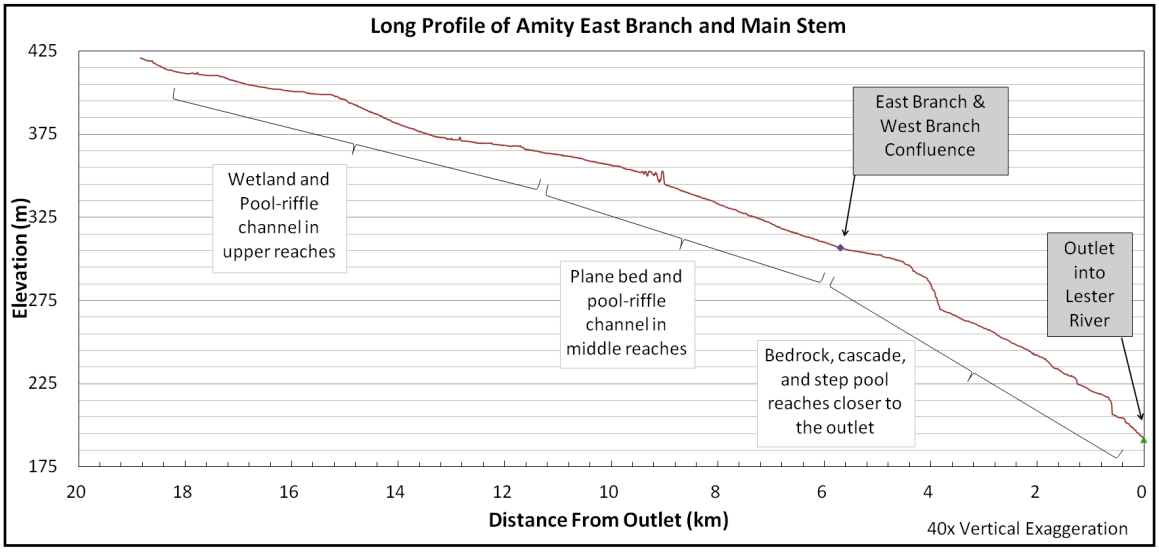

Figure 3.2. Annotated longitudinal profile of Amity Creek. As is typical of North Shore streams, the long profile has a concave-down shape, with increasing slope towards the outlet (Wick, 2013).

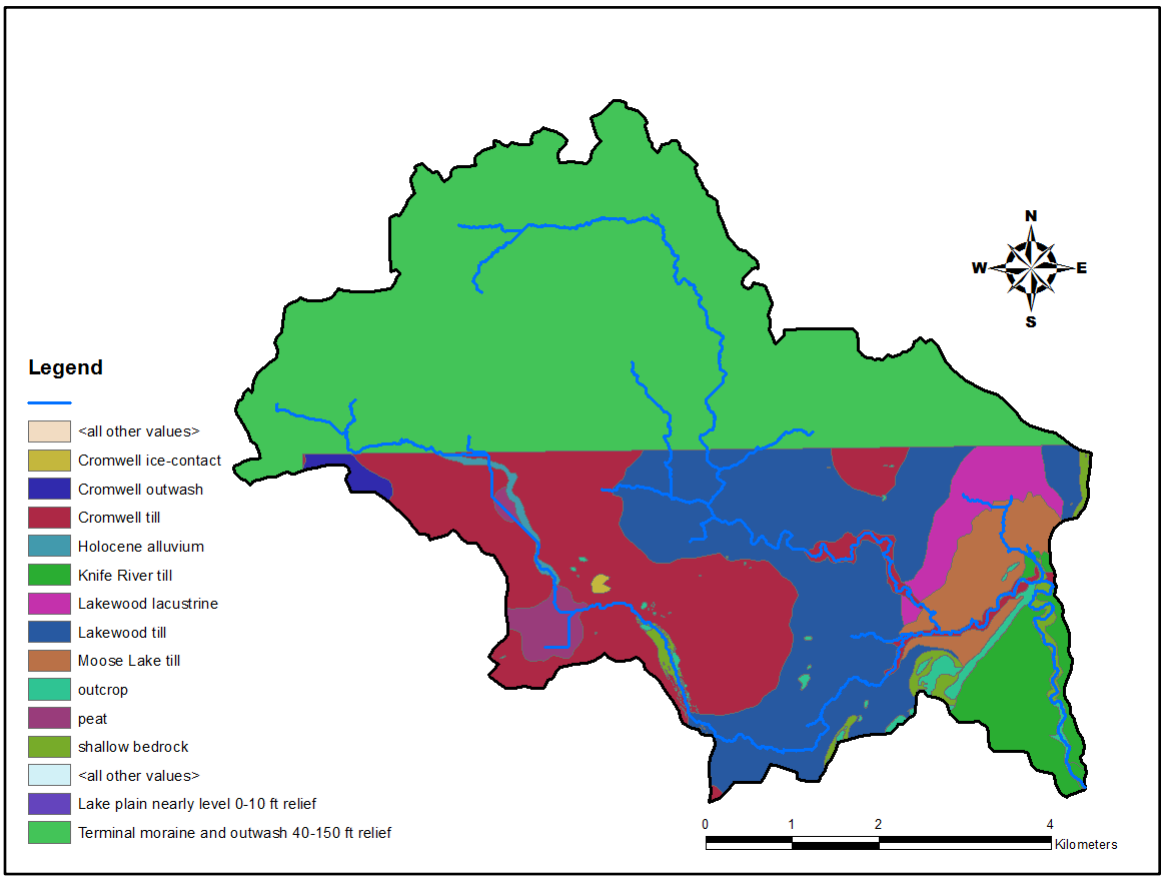

Figure 3.3: Surficial Geology of the Amity Creek watershed (southern half of watershed was mapped by the MN Geological Survey; northern half of watershed is data retrieved from MN DNR Data Deli; upper green region on map represents lumped terminal moraine and outwash deposits 40-150 feet relief – see legend).

4.0 METHODS

4.1 Terrestrial Laser Scanning

TLS technology was utilized in this experiment to investigate the severity of erosion occurring on stream bluffs in the Amity Creek watershed in northern Minnesota. In order to measure the amount of bluff erosion attributed to individual high-flow events – or to determine if bluff erosion can be correlated with individual events – we used TLS methodology to scan eight study sites (Figure 4.1) before and after each major flow event that occurred during the study period. Scans were also conducted in late fall and early

spring to determine if processes such as freeze-thaw cycling and spring melt had any effect on bluff erosion. Soil samples were collected from study sites to characterize bulk density and grain size. Bluffs were mapped with GIS software to determine size and location within the Amity watershed; these data were combined with erosion rates from our study bluffs to extrapolate results to the entire watershed.

4.1.1 Data Collection

The selection of TLS sites for this study incorporated 3 variables: size (surface area); location and relative ease of access; and vegetative cover present. Sites ranged in size from approximately 30 to 700 m^2, and all were accessible via road and/or hiking trail. A fundamental feature among bluffs selected for analysis was a general lack of vegetative cover, as vegetation drastically increases the post-processing time required and decreases the accuracy of the surface being generated.

Eight sites were selected for TLS analysis, each of which had three or four control points established. These points were later used in post-processing to link scans from different time periods together into a common framework. Control points consisted of 5/8 inch diameter rebar posts that were set in the ground, often at the toe of the study bluff, which acted as permanent markers that would remain stationary for the duration of the experiment. The length of the rebar varied from 2.5 to 4 feet, depending on the surficial geology present (i.e. how far the post could be pounded before reaching bedrock or large cobble/boulders). Spheres – automatically detectable objects in Faro Scene post-processing software – were secured to the top of each rebar control point while scans were being conducted. The purpose of the control points/spheres was twofold: (1) scans

taken from different locations on the same date could be registered/combined; and (2) scans conducted over the course of the experiment could be registered together. Spheres are essentially common reference points that allowed successive TLS campaigns to be compared, and thus, any geomorphic change to be detected.

Terrestrial laser scans were conducted using a Faro Focus 3-D laser scanner, capable of 976,000 measurement points per second at millimeter-scale accuracy. The range of the instrument is 0.6-120 meters, provided a low ambient light source (i.e. the sun) and normal incidence to a 90% reflective surface. All bluffs selected for analysis are well within the 120m threshold, yet angles of incidence and lower reflectivity values reduce the specified limits. The scanner functions by emitting a laser beam off a rotating mirror toward the area or object being scanned. The beam is reflected back to the instrument by objects in its path, which allows for distance and relative vertical and horizontal angles to be determined. The Focus 3-D uses phase-shift technology to collect up to 976,000 points per second (pps) versus 1,000 to 5,000 pps achieved with time-of-flight scanners. Rather than emitting a single pulse and measuring the time-of-flight, phase-shift scanners emit waves of varying length and measure the "phase shifts" in the waves of infrared light. The instrument has a vertical range of 305° and a horizontal range of 360° (Faro, http://www.faro.com). When conducting a scan utilizing the full window, virtually every object within the 120m threshold is detected, excluding a circular footprint at the base of the instrument that accounts for the 55° absent from a full vertical range.

The Faro scanner allows the operator to determine the instrument resolution, often dictated by the goals of the user. In this experiment, two resolution settings were utilized

to complete a campaign. First, a full-window scan was conducted at 1/8 resolution. Using the instrument's touch screen display, a window was then selected around the bluff and the scanner was set at a higher resolution (1/4) to capture the surface of interest in more detail. This technique resulted in two scans being collected from each instrument set-up. However, because vegetation and other objects often obstruct line of site to the bluff, multiple instrument locations were needed to prevent large holes in the dataset. For smaller bluffs, two instrument set-ups (4 scans) were often sufficient, while larger sites required up to four (8 scans). Thus, in this experiment, a TLS campaign consisted of anywhere from four to eight scans, depending on the size of the bluff. A campaign can be thought of as a set or series of scans conducted on the same date at one study site.

Four or five TLS campaigns were completed at each study bluff beginning in November 2011, and continuing through November 2012. Scans were conducted in the spring of 2012 following snowmelt, and in late fall (2011 & 2012) after most deciduous foliage was lost. Scans were also carried out following the two large precipitation events (May 23-28; June 19-20) that occurred during the study. As discussed previously, scanning in early spring and late fall minimized holes in the dataset caused by vegetation, thereby mitigating post-processing work. Additionally, scanning in the spring allowed any erosion and/or deposition induced by snowmelt and freeze-thaw cycling to be detected.

4.1.2 Data Analyses

In order to determine the quantity of erosion/deposition occurring on our study bluffs between scan campaigns, an immense amount of post-processing work had to be

completed. Two significant obstacles in detecting geomorphic change from raw point cloud files are removing vegetation from the surface of interest, and merging successive point clouds collected throughout the experiment.

Post-processing and analysis of the TLS field data were completed utilizing three software programs. Faro Scene was used for preliminary post-processing that included vegetation removal; trimming point cloud extents; individual campaign registration (merging scans conducted at different locations on the same date); and registration of campaigns collected throughout the experiment at each site. Topographic Point Cloud Analysis Toolkit (ToPCAT; also referred to as "PCTools") – a decimation software program originally developed by James Brasington and Igor Rychkov – was used to reduce the file size of TLS point clouds, making them manageable in GIS software (https://code.google.com/p/point-cloud-tools/). The final stage of data analysis was conducted using a combination of ArcMap and Geomorphic Change Detection (GCD) software, an ArcMap plug-in developed by Joe Wheaton and colleagues at Utah State University (http://gcd.joewheaton.org/).

4.1.2A Faro Scene

The first stage in post-processing TLS point cloud data involves the removal of vegetation and objects other than the surface of interest from the data set. Shadows (holes) result when vegetation and/or topographic irregularities obstruct the line of sight from the scanner to the surface of interest. Vegetation was particularly troublesome in this experiment for scans conducted during late spring/early summer when foliage was most prominent. Any vegetation present in the scan window is detected by the

instrument, and must be removed from the point cloud manually using a basic select and delete process. However, due to the concave nature of the study bluffs, removal of vegetation was challenging. When viewing the entire bluff in three-dimensional space, it is difficult to remove vegetation without inadvertently deleting portions of the surface. To alleviate this issue, bluffs were first viewed using a planar perspective within Scene. Next, vertical slices of the bluff were examined in 3-D, allowing points to be more readily selected and deleted without losing data representing the bare-earth surface. This procedure was similar to that used by Day *et al*. (2012) to remove vegetation from point clouds collected from river bluffs in Southern Minnesota.

After removing vegetation, overlapping point clouds collected from different instrument locations on the same date could be registered or combined using common reference spheres. Scene makes this process fairly simple by automatically detecting spheres present in a scan image. By recognizing the relationship (angle and distance) between the spheres present in multiple scans, the software is able to register scans collected in a single campaign. Scene requires three common reference points/spheres be visible in each scan for registration to work properly. However, when additional references are added (≥4), registration typically becomes more accurate as there is less error associated with positioning of the point clouds. Once scans from an individual campaign were registered, they could then be co-registered with other campaigns to generate a point cloud encompassing all scans collected at a given site in a common coordinate system. Point clouds associated with individual campaigns were then exported separately as a ".pts file", with each point having an (x,y,z) position representing a three-dimensional location within a local coordinate system.

The 500-year flood that Duluth and the surrounding region experienced in late June 2012 resulted in many rebar posts being lost or destroyed. This made registration of successive campaigns considerably more challenging. Spheres were still used to register scans collected in a single campaign, but were placed on rocks or directly on the face of the bluff rather than being attached to the rebar control posts. Because the spheres could no longer be placed in a fixed location (rebar), objects such as rocks and trees that existed pre and post-flood were used to co-register multiple campaigns. This process requires the user to manually establish common reference points and often results in larger registration errors, as it must be assumed that the reference objects are in precisely the same location for successive campaigns. Due to the extreme power of the floodwaters, many sites and their control networks were more or less destroyed, leaving limited options for common reference points.

4.1.2B ToPCAT (PCTools) Decimation Software

TLS point cloud files are immense in size. Depending in part on the selected instrument resolution, individual scans typically contain millions of points, each representing a unique 3-D location in space (Buckley et al., 2008). Although GIS software packages such as ArcMap have become increasingly TLS-friendly, it is often necessary to reduce the file size in order to eliminate large delays when regenerating graphics or running various analyses. ToPCAT (formerly PCTools), a decimation software package designed for processing large TLS datasets, was used to condense point cloud file size in this experiment. The 32-bit version of the software was used in this study, though a more recent 64-bit version exists.

ToPCAT works by sorting the point cloud into a 2-D grid of square domains (Δx,Δy) specified by the user. ToPCAT's geospatial algorithm then extracts various terrain products (e.g. minimum, maximum, mean elevation) from each domain or cell (Brasington et al., 2012). In this experiment the resolution for the domains used in ToPCAT varied from 0.02 to 0.06 meters, based on the size of the point cloud (i.e. the size of the bluff). In order to generate the most accurate representation of the bluff surface and minimize the effects of unwanted vegetation, z_{min} (minimum elevation) values were utilized in this study. Therefore, any bare surface points existing within the Δx, Δy cell would be selected, effectively filtering any remaining vegetation. The final products of ToPCAT's algorithm are simple text files, which were then imported into ArcMap. Files generated by ToPCAT to be imported into ArcMap averaged approximately 5-6 MB in size.

4.1.2C ArcMap/GCD

The final stage in post-processing of the TLS point cloud data for this experiment was completed using ArcMap GIS (TIN and DEM creation) and GCD software (DEM differencing). After decimating the raw point clouds using ToPCAT, the output .txt files were imported into ArcMap and displayed. The y and z-axes were re-oriented; the z-axis was now perpendicular to the face of the bluff (as opposed to perpendicular to the ground) and the y-axis perpendicular to the earth's surface. Next, the .txt files were converted to shapefiles, allowing TINs (Triangular Irregular Networks) to be built (ArcMap 3D Analyst Toolbox). TINs were checked for any interpolation or extrapolation errors – basically, did the TIN accurately portray the topography in the scan

image? Subsequently, DEMs (Digital Elevation Models) were generated from the TIN surface using ArcMap's 3D Analyst. In this stage of data processing, each bluff had a corresponding series of DEMs, each of which represented an individual scan campaign.

The principles by which the GCD software works are fairly straightforward – two DEMs representing the same surface at different time periods are differenced, meaning each cell has a calculated volume of erosion, deposition, or no net change. Because of the coordinate shift, the z values being differenced were now normal to the bluff surface; thus, negative numbers indicate erosion or a retreat of the bluff (Figure 4.2) while a positive numbers represent deposition on the bluff surface. The product of two differenced DEMs is termed a DoD, or DEM of difference.

DEMs are raster files composed of hundreds of thousands of grid cells, each representing a 3-D location on the bluff surface. As per GCD input requirements, the resolution used when creating the DEM was matched with the resolution used in ToPCAT to decimate the point cloud. Additionally, each series of DEMs have to meet the conditions of being orthogonal (same grid resolution and common grid centers) and concurrent (same extents). In summary, DEMs have to be properly aligned for the GCD software to function correctly.

To achieve the orthogonal and concurrent requirements, the resolution used for a series of DEMs (i.e. series of campaigns) was held constant. In order to ensure concurrency among a series of DEMs, a shapefile was first created that would serve as the "processing extent" for the overlapping point clouds. This shapefile can be viewed as a common extent or boundary to be used later when creating DEMs. When generating TINs, however, it was necessary to create extents unique to each individual campaign in

order to prevent extrapolating or interpolating to regions with no data. Therefore, new polygon shapefiles were generated for each TLS campaign using the processing extent shapefile as a template. A combination of ArcGIS tools (Editor; Clip) were used for this process. Next, points from a single campaign were overlaid on their corresponding extent shapefile. Holes in the dataset –typically a result of dense vegetation or uneven topography – were subsequently trimmed from the new shapefiles using the Editor toolbar. Initially, any holes greater than 0.20 meters in diameter were removed. Depending on the size of the bluff, this process was very time-intensive, requiring up to 8 hours to complete the trimming on one campaign. For this reason, a higher threshold was used with later DEMs, and voids greater than or equal to approximately 0.50 by 0.25 meters were removed. Previous studies indicate that while removing holes in the dataset leaves less area over which change can be measured, errors are greatly reduced (Day et al., 2012). Resulting trimmed extents (polygon shapefiles) were then used in conjunction with TLS points (point shapefiles) as TIN inputs. Due to the coordinate shift, the y attribute now represented the height field and the polygon shapefile served as a "hardclip" – basically a boundary for triangulation.

When creating the first DEM in a series, the common extent shapefile was used to define the processing extent. Next, these extents were modified; the top and right extents were rounded up to the nearest whole number, or a value evenly divisible by the cell resolution. The bottom and left extents were rounded down following the same guidelines. This procedure was completed to ensure that no portion of the TIN was omitted when converting to a DEM. Subsequent DEMs were generated using the original DEM for the processing extent, resulting in an orthogonal, concurrent series.

The final stage in post-processing of our TLS dataset utilized the GCD software plug-in for generating DoDs. First, concurrent DEMs from a given site were added to the software's survey library; the single method survey was specified as TLS. The GCD Analysis Change Detection tool was then used to difference the DEMs. Overlapping cells from two concurrent DEMs are differenced, typically by subtracting the old DEM from the new DEM. However, because of a sign convention related to our swapping the y and z-axes and the orientation of +/- z values within Faro Scene, we subtracted the new DEM from the old to give correct erosional/depositional calculations. For example, slumps in some of our study bluffs following spring melt in 2012 were displayed accurately, with positive values (deposition) at the toe of the slump and negative values (erosion) along the scarp faces, indicating that DEM differencing was in fact correct.

After a DoD was generated, a threshold value was applied in the GCD Change Detection tool. For this experiment, a threshold of 0.10 meters was used to filter the erosional/depositional statistics in the previously created DoD. This meant that any cells in the DoD ranging from -0.10 to 0.10 m were removed from the calculations. A threshold is used to filter out any "noise", which can be thought of as the cumulative error or uncertainty in the data (e.g. errors from the instrument, vegetation removal, TIN creation, scan alignment, etc.). The ten-centimeter threshold value was based on same-day error validation results from a similar TLS bluff erosion study conducted by Day *et al*. (2012). The root mean square errors for their experiment ranged from 0.023 to 0.087 meters. Therefore, our use of 0.10 m was a somewhat conservative estimate based on their error calculations. Results generated by the GCD software show both thresholded and un-thresholded areas and volumes of erosion/deposition. The benefit of having

captured a 500-year flow event in the dataset of this experiment is that the signal greatly exceeds the noise – erosional/depositional calculations exceed errors in the data. Average bluff retreat distances were calculated from the thresholded net volume difference (total thresholded volume of deposition – total thresholded volume of erosion) using the following equation:

$$Average\ Retreat\ Distance\ (m) = \frac{thresholded\ net\ volume\ difference\ (m^3)}{area\ over\ which\ change\ was\ detected\ (m^2)}$$

4.2 Bluff Characterization

Bulk density samples were collected at 5 study bluffs in the summer of 2012 and the spring of 2013 using an ICT International 0200 soil bulk density sampler (Figure 4.3). Two samples were collected from exposed portions of the bluff face, just above the toe. The first sample was taken at the surface, while the second was collected approximately 30-40 centimeters deep in the soil profile. Samples were dried for a minimum of 24 hours at ~105° Celsius in a hot-air oven. Next, the soil was ground in a mortar and pestle, and any small stones were carefully removed. The soil and stones were weighed separately using a beaker of known weight. The volume of the pebbles was determined by measuring the volume displaced by adding them to a test tube filled with water. Bulk density was determined using the following equation:

$$Bulk\ Density = \frac{oven\ dry\ weight\ of\ soil - weight\ of\ stones}{volume\ of\ soil\ solids\ and\ pores - volume\ of\ stones}$$

where the volume of soil solids and pores is a constant of 137.4 cm^3. Any variation in bulk density, with respect to time of year or location within the soil profile, provided insight into the effect freeze-thaw cycling and moisture content has on the erodibility of the soils comprising the bluffs in the watershed.

A soil's texture, or the proportion of sand, silt, and clay, influences its critical shear stress and how vulnerable it is to erosion. For this reason, grain size analyses were also conducted in this study (Figure 4.3). Soil samples were collected at all bulk density-sampling locations and analyzed at the Large Lakes Observatory in Duluth using a Beckman Coulter LS13 320 laser diffractometer. The instrument determines grain size distribution by measuring the patterns of light that are scattered by the particles in a given sample when exposed to a beam of light. This technique is one of the most commonly practiced methods in evaluating the size distribution of particles due to precise measurements and the relative speed at which results can be obtained. The scattering pattern produced by each particle is characteristic of its size – large particles scatter at small angles and vice versa (Beckman Coulter, 2003). Results of the grain size analysis are reported as percentages of sand, silt, clay, and percent washload (silt & clay).

4.3 Event Sampling

Water sampling was conducted during/following substantial precipitation events at 7 sites along Seven Bridges Road and Old Amity Creek Road/Trail (Figure 4.3). The farthest upstream sample was collected on the West branch of Amity Creek, just upstream of the confluence with the East branch. Samples were then taken consecutively in a downstream direction, beginning just downstream of the East/West confluence. The

intent here was to track the same "wave" of water down the channel. In doing so, the cumulative impact of bluff erosion was revealed as an increasing number of study sites were incorporated into each water sample. However, while sampling in a downstream direction effectively increased the number of bluffs incorporated into each sample, it also meant that sediment from sources such as culverts and small tributaries could potentially influence our suspended sediment calculations. Sampling in this manner helped to determine the extent to which bluff erosion contributes to the turbidity impairment of Amity Creek.

The water samples collected in the field were hand-pumped through a vacuum using 45 mm diameter ashed GF/C filters to extract any particles suspended in the water. The sediment-laden filters were then dried at ~105° Celsius to remove any remaining moisture. The dry filter and sediment were weighed and tared with the known weight of the filter to calculate the Suspended Sediment Concentration (SSC).

4.4 Flow Characterization

In order to for us to determine the effect that high flow events have on bluff erosion in the Amity watershed, we needed to combine our change detection calculations with flow data recorded by a stream gage located on the lower main branch of Amity Creek, 0.66 km upstream of the mouth. The Minnesota Pollution Control Agency (MPCA) operates and maintains the gage, and provided us with archived daily discharge data (cubic feet per second) from the time period over which we conducted our TLS analysis. Flow data was also downloaded from the Lake Superior Streams website (http://www.lakesuperiorstreams.org/). These data were used to determine the peak flow

rate and total flow volume between successive scan campaigns. Because discharge is not uniform at all study sites, peak flow values were scaled based on the following drainage area relationship:

$$\frac{Q_{peak\ gage}}{Area_{gage}} = \frac{Q_{peak\ bluff}}{Area_{bluff}}$$

where $Q_{peak\ gage}$ is the peak flow at the MPCA gage on lower Amity, $Area_{gage}$ is the drainage area above the gage, $Area_{bluff}$ is the drainage area above a given study bluff, and $Q_{peak\ bluff}$ is an unknown. The MPCA gage on lower Amity was destroyed during the June flood, and therefore, peak flow data for the May to June 2012 time period was unavailable. Because of this, $Q_{peak\ gage}$ for the time period encompassing the June flood was scaled from the peak discharge at a USGS gage on the nearby Knife River using a simple drainage area/discharge relationship. Upstream drainage areas were determined from our flow accumulation inquiry of the 1.5 m DEM (see below, Section 4.5). Average daily flows (cfs) were converted into total daily flows (cubic feet/day); the total flow volume between scan campaigns was determined by summing daily flow totals.

4.5 Extrapolating Results

After determining the volume of sediment eroded/deposited at each study bluff and the subsequent average retreat distance between scan campaigns, we could now extrapolate our results across the entire watershed in order to estimate the extent to which bluff erosion contributes to the turbidity impairment of the creek.

The first step in extrapolating our results was mapping bluffs and delineating the drainage network using airborne LiDAR (ATLM) that was flown for the Arrowhead

Region of Northeastern Minnesota in the spring of 2011, and obtained through the Minnesota Geospatial Information Office website. The LiDAR used in this study had a resolution of 1.5 meters, significantly higher than typical DEMs having 10 to 30 meter resolution. ArcMap software was utilized in conjunction with the LiDAR DEM to map Amity Creek bluffs and delineate the drainage network in the watershed.

The fill tool in the Arc Hydrology toolbox was used to fill the DEM to remove any errors due to resolution limits and allow us to create a continuous drainage network. Next, the flow direction and flow accumulation tools (ArcMap Hydrology) were used to map the channel. A threshold value of 75,000 cells was applied to the flow accumulation layer using a simple conditional statement (ArcMap Spatial Analyst), meaning that any portions of the channel having less than 75,000 cells of accumulation were removed from the channel network. The threshold was determined by simple trial and error – basically, the value that would result in the most accurate representation of the existing channel based on field observations. To filter the delineated stream network from the accumulation layer, another conditional statement was applied. The channel was then converted from a raster to vector file using the Stream to Feature Tool (ArcMap Hydrology Toolbox). The resulting vector file representing the Amity Creek drainage network was more accurate than others available from online databases, and would allow us to determine which bluffs interact with the creek (i.e. are in close proximity to the channel), potentially contributing sediment through erosional processes.

In order to map the bluffs in the watershed, we utilized the Slope tool within the ArcMap Spatial Analyst Toolbox. Next, regions having a slope greater than 20 degrees were filtered using the Raster Calculator, leaving values of either one (true) or zero

(false). A conditional statement was then run to preserve the pixels having true values (areas having a slope ≥20 degrees). Next, the "select by location" feature was used to preserve any bluffs within 4 meters of the previously delineated channel. The resulting shapefile accurately mapped the location of bluffs interacting with the channel in the Amity Creek watershed.

Once bluffs were mapped, we overlaid the bluff shapefile (transparency applied) onto 3-inch resolution aerial photography flown in 2011. Our intent was to manually delineate unvegetated bluffs in this manner. However, shadows and poor contrast in the high-resolution photography made GIS bluff delineation difficult. The resolution in other existing aerial photos was not detailed enough for accurate bluff delineation. Moreover, some of the bluffs mapped with LiDAR were either composed of bedrock, or were completely vegetated. Therefore, we elected to inventory bluffs in the field. The height and length of unvegetated bluffs were measured using a laser altimeter and rangefinder. The approximate percentage of bluff devoid of vegetation was also recorded. The advantage to this technique was that many bluffs in the watershed experienced significant erosion as a result of the June flood, increasing in size substantially. The most recent aerial photography in the region was collected pre-flood, meaning that any estimate of total bluff area using aerial photos would have neglected to include recently eroded sections of bluff.

For the purposes of this study, we were concerned with unvegetated bluffs; hence, our results will be biased toward bluffs experiencing recent erosion. We calculated the total area of unvegetated bluffs in the watershed using measurements from the field inventory, and combined this number with areal statistics from our study bluffs. To

determine the amount of sediment that unvegetated bluffs in the Amity watershed contribute to the channel, we utilized the average retreat rate calculated for study bluffs that were scanned over the course of an entire year. Retreat distances for these four sites were assumed to be representative of all study bluffs that scanned in this experiment. By multiplying the average retreat distance (bluffs scanned for one year) by the total area of unvegetated bluffs, we estimated the total volume of sediment eroded from unvegetated bluffs in the watershed. Next, we multiplied the total volume of sediment by our average bulk density, giving us a mass of sediment eroded from bluffs. The total mass was multiplied by the average percent of silt and clay, determined from our grain size analysis. The total mass of fine sediment was then compared to annual FLUX model load estimates from the MPCA's North Shore Stream Monitoring Program (2001-2006), and NRRI estimates which were derived using continuous in-situ turbidity monitoring as a surrogate for annual TSS loads (2005-2007; 2009-2010) (Ruzycki et al., in press).

Table 4.1: Bluff Area Remaining After Removing Vegetation & Holes in the Dataset (m^2)

Site #	Total Area (m^2)	November, 2011	April, 2012	May, 2012	June, 2012[a]	November, 2012
B9	370	346	356	323	318	336
B12	36	36	26	25	27	31
B13	45	44	43	44	44	43
B14	91	NO SCAN	86	24	44	83
B15	32	25	27	28	26	26
B20	83	NO SCAN	66	76	66	77
B2	468	NO SCAN	458	451	423	439
B7	737	NO SCAN	606	497	632	684

[a]post-flood

Table 4.2: % of Bluff Area Remaining After Removing Vegetation & Holes in the Dataset (m^2)

Site #	November, 2011	April, 2012	May, 2012	June, 2012[a]	November, 2012
B9	93%	96%	87%	86%	91%
B12	99%	72%	69%	76%	86%
B13	98%	96%	96%	97%	96%
B14	NO SCAN	95%	27%	48%	91%
B15	80%	87%	89%	83%	81%
B20	NO SCAN	79%	91%	80%	93%
B2	NO SCAN	98%	96%	91%	94%
B7	NO SCAN	82%	67%	86%	93%

[a]post-flood

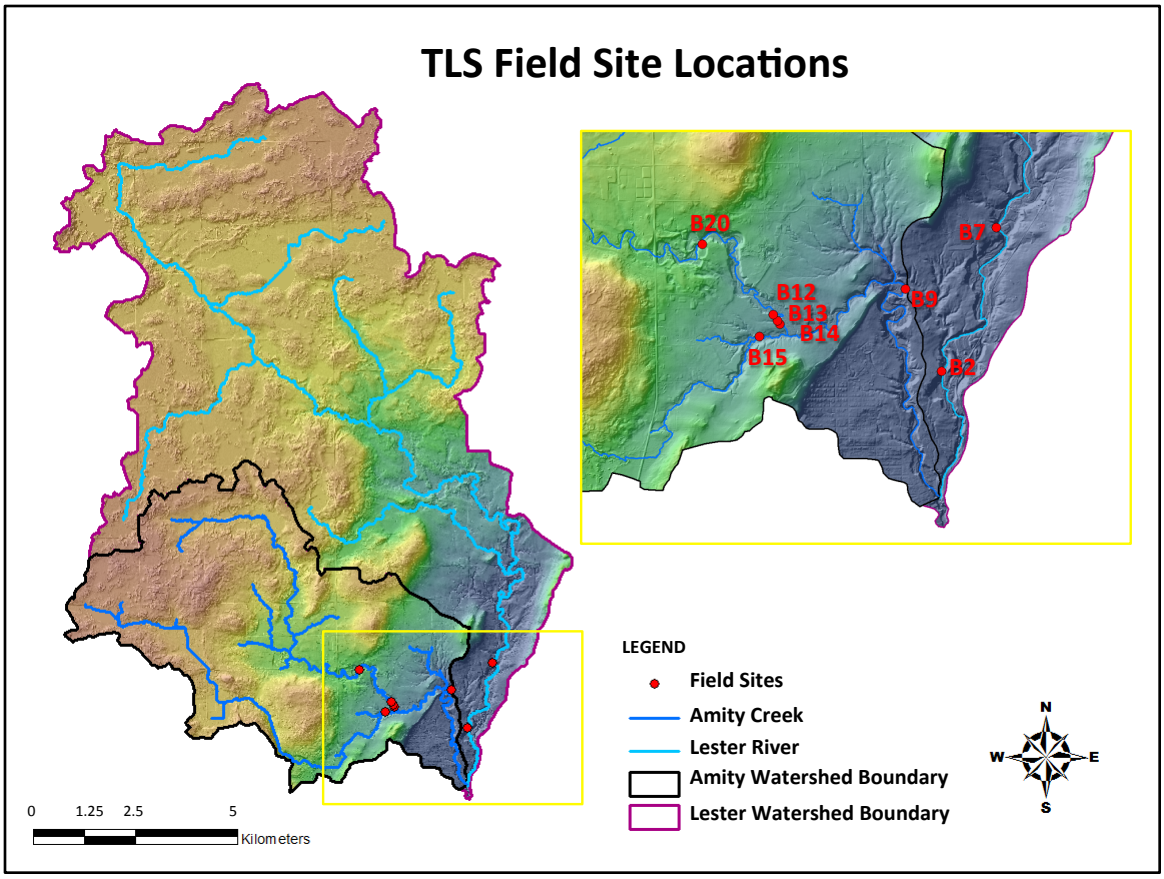

Figure 4.1: TLS field site locations within the Amity Creek and Lester River watersheds.

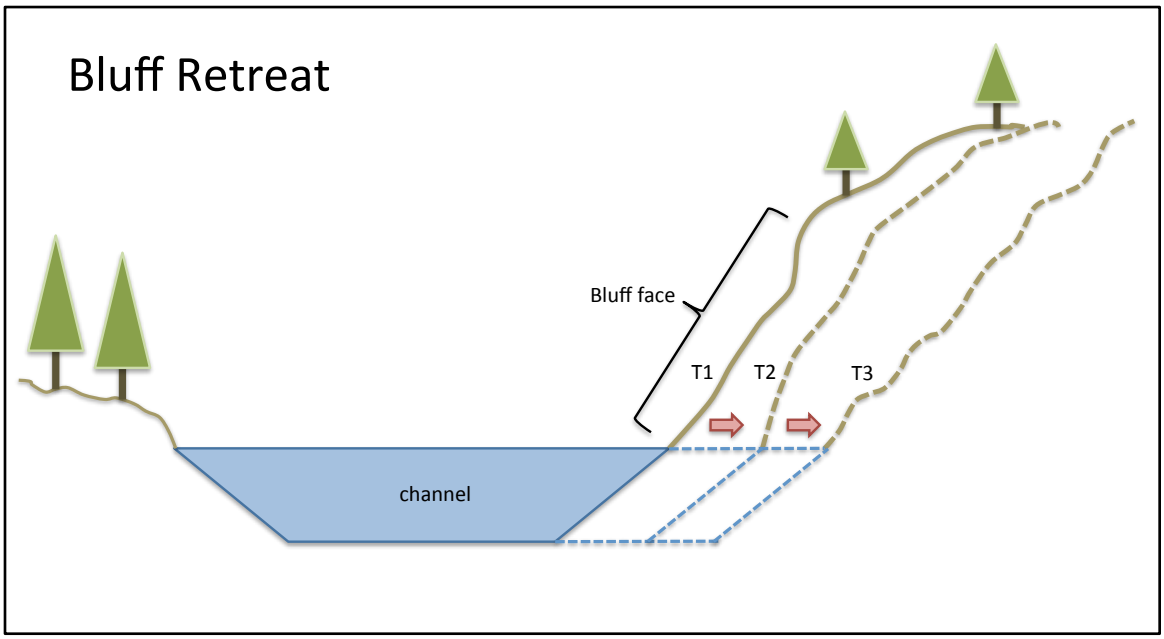

Figure 4.2: Cartoon depicting bluff retreat over time (T1 represents present location; T2 and T3 represent future bluff location).

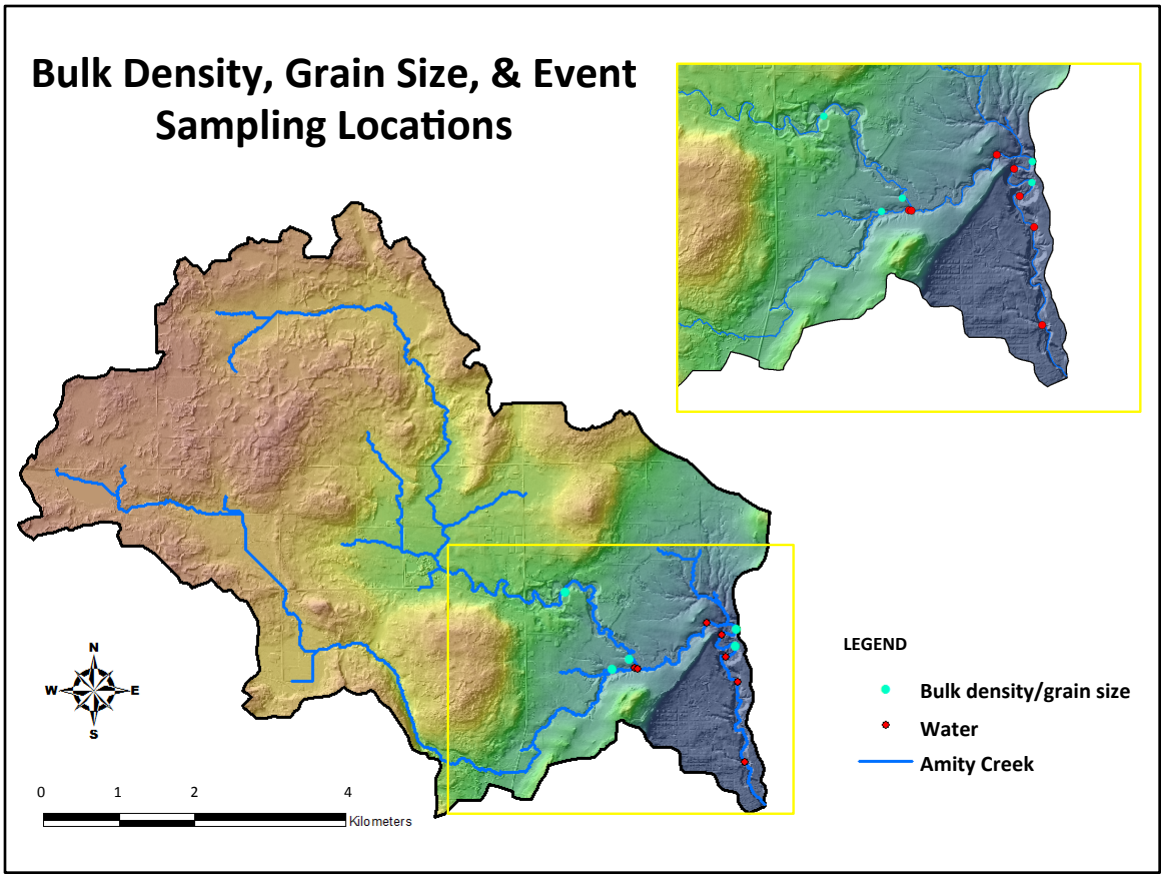

Figure 4.3: Locations of sediment samples and water samples within the Amity Creek watershed.

5.0 Error Validation

TLS technology provides a means for detecting high-resolution change in topographic features not possible with more traditional techniques such as GPS or total station instruments. However, errors in data collection and post-processing do exist and must be taken into consideration when analyzing results. Sources of uncertainty with TLS include instrument/mechanical errors, error in aligning scans comprising a single campaign, error in aligning successive TLS campaigns, error in creating a TIN, error in removing erroneous points (i.e. vegetation), and errors associated with calculating erosional/depositional volumes (Day et al., 2012).

The timescale associated with this project was fairly short from a geomorphological perspective. Consequently, one concern in experimental design was that we would see little change in the study bluffs over the year or so that scans were conducted. Our goal was to capture change related to individual events, and it was imperative that errors in our methodology did not exceed the signal. Fortunately, the Amity Creek watershed experienced multiple large precipitation events, resulting in significant erosion of the study bluffs and providing conclusive evidence that the signal was considerably greater than the noise.

Study sites in this experiment were set-up with the intention of performing error validation in the field using a total station instrument. Survey control points (rebar posts used for total station instrument set-up) were set flush with the ground at each site, typically across the stream from the surface of interest. A Trimble S6 total station was then used to survey the sphere control points. Surveying in this manner was intended to serve two purposes: (1) establish a local coordinate system that could be applied to control points/spheres in Faro Scene; and (2) provide a means for surveying sphere control points at the end of the experiment to verify that rebar posts remained stationary. However, due to the severe flooding in late June 2012, most survey control points were either lost or buried by sediment deposition.

To confirm the legitimacy of scan alignment (registration) for this study, statistics from Faro Scene's internal Scan Manager were utilized. Scene provides "mean tension" results within the Scan Manager, allowing the user to determine how tight of fit has been achieved in the registration process, whether with individual scans conducted on the same day, and/or successive campaigns carried out over the course of the experiment.

Furthermore, "reference tension" values are also provided, indicating which pairs of control points or reference objects have acceptable fits and which negatively impact the overall mean tension. A mean tension value of zero indicates that a perfect fit has been achieved; the larger the mean tension value, the greater the error in fitting the scans together.

In addition to using Faro Scene to validate scan alignment, a simple experiment was designed which essentially combined all potential uncertainties associated with the instrument and the change detection methodology used in this research. It did not, however, include errors induced by environmental factors such as vegetation, which will be addressed later in this section. To conduct this test, a small box was mounted to a flat, vertical surface. Scans were taken of the surface from multiple angles with and without the box, and the normal post-processing procedure was employed to difference the two campaigns. The calculated volume of erosion (or deposition, depending on how the difference was determined) was 0.069 m^3 after differencing the DEMs, and 0.061 m^3 with a 10 cm threshold applied. These numbers were compared to the actual measured volume of the box, which was 0.052 m^3. The calculated percent errors for these DoDs were 25% and 15%, respectively.

One source of error introduced solely as a result of the change detection methodology used in this experiment involves the angle or perspective from which change is measured. Because the vast majority of stream bluffs lie to the outside of the channel meander, most are concave in shape. Day *et al*. (2012) show that retreat rates can be calculated more accurately when multiple vectors are used to measure change normal to the face of the bluff. As can be seen in Figure 5.1, and depending on the

severity of the curvature, change is overestimated on bluff edges when only one vector is used for analysis. However, results from their experiment suggest that errors introduced when using only one vector – as was the case for our experiment – are comparable to those created when measuring change along multiple vectors (Figure 5.1; table III in Day et al., 2012). Bluffs in this experiment were positioned in Faro Scene; change in DEMs was measured along one vector, approximately normal to the bluff face in the midpoint of the curvature.

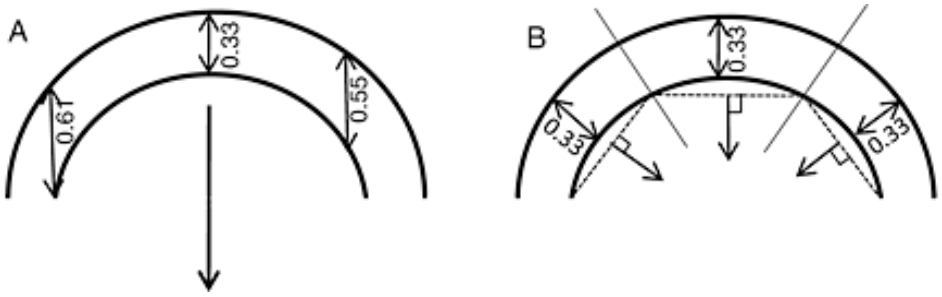

Figure 5.1. (A) If only one vector is used to compare a curved bluff the change on the edges will be overestimated. (B) When the bluff is broken into nearly planar areas, comparisons can be made more accurately. (Day et al., 2012)

When creating a DoD within GCD, the software automatically generates a corresponding summary file, which provides the user with DoD statistics such as total area of erosion/deposition, total volume of erosion/deposition, and both areal and volumetric histograms for each combination of DoD produced. Summary files also list the uncertainty associated with each combination of DoD created, reported as a +/- error volume and corresponding percent error. For this experiment, we assumed a spatially uniform error surface of 0.10 meters in GCD (see methods section). Error volumes are calculated by multiplying the area of the non-thresholded cells by the error surface, resulting in a somewhat conservative estimate of error volume. Most importantly, this

number gives the user an indication of whether or not they have a clear signal of erosion/deposition or an indeterminate sediment budget. Essentially, the greater the signal, the lower the percent error that is typically attributed to the DoD. GCD summary statistics were used as the final step in our error analysis for this experiment.

Vegetation often presents a challenge when using TLS to monitor change in a natural environment. Several studies have investigated the effect that vegetation has on introducing error to various TLS change detection techniques. Coveney and Fotheringham (2011) found vegetation-derived error to be significant in areas having dense ground vegetation, often times inhibiting an accurate representation of the surface of interest even in relatively flat terrain. Day *et al*. (2012) suggest being aggressive in removal of vegetation and other erroneous points. This results in an increased number of holes in the DEM, and therefore, less area over which change can be detected. However, because many holes exist in areas where vegetation was removed from the surface of the bluff, it is also likely that these sections of bluff undergo less change over the short timescales (Day et al., 2012).

Due to the potential error and difficulties associated with vegetation when using TLS to measure geomorphic change, the majority of bluffs in this experiment were selected for analysis based primarily on their lack of vegetative cover (two bluffs were selected for analysis to evaluate the effectiveness of restoration techniques; both of these sites had substantially more ground vegetation than other bluffs). Nonetheless, vegetation was still abundant at certain sites, particularly during late spring and early summer months. To reduce the potential error introduced as a result of vegetation producing a false signal, we were liberal in removing vegetated areas from the dataset.

When generating a DoD, areas with no data (i.e. holes) were excluded from change detection calculations, and thus, error caused by erroneous points was significantly reduced.

6.0 RESULTS

6.1 Bluff Characterization Results

The average bulk density value for soil samples collected at field sites was calculated at 1.426 ± 0.280 g/cm^3 (Table 6.1). Typically, bulk density increases with depth in the soil horizon (USDA, http://soils.usda.gov), and our results generally support this trend. However, samples collected below the surface at site B5 had lower values for both sampling dates.

In order to investigate the effect that freeze-thaw cycling has on soils comprising the bluffs in our experiment, we collected bulk density samples in both early spring and summer months. Presumably, bulk density values would be lower in the spring, especially in samples collected at the bluff surface due to freeze-thaw cycling reducing the granular interlocking structure between soil particles and lessening its resistance to erosional forces (Kok and McCool, 1989; Dietrich and Gallinatti, 1991; Asare et al., 1997; Wynn and Mostaghimi, 2006). However, our calculations showed little trend in values from spring to summer months, with 60% of samples having a lower bulk density in the spring following snowmelt, and 40% having higher values in the spring. Because our bulk density samples showed little seasonal trend, we felt that an average bulk density for the entire dataset could be used to estimate the mass of sediment lost from bluffs throughout the year.

Grain size analyses conducted on samples collected at study bluffs illustrate why excess turbidity plagues the Amity Creek watershed. As can be seen in Table 6.2, the average ratio (percent) of sand, silt, and clay in our samples was approximately 2/28/70, respectively. The high percentage of silt and clay, which account for almost all of the soil texture, have major implications for turbidity – the smaller the particle size, the greater the chance they will be suspended in the water column even at times of relatively low flow. As discussed in the Field Site section of this paper, the Amity Creek watershed is covered in various glacial tills deposited by multiple advancements of the Superior lobe, with very fine-grained lacustrine sediments sourced from Glacial Lake Duluth interspersed in the lower portion of the watershed (Hobbs, 2004; Hobbs, 2009; Hobbs and Breckenridge, 2011) (Figure 3.3). The successive retreat and advancement of the Superior Lobe likely accounts for the differences in the sample textures. Clay content in the samples ranged from 47-90% overall; however, less variability was seen in samples belonging to the same till unit collected in close proximity of one another. For example, clay content in samples collected at sites B5 and B7 (Knife River till; highest clay content among tills in the watershed) ranged from 73-90%.

6.2 TLS/GCD Results

Repeat terrestrial laser scanning was conducted at eight study bluffs throughout this experiment. The net volume of erosion and deposition (net change) and average retreat distance were calculated at four sites spanning approximately one year, while net change and average retreat distance were measured at the remaining four sites over the course of approximately seven months (Tables 6.3, 6.4). Discrepancies in the time period

over which geomorphic change was calculated were due to snowfall in November 2011, prior to all study bluffs being scanned.

Net change and average retreat distance were determined using summary files generated by the GCD software. Table 6.5 summarizes the outputs contained in GCD summary files, which include information such as areas and volumes of erosion and deposition (thresholded and non-thresholded), and the net volume difference. The error or uncertainty associated with our change detection analyses is also included in summary files, and will be discussed later in this section. For purposes of this study, net change (net volume difference) can be defined as the difference between erosion (-) and deposition (+) at a given bluff. Thresholded volumes were used to calculate net change. We also determine average retreat distances, which we calculate by dividing the net change by the area over which change analysis was conducted (see Methods).

In this experiment, erosional and depositional volumes were calculated only for portions of the bluff over which change was measured; if portions of a bluff were removed from the dataset of a given campaign due to thick vegetation, for instance, they were omitted from retreat distance calculations. Retreat distances were determined using the area (m^2) over which change was measured, and therefore, account for the considerable size difference among study bluffs.

There were two large precipitation events that occurred during the experiment – May 23 to May 28 (4.75 in), and June 19 to June 20 (7.25 in) (Western Lake Superior Sanitary District rainfall data provided by MPCA). Both events were captured in our bluff erosion analysis, as each site was scanned before and after these major events. Change was also measured over a period of base flow with no significant precipitation

events (June to November 2012) and over winter and spring melt (November 2011 to April 2012).

For each time period in which geomorphic change was analyzed at a given study site (i.e. for any DoD created), the GCD software generates a colorized change map of the bluff showing the location and retreat (or advancement) distance of any erosion and/or deposition that occurred (red values represent erosion; blue values represent deposition; the darker the tone of color, the greater the amount of erosion/deposition occurring in that time period; grey values represent thresholded regions of the bluff where measured change was below a threshold) (Figure 6.1). These maps also allow for interpretation of the dominant process of erosion at a given study site. Figures 6.2, 6.3, and 6.4 represent three bluffs that we analyzed using GCD software.

Figure 6.2 shows the four time periods over which change detection was completed on Bluff 9, which spans roughly 370 m^2 and is located approximately 3.4 km upstream of the Lester confluence on the main branch of Amity Creek (Figure 4.1). Five scan campaigns were conducted at this site. The November 2011 to April 2012 change map shows a fairly large slump (erosion) in the middle of the bluff face with the material deposited beneath the slump, along the toe. Two smaller such areas can be seen in the lower right side of the image, with the eroded material again deposited along the base of the bluff. Typically, these toe deposits are temporary; these scans capture a moment when fluvial erosion has not yet removed this material. The April to May time period for Bluff 9 is much more depositional in nature, possibly due to material eroded from the very upper portion of the bluff (removed from DoD analysis due to vegetative cover) being deposited on the bluff face. Other possible explanations for the depositional nature

of the time period are decreased bulk density in residual slump deposits or freeze-thaw expansion of the upper soil horizon. However, freeze-thaw expansion exceeding the 0.10 m threshold seems unlikely, making this scenario questionable. Figure 6.2.B shows the slump from the previous time period extended up the face of the bluff, with a line of erosion (scarp) running horizontally through the middle of the bluff. Again, slumped material is deposited directly below the scarp. This time period captured a high flow event in late May (23-28th), and the band of erosion along the toe of the bluff is presumably due to high flows removing the slumped deposit from the previous time period. The May to June time period captured the 500-year flood event, and the GCD image shows a large band of erosion along the bottom half of the bluff, with much of this region retreating ≥2.5 meters. Again, fluvial erosion has removed large quantities of material from the toe of this bluff due to extremely high flows in the few days during and following the flood. The bluff was fairly stable during the June to November time period due to low base flows and little precipitation, with a large portion lying below the threshold (change ≤0.10 m), meaning most change was not discernable from noise in the dataset.

Figure 6.3 shows changes detected in Bluff 20 (83 m^2), located on the East Branch of Amity Creek 7.14 km upstream. Four scan campaigns were conducted at this site, beginning in April 2012. The April to May time period shows a band of erosion along the top of the bluff, with the eroded material deposited along the toe. The bottom left portion of the bluff shows some irregular patterns of erosion and deposition, likely the result of cobbles having been rearranged by the flow or eroded from above. The May to June time period illustrates extreme erosion on the downstream end of the bluff, where

much of the flow was directed during the flood. The right toe of the bluff shows deposition, resulting from material being eroded from directly above. As was the case with Bluff 9, Bluff 20 was very inactive from June (post-flood) to November, when base flow was low.

Geomorphic change that occurred in Bluff 2 (468 m^2) – one of two study sites located on the Lester River in the adjacent watershed – are shown in Figure 6.4. Bluff 2 was hit particularly hard by the June 2012 flooding, resulting in 347 ± 23 m^3 of net sediment loss in the time period from May to June 2012. One factor likely influencing this substantial change is the bluff's large upstream drainage area of just over 9.88 km^2. Four campaigns were conducted at Bluff 2, beginning in early April 2012. The time period from April to late May shows a somewhat random pattern of erosion and deposition. There is a fairly distinct band of erosion that can be seen along the top of the bluff. Much of this material was deposited below, in the middle of the bluff face. Another band of erosion is present on the toe of the bluff, caused by fluvial erosion during high flows resulting from the substantial precipitation in late May. The May to June time period encompasses the flooding, resulting in extreme erosion along the bottom half of the bluff due to fluvial scour. A band of deposition spans the middle of the bluff, which was eroded from above. Small rills appear as vertical lines of erosion in the middle right of the bluff face. The late June to November 2012 time period was very inactive at this study site, with much of the bluff falling below the threshold. Small pockets of erosion span the very top of the bluff, probably a result of over-steepening, which occurred during the unprecedented flow rates reached in the June floods.

Average retreat distances were determined to be negative (i.e. erosional) for three of the four time periods over which change was measured (Table 6.4). Retreat distances were highest from May to June, and averaged -0.41 ± 0.06 m over all of the bluffs. Retreat distances were lowest for the period from June 2012 (post-flood) to November 2012, averaging +0.01 ± 0.01 m over all of the bluffs, meaning geomorphic change occurring in our bluffs during this time was negligible. The Amity watershed experienced minimal precipitation during this time period, and flow rates remained low. Our change detection results reflect this relatively inactive period in the watershed.

The relationship between scaled peak flow rates and average retreat distance can be seen in Figures 6.5 and 6.6. Peak flow rates were scaled based on the upstream drainage area at a given site. Bluffs 2 and 9 experienced the greatest retreat distance, both as a result of the June flood. Scaled peak flow rates were highest spanning the May to June time period, also as a result of the flood. Flow rates were also relatively high for the April to May time period, which captured heavy precipitation received from May 23-28.

Figures 6.7 and 6.8 show the relationship between total scaled flow volume between scan dates and average retreat distance. Total flow volumes were again scaled based on the upstream drainage area. Total flow between scans was greatest from May to June; although the timeframe was short, the extreme flow rates which resulted from the flooding accounted for the highest flow volumes between scans. As was the case with net change, total flow volume was lowest for the time period spanning late June to November. Bluff retreat distance correlated fairly well with flow volume – six of eight

sites experienced significant retreat (≥ -0.25 m) when volume of flow was highest in the May to June time period.

Net change values were highest spanning the time period from May to June, which encompassed the severe flooding of the June storm, and lowest from June to November, when base flow remained low (Table 6.3). The relationship between scaled peak flow and net change is shown in Figures 6.9 and 6.10. The largest net changes in our study bluffs occurred as a result of the June flood; bluffs 2, 7, and 9 lost 347 ± 23 m^3, 141 ± 23 m^3, and 247 ± 26 m^3, respectively. Significant net change was also seen in Bluff 9 during the Nov 2011 to April 2012 time period.

There was little correlation between the number of days spent above a threshold discharge and average retreat distance of our study bluffs. This relationship is shown in Figure 6.11; as indicated, one-third of the bankfull discharge rate was used for the threshold value. The two major precipitation events during this study – 4.75 inches and 7.25 inches, occurring in the April to May and May to June time periods, respectively – accounted for the vast majority of days spent above the threshold flow. The base flow time period (June to November 2012) and over-winter time period (November 2011 to April 2012) had few, if any, days during which the threshold discharge was reached.

6.2.1 Faro Scene/GCD Error Results & Uncertainties

As discussed in the error analysis section of this paper, errors were analyzed at multiple stages in this experiment. Faro Scene software was used to check mean tension values (errors in registration/alignment) in individual scans conducted at a given site on the same day. Scene was also used to validate scan alignment in successive campaigns

collected over the duration of the study. Table 6.6 shows mean tension values for individual scan campaigns (dates) after vegetation was removed and successive campaigns had been registered together. Mean tensions ranged from 0.003 m to 0.076 m for individual campaigns, while site averages fell between 0.006 m and 0.055 m. The average for individual time periods remained consistent (~0.02 m), indicating that vegetation removal in Scene had little effect on how well successive campaigns were merged together. The standard deviation in reference tension between objects used to align scans (sphere control points and manually-generated control points at sites where rebar were destroyed post-flood) is also reported in Table 6.6, averaging 0.026 m overall.

The last stage in our error analysis for this study utilized summary files generated by the GCD software (see Methods sections 4.1.2C; see Error Analysis 5.0). The thresholded area of erosion/deposition and spatially uniform error surface (i.e. threshold of 0.10 m) were used to calculate ± error volumes and subsequent percent errors. Table 6.7 and 6.8 show the calculated error volumes and percent error for net change (net volume difference) and average retreat distances at our study sites for each time period over which change was measured. Error distances ranged between ± 0.01 and 0.08 m. The percent error associated with these distances ranged from 15-185%; percent error was lowest from May to June when retreat distances were greatest. Conversely, percent error was highest from June to November when change was negligible. The average percent error for sites measured for a year (Nov 2011 to Nov 2012) was 15%; sites measured from April to November had an average percent error of 12%. Period averages for net change and associated uncertainties were not calculated since these numbers do not account for bluff area. Results for individual bluff GCD summary files for each scan

date are shown in Appendix C, and include additional data such as thresholded and non-thresholded areas and volumes of erosion and deposition, ± error volume associated with volume of erosion and deposition, and percent error for volumes of erosion and deposition.

6.3 Extrapolating Results

In order to determine the effect that bluff erosion has on the turbidity impairment of Amity Creek, we extrapolated our TLS/GCD results to the entire watershed. To extrapolate, we combined data from various phases of our experiment including: areal statistics from our field inventory of unvegetated bluffs; retreat distance measurements from GCD analyses; and values from our bulk density and grain size analyses.

The total area of the Amity LiDAR study bluffs was calculated to be 656 m^2, while the total area of the other unvegetated bluffs from our field inventory was 4,940 m^2; the total area of unvegetated bluffs in the watershed was 5,596 m^2 (Table 6.9). Using the average retreat rate of 0.50 m/yr, we estimated the total volume of sediment eroded from bluffs to be 2,798 m^3. This average retreat rate was determined from our four study bluffs that were scanned over an entire year, and appeared to represent an appropriate average of all our sites. To account for larger particles contained in the bluff sediment (i.e. anything larger than coarse sand), which were removed from grain size samples prepared for the laser diffractometer, we used an estimate of 10%. After reducing the total sediment volume by 10%, we calculated a total volume of 2,518 m^3 of fine particles eroded from unvegetated bluffs in the watershed. We converted this volume of sediment to a mass by multiplying by our average bulk density of 1430 kg/m^3, giving us 3,601,000

kg of fine sediment lost as a result of bluff erosion. However, turbidity is a measurement of water clarity, and thus, we are concerned with particles that are often suspended in the water column even during times of relatively flow. Because of this, we multiplied our total fine sediment load by the average percentage of silt and clay (98%), calculated from our grain size analysis results, in order to compare our estimated loads with TSS loads. Our total fine sediment load estimate from bluff erosion in the Amity watershed was 3,532,000 kg. Table 6.10 shows annual TSS load estimates from the North Shore Stream Monitoring Program, and NRRI estimates using continuous in-stream turbidity data as a surrogate for TSS (Ruzycki et al., in press). We compared our total 2012 load estimate with those from the MPCA and NRRI and reported the percent increase in Table 6.10. Our estimated TSS load for 2012 was anywhere from 151% to 3,397% greater than MPCA/NRRI values, a definite result of the extreme flooding that occurred in late June 2012.

6.3.1 Estimating Load from June Flood

Clearly, the flood of June 2012 had a substantial impact on our GCD volume calculations, and in turn, affected our 2012 load estimates. Bluff erosion is temporally variable; retreat rates are not uniform throughout the year, and our numbers show that individual events – especially the June flood – account for a large percentage of the total mass of sediment being eroded from bluffs in the watershed. In order to estimate the mass of sediment removed from Amity Creek bluffs during the flood, we multiplied our average retreat distance for that time period (0.41 m of erosion) by the total area of unvegetated bluffs in the watershed, giving us a volume of 2,294 m^3. After accounting

for particles larger than sand – estimated to be 10% of the sediment composing the Amity bluffs – we were left with a total volume of 2,065 m^3. Again, we used our average bulk density value to turn this volume into a mass of sediment. After multiplying the mass by the average percentage of silt and clay, we estimated a total load of 2,896,000 kg of fine sediment removed from Amity bluffs in the June flood. This number accounts for 82% of the total load for the year. When the flood load is removed from our total bluff erosion load for 2012, our annual total becomes 636,000 kg, much closer to annual loads estimated by the MCPA from 2001 to 2006.

6.4 Event Sampling Results

By incorporating an increasing number of bluffs into water samples collected along the creek, we intended to investigate the extent to which bluffs affect turbidity levels in the Amity watershed. Water samples were collected along the lower reaches of Amity Creek during/following precipitation events on May 24th and June 14th, 2012. Both sets of samples show increasing Suspended Sediment Concentrations moving in a downstream direction in the watershed (Table 6.11). For example, the samples with the highest concentration of suspended sediments were collected at Bridge 1 (May 24) and Bridge 3 (June 14), which are the farthest downstream sites. Evidence from our GCD analyses suggest that bluffs contribute large quantities of sediment to the channel; therefore, increases in the concentration of suspended sediment in our samples is likely the result of bluff erosion rather than an increase in discharge as you move downstream

in the watershed. Surprisingly, samples collected immediately downstream of the East/West confluence did not show a large increase in the concentration of suspended sediments when compared with those taken just upstream on the West Branch.

Table 6.1: Amity Creek Bulk Density Sampling

	Bulk density (grams/mL)	
Site/Sample	Summer 2012	Spring 2013
B5A[a]	1.143	1.767
B5B[b]	1.083	1.022
B9A[a]	1.290	1.653
B9B[b]	1.774	1.627
B14A[a]	1.108	0.967
B14B[b]	1.876	1.471
B15A[a]	1.186	1.417
B15B[b]	1.345	1.485
B20A[a]	1.686	1.614
B20B[b]	1.701	1.312
Average	1.419	1.434
Overall Average	1.426	
Standard Deviation	0.280	

[a]Sample collected at surface

[b]Sample collected 30-40 cm deep

Table 6.2: Amity Creek Grain Size Analysis

Sample #	% Sand	% Silt	% Clay	% Silt/Clay
B5-1	1.1	29.9	69.1	98.9
B5-2	1.0	29.8	69.2	99.1
B5-3	0.9	29.7	69.4	99.1
B5-4	1.3	21.4	77.3	98.7
B5-5	1.1	21.3	77.6	98.9
B5-6	1.0	21.1	77.8	99.0
B9-1	0.0	5.8	94.3	100.0
B9-2	0.0	5.7	94.3	100.0
B9-3	0.0	5.7	94.3	100.0
B9-4	0.0	17.1	82.9	100.0
B9-5	0.0	17.0	83.0	100.0
B9-6	0.0	17.0	83.0	100.0
B14-1	3.6	49.0	47.4	96.4
B14-2	3.5	49.0	47.6	96.5
B14-3	3.4	48.9	47.7	96.6
B14-4	3.5	49.2	47.3	96.5
B14-5	3.3	49.2	47.5	96.7
B14-6	3.3	49.1	47.6	96.7
B15-1	7.4	38.6	54.0	92.6
B15-2	7.2	38.5	54.3	92.8
B15-3	7.2	38.5	54.3	92.8
B15-4	2.4	30.9	66.7	97.6
B15-5	2.3	30.8	66.9	97.7
B15-6	2.3	30.8	67.0	97.7
B20-1	0.0	12.6	87.4	100.0
B20-2	0.0	12.6	87.4	100.0
B20-3	0.0	12.6	87.4	100.0
B20-4	0.7	31.3	68.0	99.3
B20-5	0.6	31.3	68.1	99.4
B20-6	0.7	31.3	68.1	99.4
Average	1.9	28.5	69.6	98.1

Table 6.3: DoDs -- Net Change with 10cm threshold applied (m3)

Site #	Nov 2011 to Apr 2012	Apr to May 2012	May to June 2012	June to Nov 2012	Nov 2011 to Nov 2012	Apr to Nov 2012
B9*	-83.45	32.18	-247.40	10.43	-288.73	N/A
B12	-7.13	1.52	-1.03	-0.02	-2.91	N/A
B13	-10.51	-2.17	-3.49	0.04	-17.69	N/A
B14*	N/A	0.31	-7.71	0.78	N/A	-19.43
B15*	-1.45	-6.18	-6.43	0.35	-10.32	N/A
B20*	N/A	-4.58	-27.33	0.24	N/A	-23.37
B2	N/A	-23.28	-347.46	-0.89	N/A	-382.20
B7	N/A	-10.03	-140.55	-7.92	N/A	-297.22

* indicates bulk density & grain size sample collected/analyzed

Table 6.4: Average Retreat Distances (m)

Site #	Nov 2011 to Apr 2012 (1)	Apr to May 2012 (2)	May to June 2012 (3)	June to Nov 2012 (4)	Nov 2011 to Nov 2012	Apr to Nov 2012
B9	-0.25	0.10	-0.86	0.03	-0.91	N/A
B12	-0.32	0.09	-0.05	0.00	-0.13	N/A
B13	-0.25	-0.05	-0.08	0.00	-0.42	N/A
B14	N/A	0.01	-0.47	0.02	N/A	-0.25
B15	-0.06	-0.24	-0.26	0.01	-0.50	N/A
B20	N/A	-0.07	-0.44	0.00	N/A	-0.37
B2	N/A	-0.05	-0.84	0.00	N/A	-0.89
B7	N/A	-0.02	-0.30	-0.01	N/A	-0.51
Period Average	-0.22	-0.03	-0.41	0.01	-0.49	-0.50

Table 6.5: GCD Outputs Summary

GCD Output:	Description:
Total Area of Erosion (m^2)	Total area of cells having negative change
Total Thresholded Area of Erosion (m^2)	Total area of cells having negative change > 0.10 m
Total Area of Deposition (m^2)	Total area of cells having positive change
Total Thresholded Area of Deposition (m^2)	Total area of cells having positive change > 0.10 m
Total Volume of Erosion (m^3)	Total volume of cells having negative change
Total Thresholded Volume of Erosion (m^3)	Total volume of cells having negative change > 0.10 m
Total Volume of Deposition (m^3)	Total volume of cells having positive change
Total Thresholded Volume of Deposition (m^3)	Total volume of cells having positive change > 0.10 m
Total Net Volume Difference (m^3)	Net volume difference among all cells
Total Thresholded Net Volume Difference (m^3)	Net volume difference among all cells having > 0.10 m of change
+/- Error Volume (total volume of erosion)	Thresholded total area of erosion ÷ spatially uniform error surface (0.10 m)
+/- Error Volume (total volume of deposition)	Thresholded total area of deposition ÷ spatially uniform error surface (0.10 m)
+/- Error Volume (total net volume difference)	Thresholded total area of change ÷ spatially uniform error surface (0.10 m)
% Error (total volume of erosion)	+/- Error Volume ÷ Thresholded volume of erosion
% Error (total volume of deposition)	+/- Error Volume ÷ Thresholded volume of deposition
% Error (total net volume difference)	+/- Error Volume ÷ Thresholded net volume difference (net change)

Table 6.6: Faro Scene Scan Manager Mean Tension Results (m) and Standard Deviation

Site #	November, 2011	April, 2012	May, 2012	June, 2012	November, 2012	Site Average	Standard Deviation
B9	0.019	0.054	0.042	0.011	0.011	0.027	0.044
B12	0.003	0.003	0.004	0.011	0.012	0.006	0.011
B13	0.015	0.009	0.016	0.023	0.018	0.016	0.019
B14	NO SCAN	0.009	0.009	0.009	0.007	0.008	0.008
B15	0.045	0.076	0.050	0.061	0.044	0.055	0.050
B20	NO SCAN	0.010	0.017	0.016	0.017	0.015	0.019
B2	NO SCAN	0.006	0.013	0.032	0.017	0.017	0.035
B7	NO SCAN	0.021	0.019	0.016	0.015	0.017	0.022
Time Period Average	0.020	0.024	0.021	0.022	0.017		
Average Standard Deviation							0.026

Table 6.7: DoDs -- Net Change & Associated Uncertainties (10 cm threshold applied)

	Nov 2011 to Apr 2012			Apr to May 2012			May to June 2012		
Site #	Net Change (m^3)	± Error (m^3)	% Error	Net Change (m^3)	± Error (m^3)	% Error	Net Change (m^3)	± Error (m^3)	% Error
B9	-83.45	31.10	37%	32.18	14.45	45%	-247.40	25.96	10%
B12	-7.13	1.84	26%	1.52	0.05	3%	-1.03	0.33	31%
B13	-10.51	4.03	38%	-2.17	1.25	58%	-3.49	3.27	94%
B14	N/A	N/A	N/A	0.31	0.01	4%	-7.71	1.27	17%
B15	-1.45	0.80	56%	-6.18	2.25	37%	-6.43	1.97	31%
B20	N/A	N/A	N/A	-4.58	1.51	33%	-27.33	3.32	12%
B2	N/A	N/A	N/A	-23.28	12.65	54%	-347.46	23.46	7%
B7	N/A	N/A	N/A	-10.03	4.06	40%	-140.55	23.24	17%

	June to Nov 2012			Nov 2011 to Nov 2012			Apr to Nov 2012		
Site #	Net Change (m^3)	± Error (m^3)	% Error	Net Change (m^3)	± Error (m^3)	% Error	Net Change (m^3)	± Error (m^3)	% Error
B9	10.43	7.99	77%	-288.73	29.33	10%	N/A	N/A	N/A
B12	-0.02	0.29	1456%	-2.91	0.10	3%	N/A	N/A	N/A
B13	0.04	0.03	80%	-17.69	4.17	24%	N/A	N/A	N/A
B14	0.78	0.02	3%	N/A	N/A	N/A	-19.43	3.40	17%
B15	0.35	0.16	46%	-10.32	2.02	20%	N/A	N/A	N/A
B20	0.24	0.01	4%	N/A	N/A	N/A	-23.37	2.78	12%
B2	-0.89	0.82	93%	N/A	N/A	N/A	-382.20	28.38	7%
B7	-7.92	34.66	438%	N/A	N/A	N/A	-297.22	45.96	15%

Table 6.8: Average Retreat Distances & Associated Uncertainties

	Nov 2011 to Apr 2012			Apr to May 2012			May to June 2012		
Site #	Retreat Distance (m)	± Error (m)	% Error	Retreat Distance (m)	± Error (m)	% Error	Retreat Distance (m)	± Error (m)	% Error
B9	-0.25	0.09	37%	0.10	0.05	45%	-0.86	0.09	10%
B12	-0.32	0.08	26%	0.09	0.00	3%	-0.05	0.02	32%
B13	-0.25	0.09	38%	-0.05	0.03	58%	-0.08	0.08	94%
B14	N/A	N/A	N/A	0.01	0.00	3%	-0.47	0.08	16%
B15	-0.06	0.03	55%	-0.24	0.09	36%	-0.26	0.08	31%
B20	N/A	N/A	N/A	-0.07	0.02	33%	-0.44	0.05	12%
B2	N/A	N/A	N/A	-0.05	0.03	54%	-0.84	0.06	7%
B7	N/A	N/A	N/A	-0.02	0.01	40%	-0.30	0.05	17%
Average	-0.22	0.08	35%	-0.03	0.03	98%	-0.41	0.06	15%

	June to Nov 2012			Nov 2011 to Nov 2012			Apr to Nov 2012		
Site #	Retreat Distance (m)	± Error (m)	% Error	Retreat Distance (m)	± Error (m)	% Error	Retreat Distance (m)	± Error (m)	% Error
B9	0.03	0.03	77%	-0.91	0.09	10%	N/A	N/A	N/A
B12	0.00	0.01	1450%	-0.13	0.00	3%	N/A	N/A	N/A
B13	0.00	0.00	75%	-0.42	0.10	24%	N/A	N/A	N/A
B14	0.02	0.00	3%	N/A	N/A	N/A	-0.25	0.04	17%
B15	0.01	0.01	46%	-0.50	0.10	20%	N/A	N/A	N/A
B20	0.00	0.00	4%	N/A	N/A	N/A	-0.37	0.04	12%
B2	0.00	0.00	92%	N/A	N/A	N/A	-0.89	0.07	7%
B7	-0.01	0.06	438%	N/A	N/A	N/A	-0.51	0.08	15%
Average	0.01	0.01	185%	-0.49	0.07	15%	-0.50	0.06	12%

Table 6.9: Amity Creek Total Bluff Area (un-vegetated)

Study Bluffs:	Height	Length	% Un-vegetated	Total area (m^2)
B9	N/A	N/A	N/A	370
B12	N/A	N/A	N/A	36
B13	N/A	N/A	N/A	45
B14	N/A	N/A	N/A	91
B15	N/A	N/A	N/A	32
B20	N/A	N/A	N/A	83
Study Bluff Total	N/A	N/A	N/A	656
Field Inventory:	Height	Length	% Un-vegetated	Total area (m^2)
1	2	12	60	14
2	2.5	38	50	48
3	2	43	75	65
4	2.5	35	30	26
5	5	58	30	87
6	20	100	60	1,200
7	13	120	75	1,170
8	22	30	85	561
9	13	52	35	237
10	5	63	95	299
11	2	10	75	15
12	3.5	45	60	95
13	3.5	60	60	126
14	2.5	30	95	71
15	3	30	65	59
16	3.5	15	65	34
17	2.5	18	40	18
18	4.5	20	65	59
19	1.8	22	60	24
20	3.5	38	70	93
21	5.5	5	80	22
22	4.5	22	80	79
23	3.5	15	80	42
24	3.5	38	60	80
25	3.5	45	85	134
26	2	10	65	13
27	7	30	50	105
28	4	15	65	39
29	8	23	40	74
30	3.5	15	25	13
31	5	40	20	40
Inventory Total				4,940
TOTAL				**5,596**

Table 6.10: Amity Creek TLS/GCD TSS Load Estimates (kg)

Year	Estimated Load[a]	Estimated Load[b]	2012 % increase (total)
2002	895,000		295%
2003	184,000		1820%
2004	946,000		273%
2005	251,000	117,000	2919%
2006	168,000	101,000	3397%
2007	--	679,000	420%
2008	--	--	--
2009	--	1,044,000	238%
2010	--	1,406,000	151%
2012 Total Estimate:	**3,532,000**		
2012 Flood Estimate:	**2,896,000**		
2012 Total w/out Flood:	**636,000**		

[a] Estimate from MPCA North Shore Stream Monitoring Program (FLUX)

[b] Estimate from NRRI (turbidity surrogate); used to calculate 2012 % increase

* 2005 & 2006 % increase calculated from NRRI data

Table 6.11: Amity Creek Event Sampling Data

Site	Sample site X coordinate:	Sample site Y coordinate:	Distance Upstream (km):	Upstream Area (km^2):	SSC (g/mL) 24 May 2012	SSC (g/mL) 14 June 2012
West Branch	574007	5189591	5.17	1.64	0.00005632	0.00001202
E/W Confluence[a]	574029	5189592	5.15	2.27	0.00007871	0.00001200
Bridge 8	574967	5190172	3.83	3.99	0.00013114	0.00001596
Bridge 6	575149	5190030	3.15	4.46	0.00012038	0.00001816
Bridge 4	575210	5189728	2.45	4.47	0.00013148	0.00002093
Bridge 3	575358	5189387	1.93	4.50	0.00012613	0.00002321
Bridge 1	575469	5188329	0.66	4.62	0.00018012	0.00002104

[a]Sample collected just below confluence

Table 6.12: GCD Area (m2) *Bluff area over which changes were analyzed in GCD

Site #	Nov 2011 to Apr 2012	Apr to May 2012	May to June 2012	June to Nov 2012	Nov 2011 to Nov 2012	Apr to Nov 2012	Total Bluff Area
B9	339.04	318.23	286.87	310.30	317.95	N/A	369.88
B12	22.57	16.81	20.61	25.34	22.28	N/A	36.07
B13	42.57	42.19	42.48	43.02	42.60	N/A	45.1
B14	N/A	23.27	16.29	42.27	N/A	78.45	90.83
B15	22.89	25.82	24.27	24.61	20.61	N/A	31.51
B20	N/A	63.86	62.40	65.68	N/A	62.66	83.16
B2	N/A	447.00	412.03	417.01	N/A	431.48	467.56
B7	N/A	488.05	461.46	626.46	N/A	584.77	736.62

Table 6.13: Field Site Data (**NAD 1983 UTM Zone 15)

Site	Bluff Location X coordinate:	Bluff Location Y coordinate:	Distance Upstream (km):	Upstream Drainage Area (km^2):	Bluff Area (m^2):	Dates Scanned:
$B5^{AM}$*	575354	5189858	2.68	4.47	N/A	N/A
$B9^{AM}$	575350	5190097	3.41	4.46	369.88	11-18-11; 4-30-12; 5-30-12; 6-27-12; 11-3-12
$B12^{AE}$	573879	5189813	5.43	2.26	36.07	11-30-11; 5-2-12; 5-31-12; 6-28-12; 11-7-12
$B13^{AE}$	573923	5189740	5.34	2.26	45.1	11-9-11; 4-12-12; 6-4-12; 6-28-12; 11-7-12
$B14^{AE}$	573950	5189703	5.29	2.27	90.83	4-12-12; 6-7-12; 6-28-12; 11-7-12
$B15^{AW}$	573721	5189568	5.46	1.62	31.51	11-9-11; 5-2-12; 5-31-12; 6-27-12; 11-7-12
$B20^{AE}$	573086	5190594	7.14	2.12	83.16	4-5-12; 5-30-12; 6-25-12; 11-4-12
$B2^{L}$	575754	5189179	1.75	9.88	467.56	4-5-12; 6-5-12; 6-26-12; 11-14-12
$B7^{L}$	576366	5190781	4.11	9.67	736.62	4-30-12; 6-5-12; 6-26-12; 11-14-12

^{A}Amity site; ^{M}Main branch; ^{E}East branch; ^{W}West branch; ^{L}Lester site

* site used only for bulk density sampling and grain size analysis; no GCD analysis completed at this location

Table 6.14: Average Retreat Rates (m/yr)

Site #	Nov 2011 to Apr 2012	Apr to May 2012	May to June 2012	June to Nov 2012	Nov 2011 to Nov 2012	Apr to Nov 2012
B9	-0.55	1.23	-11.24	0.10	-0.95	N/A
B12	-0.75	1.10	-0.63	0.00	-0.14	N/A
B13	-0.59	-0.35	-1.25	0.00	-0.42	N/A
B14	N/A	0.09	-8.23	0.05	N/A	-0.43
B15	-0.15	-2.88	-3.19	0.03	-0.50	N/A
B20	N/A	-0.48	-6.15	0.01	N/A	-0.64
B2	N/A	-0.31	-14.66	-0.01	N/A	-1.45
B7	N/A	-0.21	-5.29	-0.03	N/A	-0.93
Period Average	-0.51	-0.23	-6.33	0.02	-0.50	-0.86

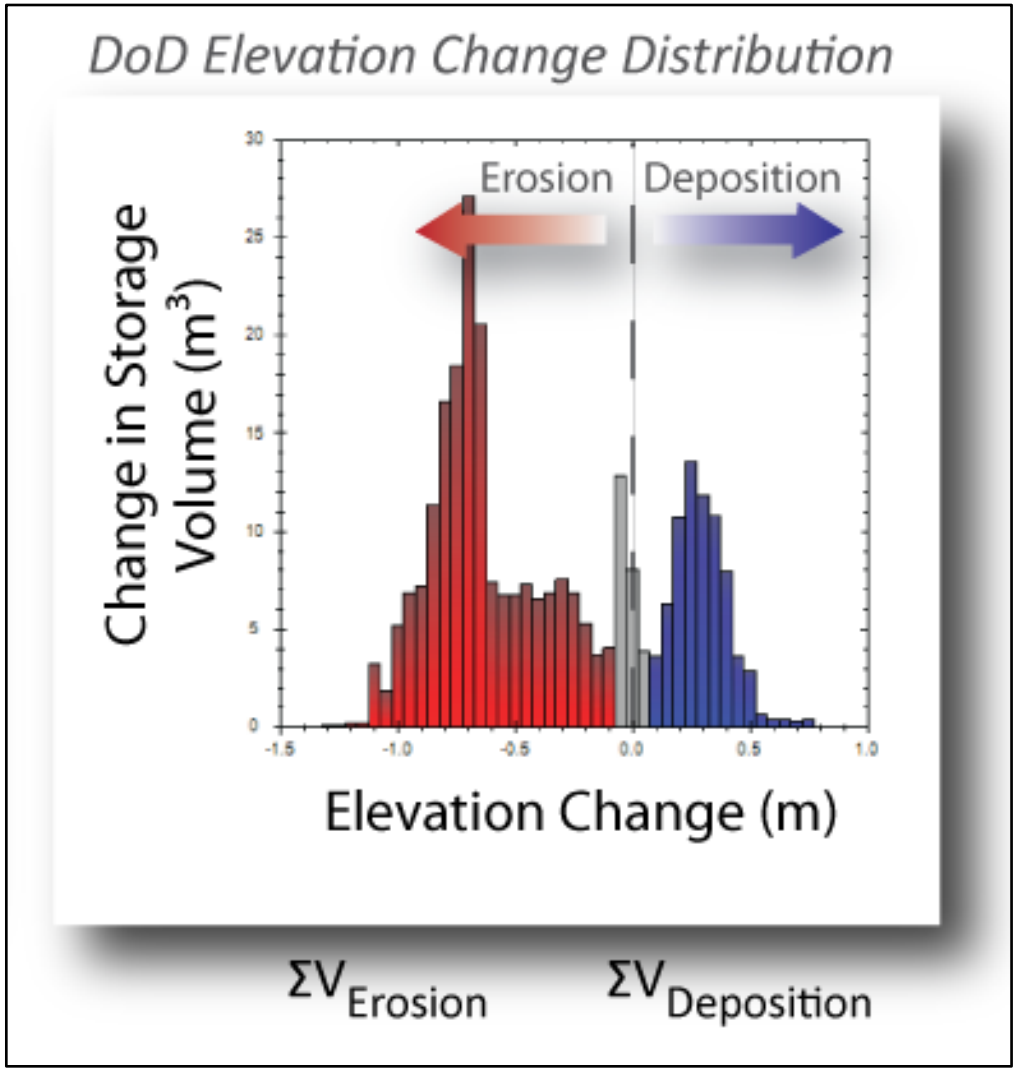

Figure 6.1: DoD histogram showing erosional and deposition volumes.

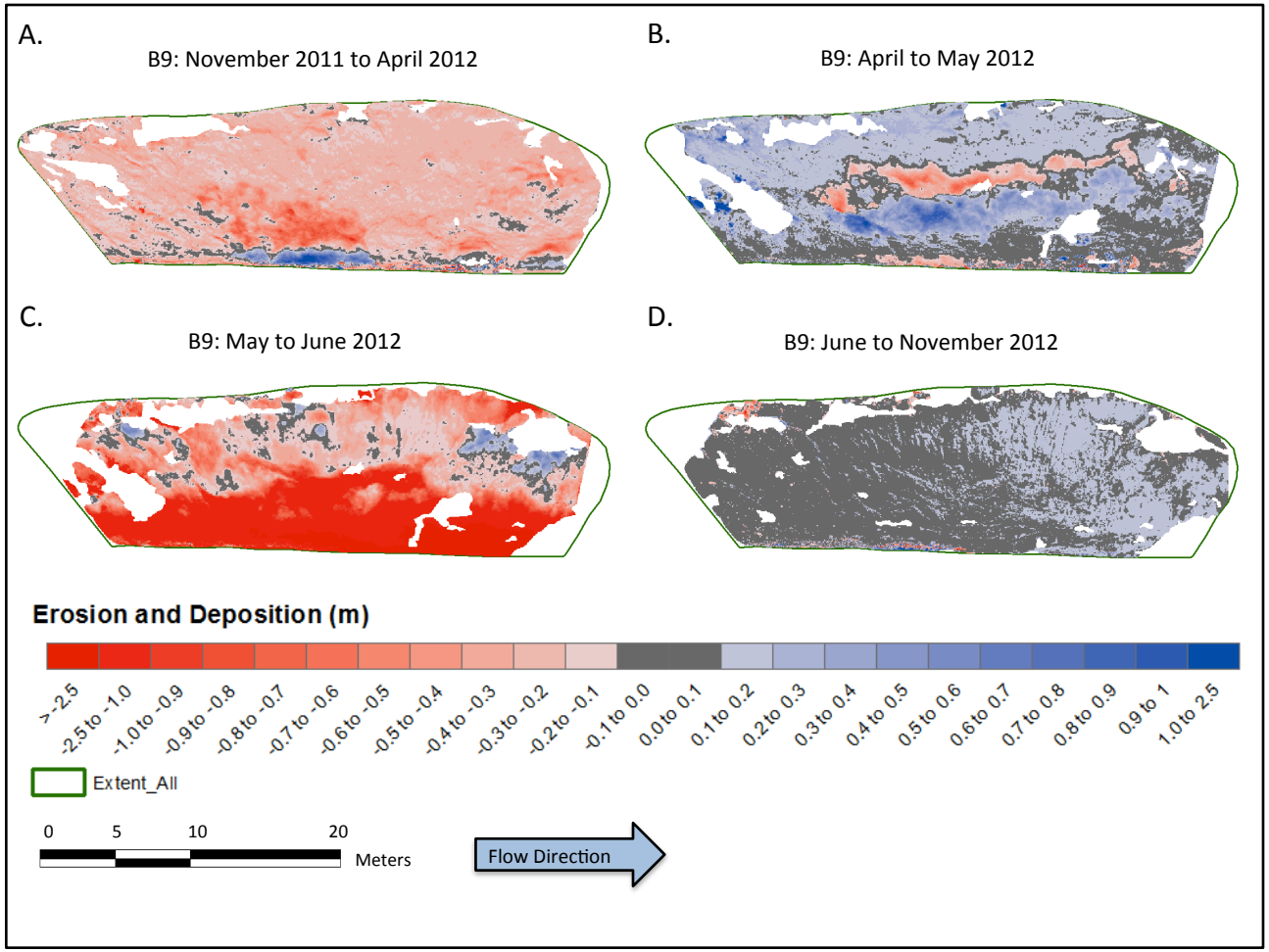

Figure 6.2: Event-scale net change at site B9 (lower main Amity); flow from L to R. (A) November 2011 to April 2012; slump observed in middle of lower face; erosion above, deposition below. (B) April to May 2012; slumping continues further up bluff face; scarp of slump can be observed as band of erosion along middle of face. (C) May to June 2012; extreme erosion following June flood (247m^3 net loss; see Table 6.3); fluvial erosion/undercutting along entire base of bluff. (D) June to November 2012; bluff inactive.

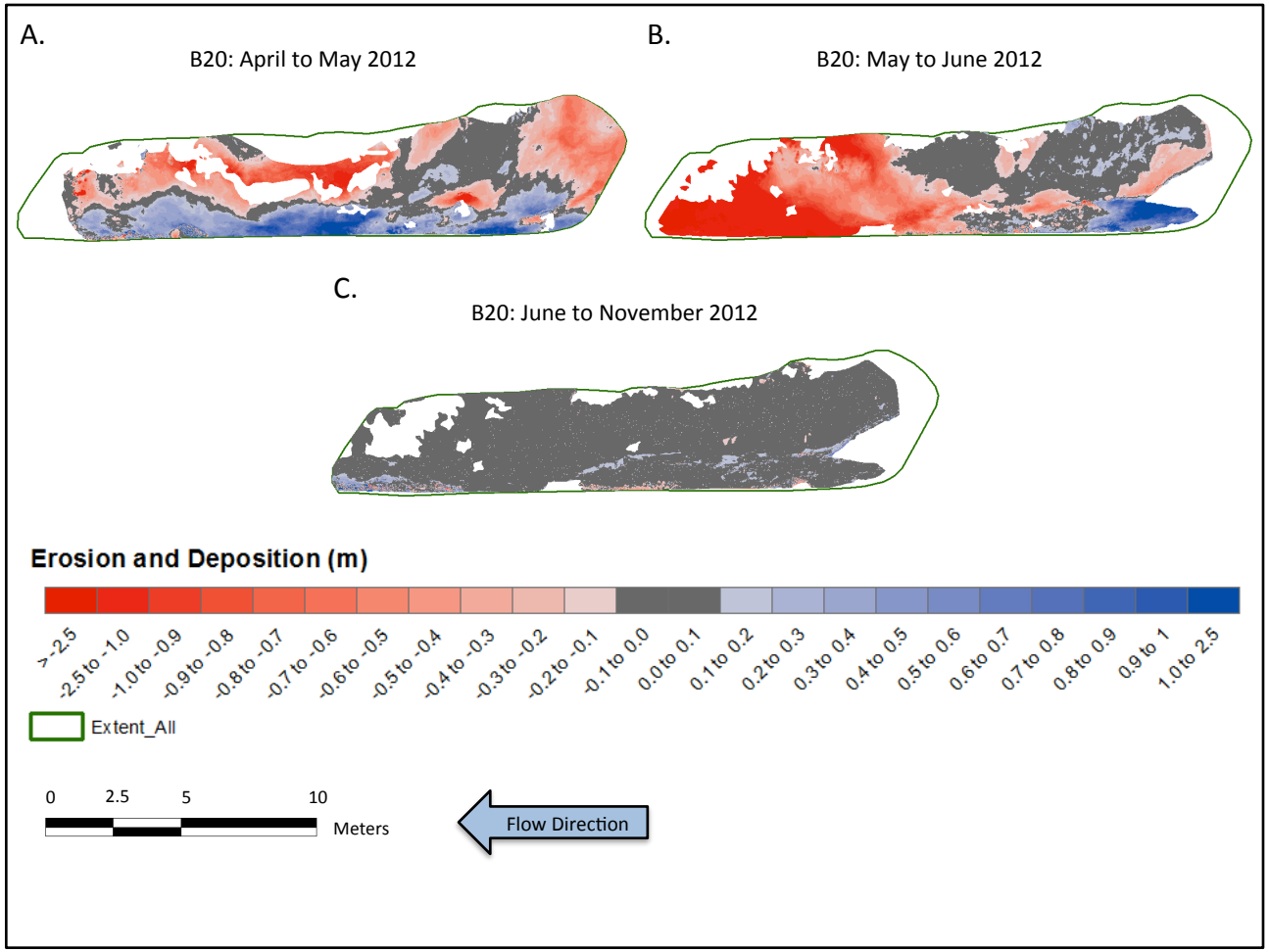

Figure 6.3: Event-scale net change at site B20 (lower East Branch Amity); flow from R to L. (A) April to May 2012; erosion along upper two-thirds of bluff, deposition of eroded material along toe. (B) May to June 2012; extreme erosion on downstream end of bluff following June flood (27m^3 net loss; see Table 6.3). (C) June to November 2012; bluff inactive.

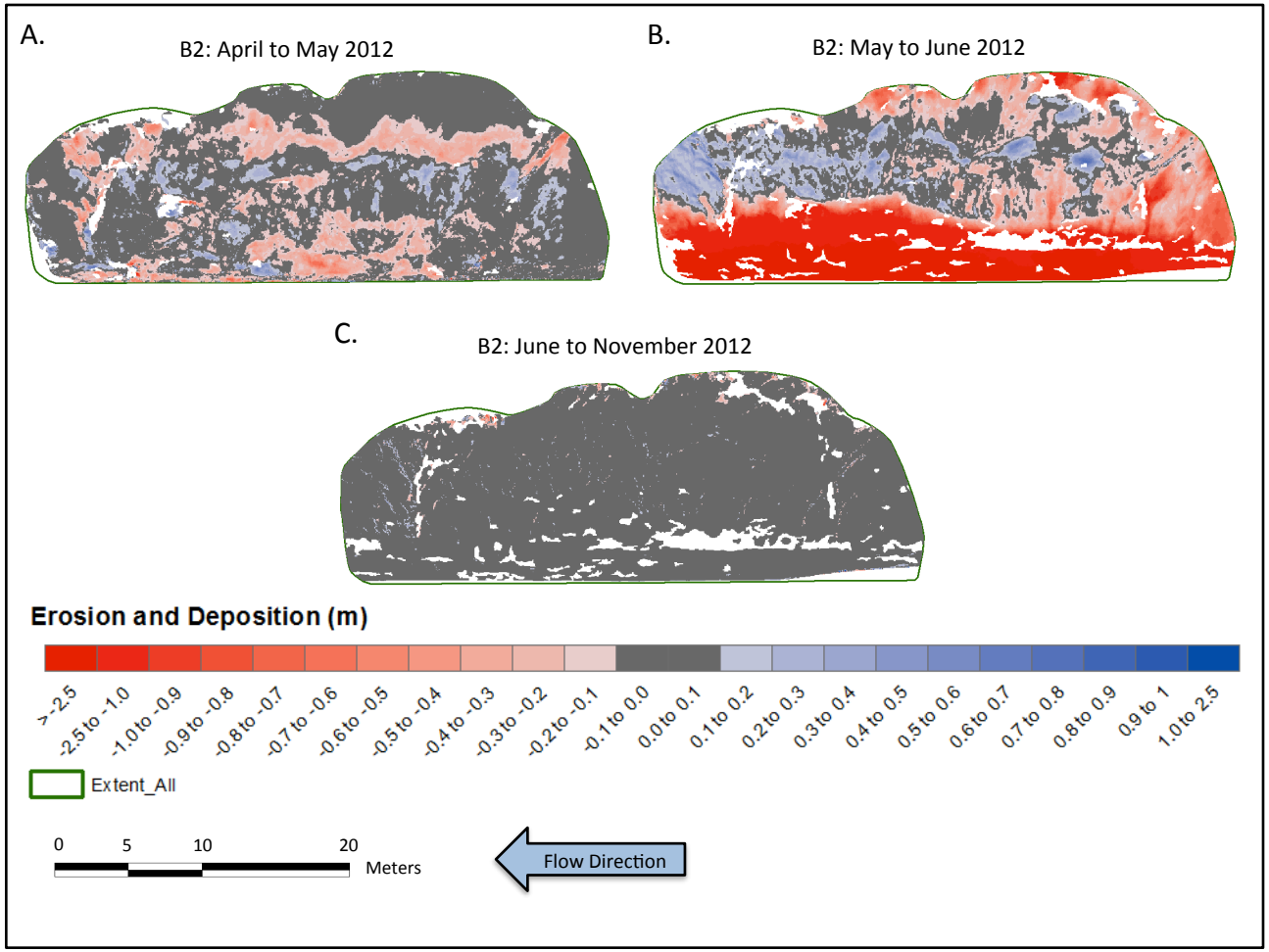

Figure 6.4: Event-scale net change at site B2 (lower Lester); flow from R to L. (A) April to May 2012; band of erosion along upper bluff with a less distinctive band of deposition below; fluvial erosion along base of bluff following heavy precipitation May 23 to 28. (B) May to June 2012; extreme erosion following June flood (347m^3 net loss; see Table 6.3); fluvial erosion/undercutting along entire base of bluff; erosion along most of top of bluff face; some erosion in upper left bluff face, likely due to erosion from above. (C) June to November 2012; bluff inactive.

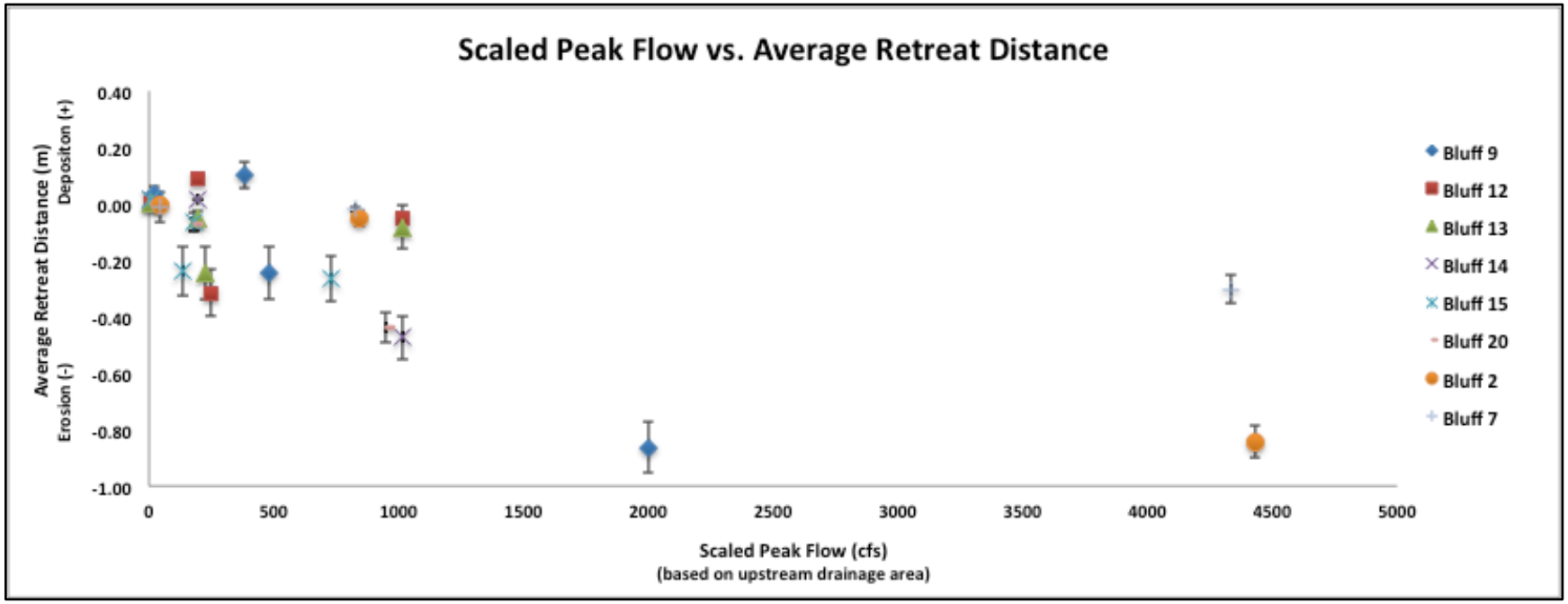

Figure 6.5: Relationship between scaled peak flow and average retreat distance of individual study bluffs.

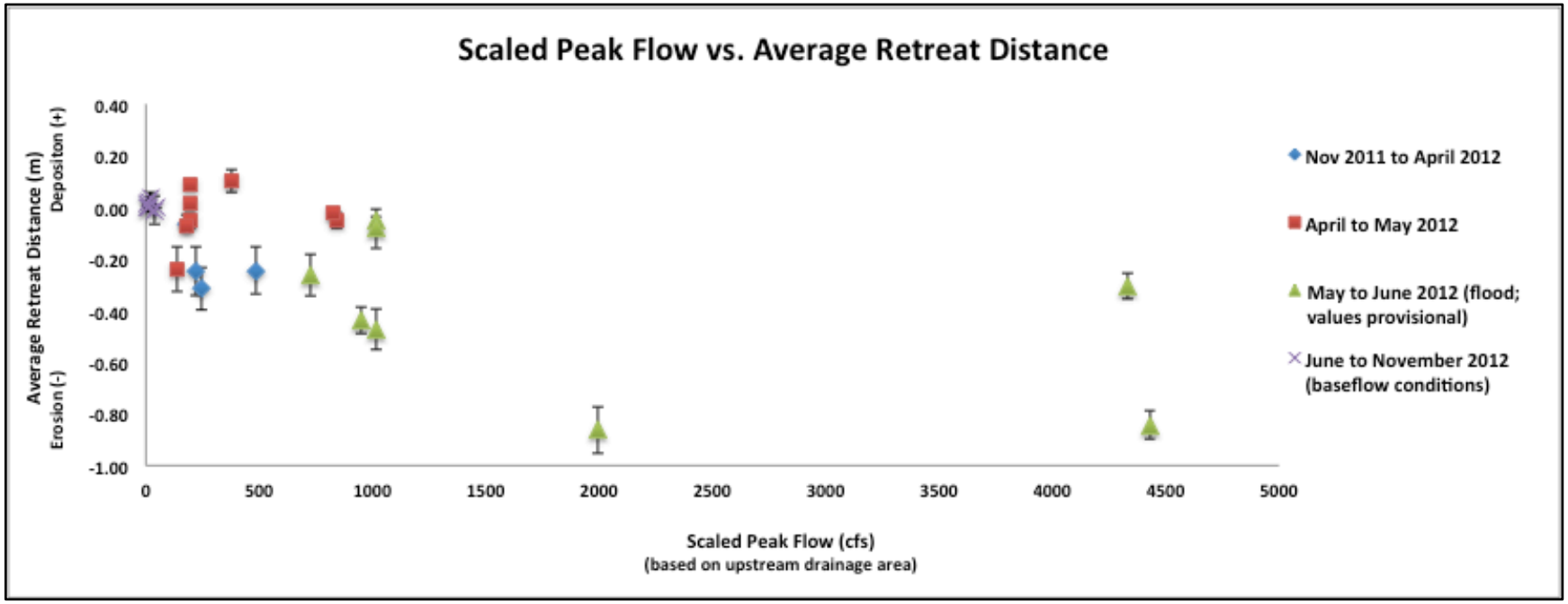

Figure 6.6: Relationship between scaled peak flow and average retreat distance in periods over which change was measured.

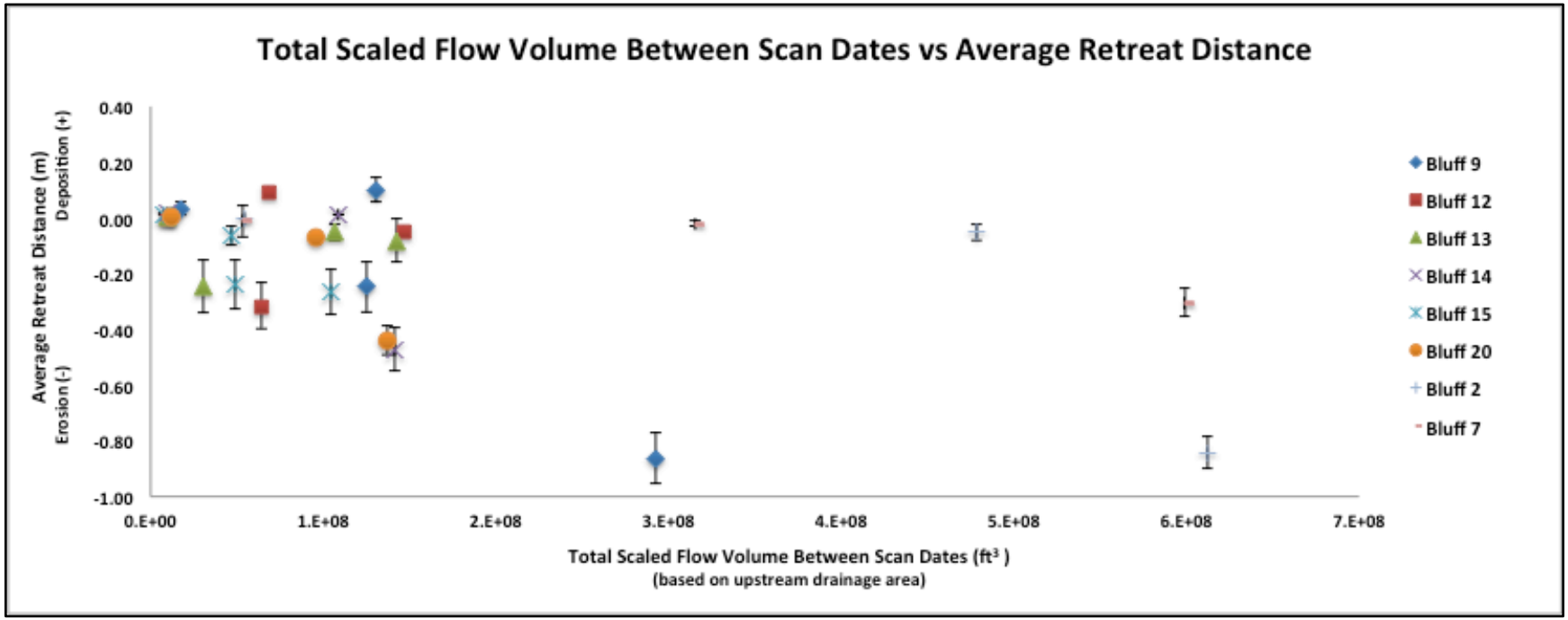

Figure 6.7: Relationship between total scaled flow volume between scan dates and average retreat distance of individual study bluffs.

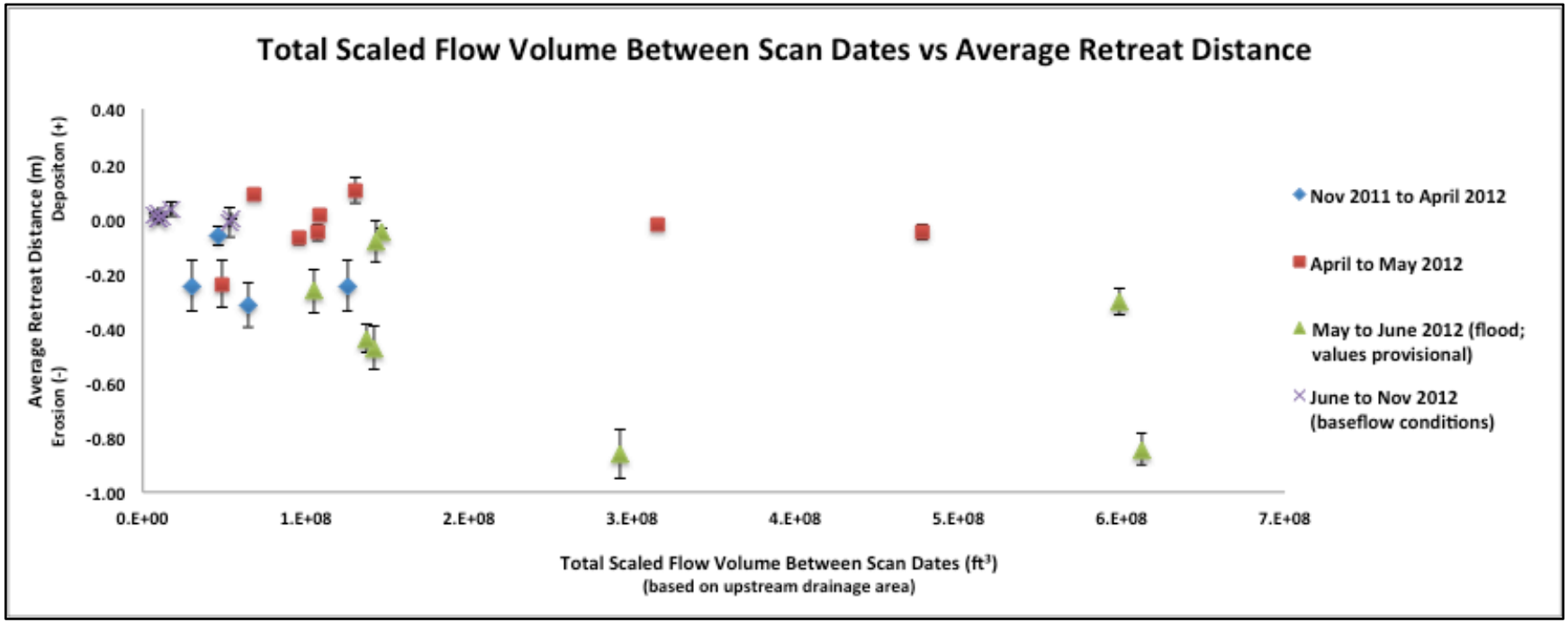

Figure 6.8: Relationship between total scaled flow volume between scan dates and average retreat distance in periods over which change was measured.

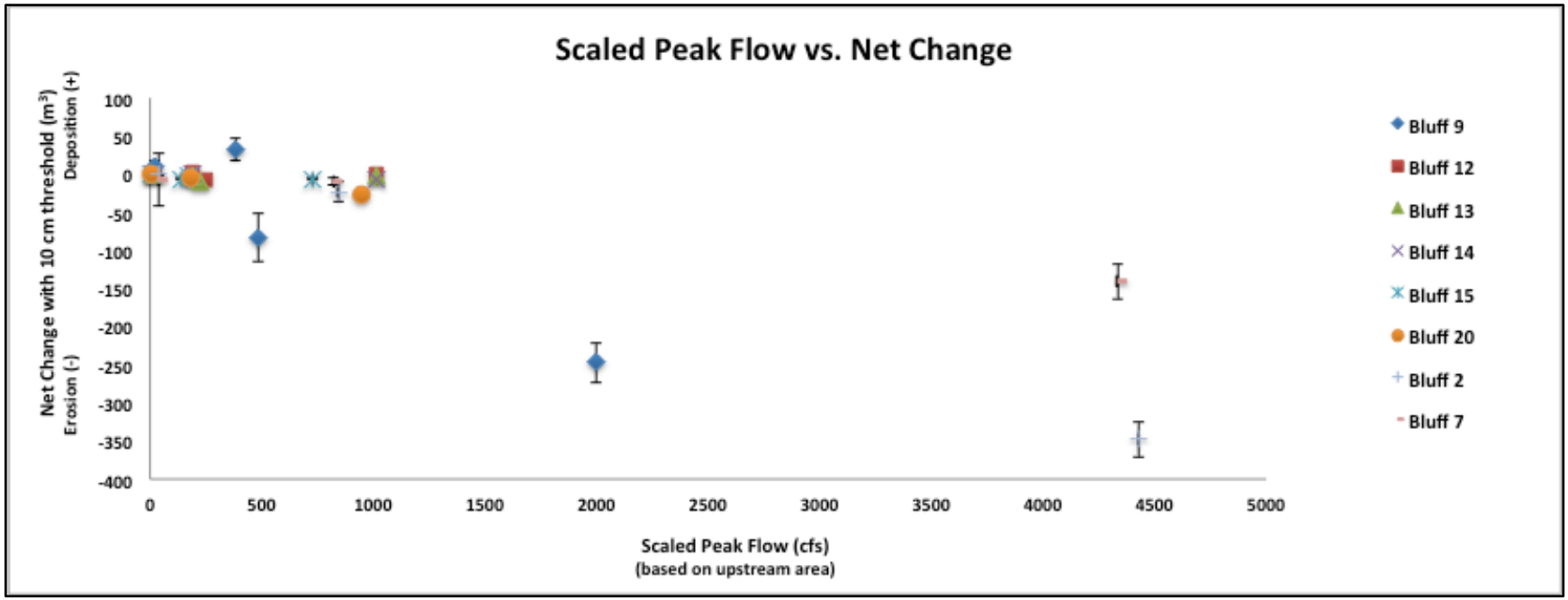

Figure 6.9: Relationship between scaled peak flow and net change of individual study bluffs.

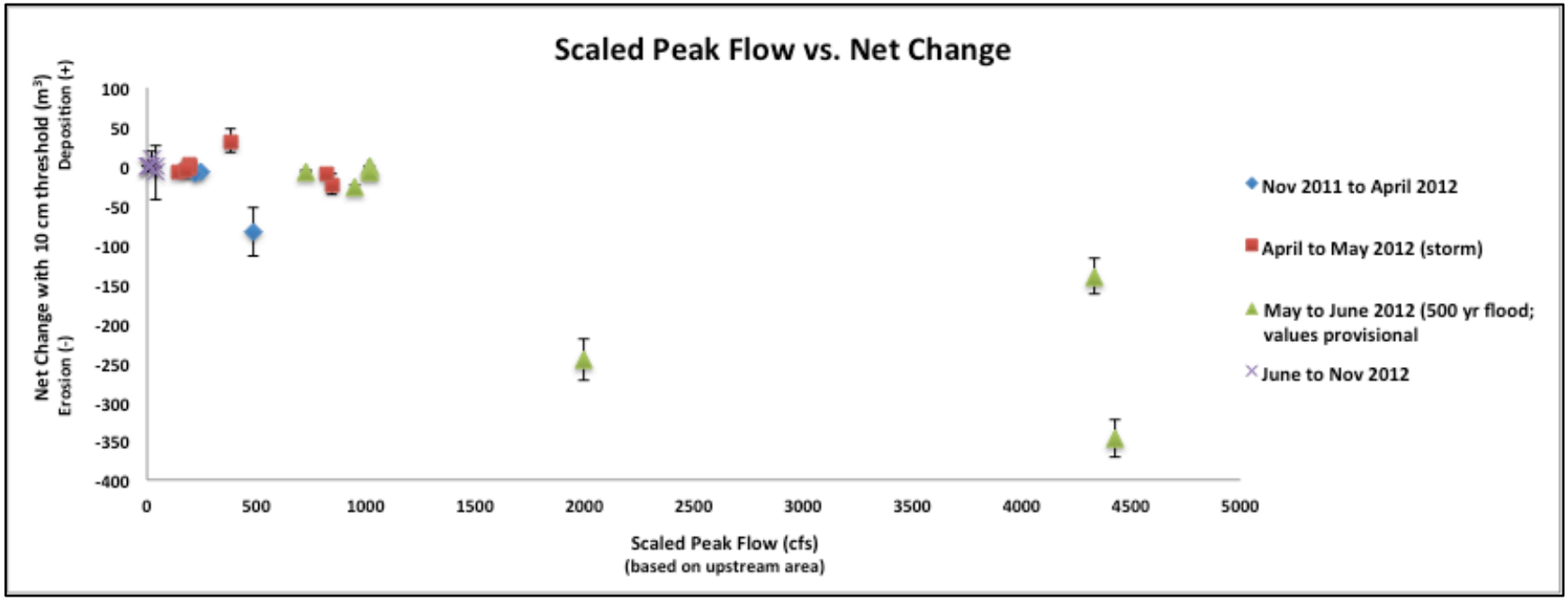

Figure 6.10: Relationship between scaled peak flow and net change in periods over which change was measured.

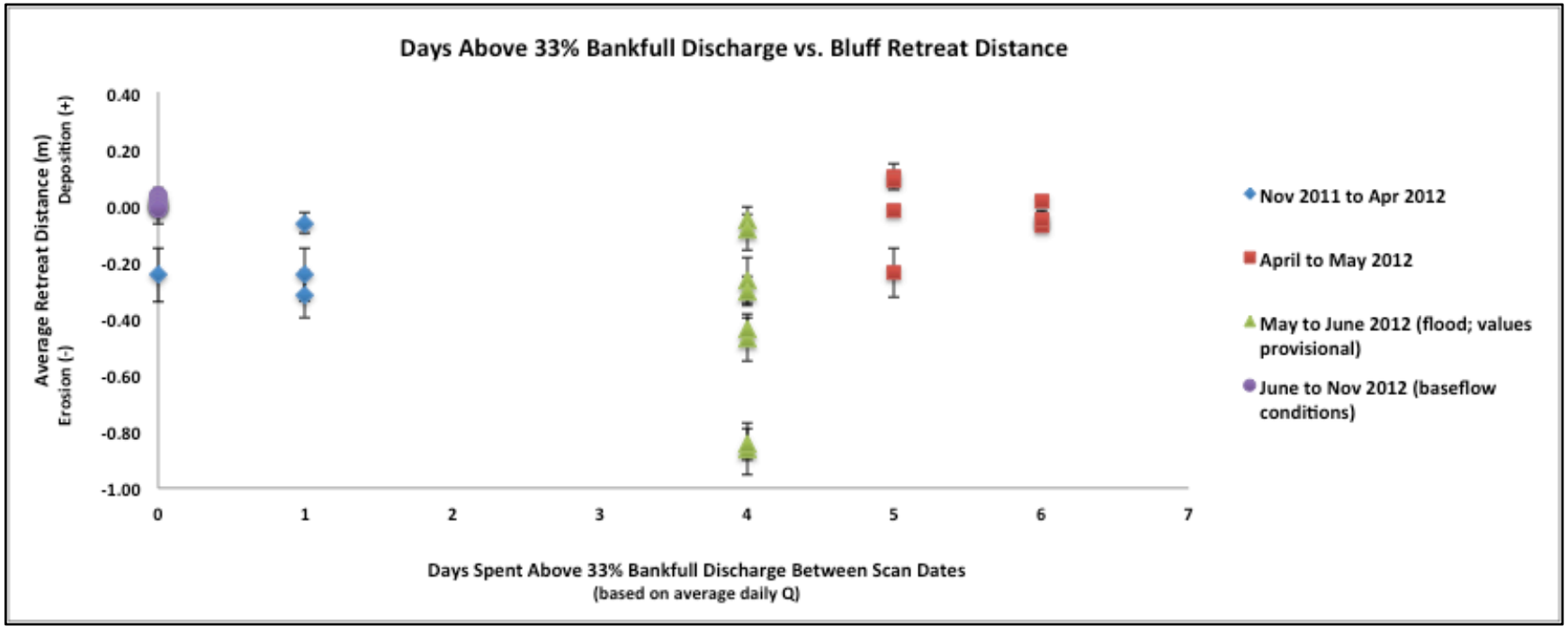

Figure 6.11: Relationship between days spent above one-third bankfull discharge and average retreat distance in periods over which change was measured.

7.0 DISCUSSION & CONCLUSIONS

Large volumes of fine sediments are being eroded from bluffs in the Amity Creek watershed. Bluff retreat distances averaged between +0.01 and -0.41 m for the four periods over which geomorphic change was measured (Table 6.4), with negligible rates of erosion occurring during times of low flows. For example, site B9 had a retreat distance of -0.86 m from May to late June following the flood, but experienced essentially no change (+0.03 m) during the period of low base flow, extending from late June to November 2012. Similarly, site B20 averaged -0.44 m of bluff retreat from late May to late June, yet retreat rates averaged 0.00 m during low base flow. At sites where change was measured over the duration of a year, retreat rates averaged -0.50 m/yr (Table 6.14). Although erosional volumes were greatest during the June flood, results also indicate that processes other than scour during high-flow events influence bluff erosion in the watershed, as average retreat distances from November 2011 to early spring of 2012 were -0.22 m (Table 6.4), at a time when flows remained relatively low.

7.1 Processes Influencing Bluff Erosion

After conducting TLS analyses on our bluffs over the course of this study, it is evident that interactions among multiple processes influence the erosion of stream bluffs in the Amity Creek watershed, which supports previous studies elsewhere (Couper and Maddock, 2001; Wynn and Mostaghimi, 2006; Resop and Hession, 2010; Day et al., 2012, 2013). As discussed in the background section, the dominant processes of bluff erosion are near-surface processes (e.g. freeze-thaw cycling; surface erosion), groundwater-driven processes (e.g. seepage erosion/sapping; high soil moisture

content/high pore water pressure), and fluvial erosion resulting in undercutting or over-steepening. Many of these processes contribute to mass wasting or slumping.

From our data, it is apparent that the largest source of erosion in the watershed was fluvial scour related to high shear stress associated with the 500-year flood in late June 2012, as average retreat distances were at least double those from other time periods (Table 6.4, Figure 6.6). Fluvial erosion at the toe of a stream bluff results in over-steepening, which occurred at many of our study sites and can be seen in Figures 6.2-6.4 as high erosional volumes along the toe of the bluff.

Multiple sites also experienced large slumps in the spring of 2012 (Figure 7.1), despite an unusually low winter snowpack and a mild spring. Slumping was likely a result of freeze-thaw preparation, saturated conditions, and sapping/seepage erosion. Substantial net change was observed in three of the four bluffs measured over the winter/early spring (Nov. 2011 to April 2012), indicating that a combination of spring melt (i.e. saturated conditions & high pore water pressure) and freeze-thaw cycling play important roles in bluff erosion in the Amity watershed. Interestingly enough, three bluffs experienced greater retreat over the winter than any study site following high flows in late May. Again, this suggests factors other than high flow events also influence bluff erosion in the watershed. Lawler *et al*. (1997) proposed that processes such as freeze-thaw cycling and sapping are preparatory, essentially weakening the surface and priming it for other processes such as mass failure and fluvial erosion to be effective, and over-winter data from our research seem to support this with high erosion rates despite relatively low spring flows. Experiments conducted by Wynn and Mostaghimi (2006) found the effects of freeze-thaw cycling to persist for one to three months. While it is

difficult to pinpoint the extent to which near-surface processes influenced early spring slumping and fluvial erosion during high flow events in late May and June, our results do not refute the notion of near-surface processes conditioning the bluff surface for increased erosion.

There was essentially no change in our study bluffs from late June 2012 (post-flood) to November 2012; average retreat distances were calculated at +0.01 m for this period. During this time of the season, soil moisture content was minimal and temperatures rarely reached levels where freeze-thaw cycling was a factor, minimizing the efficacy of preparatory near-surface processes. Additionally, the total volume of water moving through the channel was lowest for this period, meaning fluvial erosion would be minimally effective in over-steepening bluffs and removing any material that was deposited at the toe by mass failure. Because of the absence of high flow events, slumping, and near-surface process in the post-flood time period, coupled with a lack of erosion, one could infer that these processes govern bluff erosion in the Amity watershed.

7.2 Role of Flow on Bluff Erosion

One goal in this study was to investigate the relationship between peak flow events and stream bluff erosion rates. An initial concern before commencing our TLS work was the duration of our study – if the region received no significant precipitation events during our TLS analysis, we could potentially see little change in our study bluffs. Furthermore, if minor bluff erosion had occurred, it would have been quite possible that the signal was masked by noise in the dataset. However, we were fortunate to have received two large storms over the course of our study. The 500-year flood of June 2012

presented a unique opportunity to investigate bluff erosion induced by a high flow event of unprecedented magnitude.

Although the geologic setting is different, similar TLS bluff erosion work has been recently conducted by Day *et al*. (2012, 2013) on till-based bluffs in southern Minnesota in the Le Sueur watershed. Increased flows in the Le Sueur River in recent years – likely as a result of anthropogenic land use changes (Schottler et al., 2013) – have raised questions and concerns about managing sediment loads at a watershed scale. Hydrologic management options necessitate a goal, whether it be lowering peak flows, reducing overall flow volume, or decreasing the time spent above a certain threshold flow. Results from the Le Sueur study show over half of the basin-wide TSS load is derived from fine sediment eroded from stream bluffs, and that the erosion is correlated with peak flows occurring between scans. However, scanning for their work was conducted every six months to one year, making it difficult to identify discrete events in the dataset. All of our study sites were scanned three times within a 60-80 day period extending from early April to late June 2012 (in addition to November 2011 & 2012); two of these campaigns followed major precipitation events, essentially bracketing the peak flow event between two campaigns. The frequency with which scans were conducted in this study provides insight into the relationship between discrete peak flow events and bluff erosion. Additionally, we are able to investigate how total flow volume and time spent above a threshold discharge affect erosion of stream bluffs in the watershed.

Generally speaking, net change was greatest when peak flow rates were highest, as is reflected in Figures 6.9 and 6.10, which show scaled peak flow rates and net change

(m^3) in our study bluffs. Of the five campaigns having the largest volume losses in our study, four were at sites following the June flood. For this reason, we can infer that high peak flows play a very important role in bluff erosion in the watershed. After examining GCD colorized change maps generated for each DoD (Figures 6.2-6.4), it is apparent that the main role high flow events play in bluff erosion is fluvial scour along the toe of the bluff, and removal of any sediment deposited through erosional processes such as slumping, either prior to, or during the flood event.

High peak flow events also result in higher shear stress. The depth-slope product can be used to determine shear stress acting on the basal zone of a stream bluff, and is defined by the following equation:

$$\tau_b = \rho g h \mathcal{S}$$

where τ_b is shear stress, ρg is the specific weight of water (density times gravity or $(\rho * g)$), h is the depth of the channel, and $\mathcal{S}$ is the slope of the channel. Higher peak flows result in higher flow depths, which in turn, increase the amount of shear stress the toe of the bluff is subjected to.

Although not as strong of a correlation as between net change and peak flow, the greater the volume of water flowing through the channel, the greater the chance for significant sediment loss from bluffs (Figures 6.7 and 6.8). The likely cause of this relationship is that with greater flow volumes comes a longer amount of time that the bluffs are exposed to fluvial scour.

Another important point regarding change at our bluffs relates to their location within the watershed: sites with the greatest net change had the largest upstream drainage area (Table 6.3, 6.13). This can be explained by an increase in shear stress and stream power. Unit stream power (ω) is a product of the specific weight of water ($\rho * g$), the channel slope (S), and unit discharge (total discharge divided by channel width or (Q/w)), and can be defined by the following equation:

$$\omega \propto \rho g(Q/w)S$$

As you move downstream in a watershed, discharge increases, effectively increasing the stream power at a given location. An increase in stream power provides increased force for eroding sediment from bluffs. Furthermore, many North Shore streams exhibit atypical profiles; as you move in a downstream direction in the watershed, channel slope actually increases (Figure 3.2). An increase in slope results in increased shear stress and stream power.

The amount of time sites were exposed to a given threshold flow appeared to have little effect on erosion of study bluffs. One-third bankfull discharge was used as the flow threshold, providing a more robust dataset that could be utilized to examine this relationship (as opposed to 100% bankfull, which was reached only 5 days over the course of the study). Average daily discharge values acquired through the MPCA were used to determine duration spent at or above the threshold flow. Due to the exceedingly

flashy nature of North Shore streams, and Amity Creek being no exception, this relationship would be better examined using a finer temporal resolution, such as 15-minute flow data.

7.3 Role of Bluff Erosion on Sediment Loading

In order to determine a total fine sediment load for Amity Creek bluffs, we used our average retreat rate for the year based on data from our study sites to extrapolate to all unvegetated bluffs in the watershed. Our estimated fine sediment load contributed to the channel by erosion of unvegetated bluffs in the Amity watershed from November 2011 to November 2012 was 3,924,000 kg. Unfortunately, total load estimates for Amity Creek in 2012 are unavailable. For this reason, our numbers were compared to a range of estimates from previous years where data were available. Clearly, our load estimate for 2012 bluff erosion greatly exceeds annual load estimates calculated by the MPCA and NRRI from 2001 to 2010 (Table 6.10). However, after removing our estimated June flood load (3,217,000 kg), it becomes clear that the remaining load of 707,000 kg is within the range of total loads from previous years. This point brings up two important outcomes of our study. First, when comparing our 2012 bluff erosion load estimate with flood totals removed to MPCA and NRRI estimates from 2001 to 2010, it is evident that a large percentage of the total sediment load in the watershed comes from bluffs. Because of this, mitigating the amount of bluff erosion occurring in the Amity watershed is critical to reducing the fine sediment load reaching the channel and improving water quality.

Second, it appears that much if not most of the erosion occurs during short, focused time periods. For example, freeze-thaw cycling is most efficient when temperatures fluctuate around the freezing point (late winter/early spring), while fluvial erosion and mass wasting are most effective during and following spring melt and large precipitation events when soils are saturated and high flows provide the shear stress needed to remove material from the bluff toe. While bluff retreat rates are typically reported in terms of annual rates of retreat, much of the erosion occurs during several distinct events. For example, based on our estimates the June flood accounted for approximately 82% of the total bluff erosion load for 2012. It is entirely possible that in years lacking major precipitation events, or having relatively dry springs, bluffs in the watershed are stable and undergo little retreat.

7.4 Comparison with Traditional Techniques

As discussed previously in this paper, TLS technology is appropriate for a vast range of spatial and temporal scales, and yields data having very high spatial resolution and accuracy (Heritage and Hetherington, 2007; Day et al., 2012). The increase in sampling resolution achieved with TLS provides greater insight into where erosion is occurring and thus, the processes responsible for stream bank/bluff erosion. By understanding the dynamics of the erosional processes affecting a channel, it is possible to minimize the negative effect they are having on sediment loading.

Traditional techniques such as RTK-GPS and total station instruments require more training and experience on the part of the user. For example, if measurements are not taken in the proper location, or if measurements are not collected with a sufficient

spatial resolution in areas displaying rough terrain, estimates of erosion/deposition could be significantly underestimated or overestimated. Additionally, bluff erosion is spatially variable. When collecting elevation data with more traditional methods, proper technique alone may not be enough to accurately capture any geomorphic change occurring. With TLS, data collection is much less burdensome. So long as a sufficient number of instrument set-ups are used to assure line-of-sight to all portions of the surface, uneven topography will be preserved and properly displayed in any subsequent DEM created.

An issue that stems from the discussion of preserving uneven topographic features in the surface of interest is our use of DEM differencing to detect change in study bluffs. Day *et al*. (2012) employ a "reference TIN technique" to detect change in their experiment. The reference TIN provides a surface against which individual points or point clouds from other scan campaigns can be compared. The advantage to using a reference TIN is that true 3D data are retained, whereas the use of a DEM reduces a dataset to "2.5D". For example, if a bluff has an overhanging feature, the top, or front of the feature will be differenced with our DEM technique; any changes occurring to the underside will not be detected. Should a TLS site contain a large number of overhanging features, using a reference TIN or similar technique is advisable. However, in order for the aforementioned TIN technique to be advantageous, the user must be able to position the instrument in a location where the underside of an overhanging feature is visible. For a study such as ours, where change is being measured in near-vertical terrain, positioning the instrument in such a manner is difficult, if not impossible, without disturbing the surface of interest.

7.5 Retrospectives: Vegetation & Control Points

Collection of TLS data in our study was typically a smooth process. Most of the time-intensive work is related to post-processing of the data, particularly with respect to removal of vegetation from scans. In order to reduce the amount of time needed to prepare a set of campaigns for DEM differencing, we recommend selecting sites with minimal vegetation. A few of our sites became heavily vegetated by late spring, making change detection impossible. As mentioned in earlier sections of this paper, TLS instrumentation is governed by the concept of line-of-sight; if the surface is obstructed by vegetation or irregularities in the topography, points will not be collected in those locations. Dealing with obstructions may be as straightforward as positioning the instrument behind the obstacles, or in a location where surface undulations are visible, terrain permitting. However, sites in this experiment were steep, with some being oriented nearly vertically. Moreover, we were interested in detecting erosional/depositional changes in bluffs, and therefore, instrument set-ups on the bluff face would have meant disturbing the surface of interest and likely altering our data and subsequent results. Because of this, we strongly suggest selecting sites having minimal vegetative cover if at all possible.

Another complication in our study came about as a result of the June flood. As discussed previously, most control points (control spheres) were located at the base of the bluff, within 2 to 4 meters of the channel. Clearly, a 500-year flood is a rarity. As such, we did not establish control points with events of extreme magnitude taken into consideration. Fortunately, we were able to link pre- and post-flood campaigns using objects other than control points (e.g. rocks, trees, etc.), though our mean tension values

typically increased. The point here is that control points are the best means by which individual campaigns can be linked together to produce a DoD. In order to reduce errors in scan alignment and generate an accurate series of DEMs, it is ideal that control points are stationary and remain intact for the duration of the study. Whenever possible, we suggest establishing control points on features such as rocks and trees that are fairly certain to remain stable throughout the scanning process. Additionally, we recommend creating back-up control points (i.e. rebar, etc) in the event that some are lost to natural processes or destroyed by human interference.

7.6 Amity Creek Bluff Stabilization & Restoration

As is the case with many North Shore drainage networks, the geology of the Amity watershed has a large impact on erosional processes. The region's steep gradient and relatively thin soils, combined with bedrock and surficial geology, greatly reduce infiltration potential. Both past and present land use practices in the region – such as draining wetlands and increasing the number of impervious surfaces – have adversely affected water resources in the greater Duluth area. A 1973 study on Duluth streams conducted by the US Army Corp of Engineers concluded that the storm water removal system in the city relies heavily on streams and ditches as conduits to Lake Superior (Anderson et al., 2000). These practices, in addition to the geologic composition of the region, have altered the natural flow regime of many urban streams such as Amity Creek by concentrating flows and increasing the volume of water reaching the channel.

From 2005 to 2011 the City of Duluth and South St. Louis Soil and Water Conservation District oversaw bluff stabilization projects on the lower East Branch of

Amity Creek and the Graves Road tributary to the main branch of the creek. Almost $2 million in externally funded grants – leveraged by the Weber Stream Restoration Initiative (WSRI) Endowment – were used to fund these restoration projects (Axler et al., 2010). WSRI is dedicated to enhancing habitat and biodiversity in tributaries to Lake Superior along the North Shore. An important element of the stabilization efforts was monitoring and assessing their overall success to determine if bluff stabilization techniques utilized elsewhere will be effective on flashy North Shore streams. For this reason, we selected two previously restored bluffs to include in our TLS study.

The two restored bluffs that we analyzed with TLS are located on the East Branch, just upstream of the West Branch confluence. Tables 6.3 and 6.4 show net change and average retreat distances for these sites (B13, B14). As mentioned in our Methods section, the prevailing characteristic of sites selected for this experiment was lack of vegetative cover. Due to stabilization efforts, B13 and B14 were heavily vegetated, especially in late spring and summer when grasses thrive. Because of this, GCD analysis was difficult; small trees, shrubs, and grasses obstructed much of the surface. Removal of vegetation in Faro Scene was particularly futile for B14, and only small portions of the bluff toe were used in change detection analysis for campaigns conducted in May and June (Table 4.1, 4.3). Stabilization of these sites has been fairly successful, and upper regions of the bluff remain stable post-flood. However, the base of these bluffs did not fare well in the high flows during the June flood. Our numbers show that erosion did occur at sites B13 and B14, as almost 20 m^3 of sediment was removed from both bluffs, and retreat distances were -0.42 m (Nov. 2012 to Nov. 2013) and -0.25 m (Apr. to Nov. 2012), respectively. It is important to note that our numbers are

somewhat skewed at these sites for a few reasons. First, upper regions of the bluff were removed during initial post-processing in Faro Scene, due to those portions being heavily vegetated. Thus, the "total bluff area" reported in Table 6.12 is the area of the point cloud remaining after removing vegetation and holes in Scene. Heavily vegetated areas were an issue only at these rehabilitated sites. Secondly, as mentioned above, only a small percentage of this remaining "total bluff area" was used in change detection calculations at site B14 for scans conducted in May and June. Hence, the area used in GCD analysis for the time periods spanning from April to May, May to June, and June to November is significantly reduced (Table 6.12). If the actual bluff area (area of bluff prior to vegetation and hole removal during initial post-processing) is used in determining average retreat distance, and assuming there was no net change in portions of the bluffs removed prior to GCD analysis, retreat rates are reduced at these rehabilitated sites. Average retreat distance changes from -0.42 m to -0.13 m at site B13, and from -0.25 m to -0.15 m at site B14, when vegetated upper portions of the bluffs are accounted for. Additionally, while bank/bluff stabilization and restoration designs should be engineered to withstand high flow events, the flood of June 2012 was unprecedented in magnitude, making it very difficult to prepare for such an occurrence.

Stream bluff restoration and stabilization projects are relatively new to the Amity watershed and the western Lake Superior region. The costs associated with these projects are often high (Axler et al., 2010), and some feel that bank/bluff restoration projects merely postpone the inevitable as the site will eventually succumb to natural erosional processes. Nonetheless, these projects may be vital to improving the water quality and overall health of the stream ecosystem, protecting (or in some cases preserving)

infrastructure, and in reducing high sediment loads that plague many North Shore tributaries today. Through our TLS research, we have concluded that bluffs in the Amity Creek watershed are responsible for contributing a high percentage of the total sediment load (Table 6.10), and therefore, long-term stabilization efforts and/or flow reduction strategies are essential in reducing fine sediment loads to the creek.

Figure 7.1: Slumps in study bluffs observed from April to May 2012. (A) Site B9 (lower main Amity); slump observed in early April. (B) Site B9; slumping continues up face of bluff following heavy precipitation May 23 to 28; significant undercutting along bluff toe. (C) Site B7 (lower Lester); slump observed in early April. (D) Site B12 (lower East Branch Amity); slump following heavy precipitation in late May

8.0 REFERENCES

Anderson, J., Estabrooks, T., and McDonnell, J. 2000. Duluth metropolitan area streams snowmelt runoff study. Minnesota Pollution Control Agency.

Asare, S.N., Rudra, R.P., Dickinson, W.T., and Wall, G.J. 1997. Frequency of freeze-thaw cycles, bulk density and saturation effects on soil surface shear and stability in resisting water erosion. *Canadian Agricultural Engineering*. 39(4): 273-279.

Axler, R., Breneman, D., Brady, V., Host, G., and Johnson, L. 2010. Weber Stream Restoration Initiative Progress Report & Prospectus, June 28, 2010.

Beckman Coulter, Inc. LS 13 320 instruction manual. 2003.

Bitelli, G., Dubbini, M., and Zanutta, A. 2004. Terrestrial laser scanning and digital photogrammetry techniques to monitor landslide bodies. In *Proceedings of the 20th ISPRS congress.* Istanbul, Turkey, 2004.

Brasington, J., Vericat, D., and Rychkov, I. 2012. Modeling river bed morphology, roughness, and surface sedimentology using high resolution terrestrial laser scanning. *Water Resources Research.* 48(W11519): 1-18.

Buckley, S.J., Howell, J.A., Enge, H.D., and Kurz, T.H. 2008. Terrestrial laser scanning in geology: data acquisition, processing and accuracy considerations. *Journal of the Geological Society, London.* 165: 625-638.

Cancienne, R.M., Fox, G.A., and Simon, A. 2008. Influence of seepage undercutting on the stability of root-reinforced streambanks. *Earth Surface Processes and Landforms.* 33: 1769-1786.

Carney, S.J. 1996. Paleohydrology of the western outlets of Glacial Lake Duluth. M.S. thesis. University of Minnesota – Duluth.

Casagli, N., Rinaldi, M., Gargini, A., and Curini, A. 1999. Pore water pressure and streambank stability: results from a monitoring site on the Sieve River, Italy. *Earth Surface Processes and Landforms.* 24: 1095-1114.

Charlton, M.E., Large A.R.G., and Fuller, I.C. 2003. Application of airborne lidar in river environments: the River Coquet, Northumberland, UK. *Earth Surface Processes and Landforms.* 28: 299-306.

Couper, P.R., and Maddock, I.P. 2001. Subaerial river bank erosion processes and their interaction with other bank erosion mechanisms on the River Arrow, Warwickshire, UK. *Earth Surface Processes and Landforms*. 26: 631-646.

Coveney, S., and Fotheringham, A.S. 2011. Terrestrial laser scan error in the presence of dense ground vegetation. *The Photogrammetric Record.* 26(135): 307-324.

Czuba, C.R., Fallon, J.D., and Kessler, E.W. 2012. Floods of June 2012 in northeastern Minnesota: U.S. Geological Survey Scientific Investigations Report 2012–5283. 42 p. with 3 app.

Day, S.S., Gran, K.B., Belmont, P., and Wawrzyniec, T. 2012. Measuring bluff erosion part 1: terrestrial laser scanning methods for change detection and determining bluff erosion processes. *Earth Surface Processes and Landforms.* DOI: 10.1002/esp.3353.

Day, S.S., Gran, K.B., Belmont, P., and Wawrzyniec, T. 2013. Measuring bluff erosion part 2: pairing aerial photographs and terrestrial laser scanning to create a watershed scale sediment budget. *Earth Surface Processes and Landforms.* 38: 1068-1082.

Dietrich, W.E., and Gallinatti, J.D. 1991. Fluvial Geomorphology. In *Field Experiments and Measurement Programs in Geomorphology,* Slaymaker, O. (ed). Balkema: Rotterdam.

Faro Focus 3-D Laser Scanner. Tech Sheet. Web. <http://www.faro.com/focus/us/downloads>.

Farrand, W.R., and Drexler, C.W. 1985. Late Wisconsinan and Holocene history of the Lake Superior Basin. In *Quarternary Evolution of the Great Lakes,* Karrow, P.F., Calkin, P.E. (eds). Geological Association of Canada Special Paper. 30: 17-32.

Fitzpatrick, F.A., Peppler, M.C., DePhilip, M.M., and Lee, K.E. 2006. U.S. Geological Survey; U.S. Department of the Interior. Geomorphic characteristics and classification of Duluth-area streams, Minnesota. Scientific Investigations Report 2006-5029.

Fox, G.A., Wilson, G.V., Simon, A., and Langendoen, E.J. 2007. Measuring streambank erosion due to ground water seepage: correlation to bank pore water pressure, precipitation and stream stage. *Earth Surface Processes and Landforms.* 32: 1158-1573.

Heritage, G., and Hetherington, D. 2007. Towards a protocol for laser scanning in fluvial geomorphology. *Earth Surface Processes and Landforms.* 32: 66-74.

Hobbs, H.C., and Breckenridge, A. 2011. Ice advances and retreats, inlets and outlets, sediments and strandlines of the western Lake Superior Basin. The Geological Society of America Field Guide. 24: 299-315.

Hobbs, H.C. 2004. Late Wisconsinan Superior-Lobe deposits in the Superior Basin northeast of Duluth. Institute on Lake Superior Geology, 4-9 May, 2004. Field Trip 3: 86-98.

Hobbs, H.C. 2009. Surficial geology of the Duluth quadrangle, St. Louis County, Minnesota. Minnesota Geological Survey. Web. <http://conservancy.umn.edu/bitstream/58230/3/m-187%5B1%5D.pdf>.

Kok, H., and McCool, D.K. 1989. Freeze-thaw induced variability of soil shear strength. ASAE Paper No. 89-2189. St. Joseph, MI: ASAE.

Lawler, D.M., Thorne, C.R., and Hooke, J.M. 1997. Bank erosion and instability. In *Applied Fluvial Geomorphology for River Engineering and Management,* Thorne, C.R., Hey, R.D., Newson, M.D. (eds). Wiley: Chichester; 137-172.

Lawler, D.M. 1993. The measurement of river bank erosion and lateral channel change: a review. *Earth Surface Processes and Landforms.* 18: 777-821.

Lindow, N., Fox, G.A., and Evans, R.O. 2009. Seepage erosion in layered stream bank material. *Earth Surface Processes and Landforms.* 34: 1693-1701.

Milan, D.J., Heritage, G.L., and Hetherington, D. 2007. Application of a 3D laser scanner in the assessment of erosion and deposition volumes and channel change in a proglacial river. *Earth Surface Processes and Landforms.* 32: 1657-1674.

Nasermoaddeli, M.H., and Pasche, E. 2008. Application of terrestrial 3D laser scanner in quantification of the riverbank erosion and deposition. In *Proceedings of Riverflow 2008.* 3: 2407-2416.

Resop, J.P., and Hession, W.C. 2010. Terrestrial laser scanning for monitoring streambank retreat: comparison with traditional surveying techniques. *Journal of Hydraulic Engineering*. 136(10): 794-798.

Rinaldi, M., Casagli, N., Daporto, S., and Gargini, A. 2004. Monitoring and modeling pore water pressure changes and riverbank stability during flow events. *Earth Surface Processes and Landforms.* 29: 237-254.

Ruzycki, E.M, Axler, R.P., Host, G.E., Henneck, J.R., and Will, N.R. In press. Estimating sediment and nutrient loads in four Western Lake Superior streams. *Journal of the American Water Resources Association*.

Schottler, S., Ulrich, J., Belmont, P., Moore, R., Lauer, J., Engstrom, D., and Almendinger, J. 2013. Twentieth century agricultural drainage creates more erosive rivers. *Hydrological Processes*. 28: 1951-1961.

South St. Louis Soil and Water Conservation District. 2009. Amity Creek sediment and erosion reconnaissance.

Simon, A., Curini, A., Darby, S.E., and Langendoen, E.J. 2000. Bank and near-bank processes in an incised channel. *Geomorphology.* 35: 193-217.

Simon, A., Curini, A., Darby, S.E., and Langendoen, E.J. 1999. Streambank mechanics and the role of bank and near-bank processes in incised channels. In *Incised River Channels: Processes, Forms, Engineering and Management,* Darby, S.D., Simon, A. (eds). John Wiley and Sons: New York.

Sims, P.K., and Morey, G.B. 1972. Geology of Minnesota: a centennial volume. Minnesota Geological Survey. 632.

Thorne, C.R. 1982. Processes and mechanisms of river bank erosion. In *Gravel-Bed Rivers,* Hey R.D., Bathurst, J.C., Thorne, C.R. (eds). Wiley: Chichester; 227-271.

U.S.D.A. Natural Resources Conservation Service. 2008. Soil quality indicators. Web. <http://soils.usda.gov/sqi/assessment/files/bulk_density_sq_physical_ indicator_sheet.pdf>.

Wick, M.J. 2013. Identifying erosional hotspots in streams along the North Shore of Lake Superior, Minnesota using high-resolution elevation and soils data. M.S. thesis. Univeristy of Minnesota – Duluth.

Wilson, G.V., Periketi, R.K., Fox, G.A., Dabney, S.M., Shields, F.D., and Cullum, R.F. 2007. Soil properties controlling seepage erosion contributions to streambank failure. *Earth Surface Processes and Landforms.* 32: 447-459.

Wynn, T., and Mostaghimi, S. 2006. The effects of vegetation and soil type on streambank erosion, southwestern Virginia, USA. *Journal of the American Water Resources Association*. 42(1): 69-82.

9.0 APPENDICES OF GCD FIGURES & RESULTS

9.1 Appendix A: Event-Scale Net Change at Study Bluffs

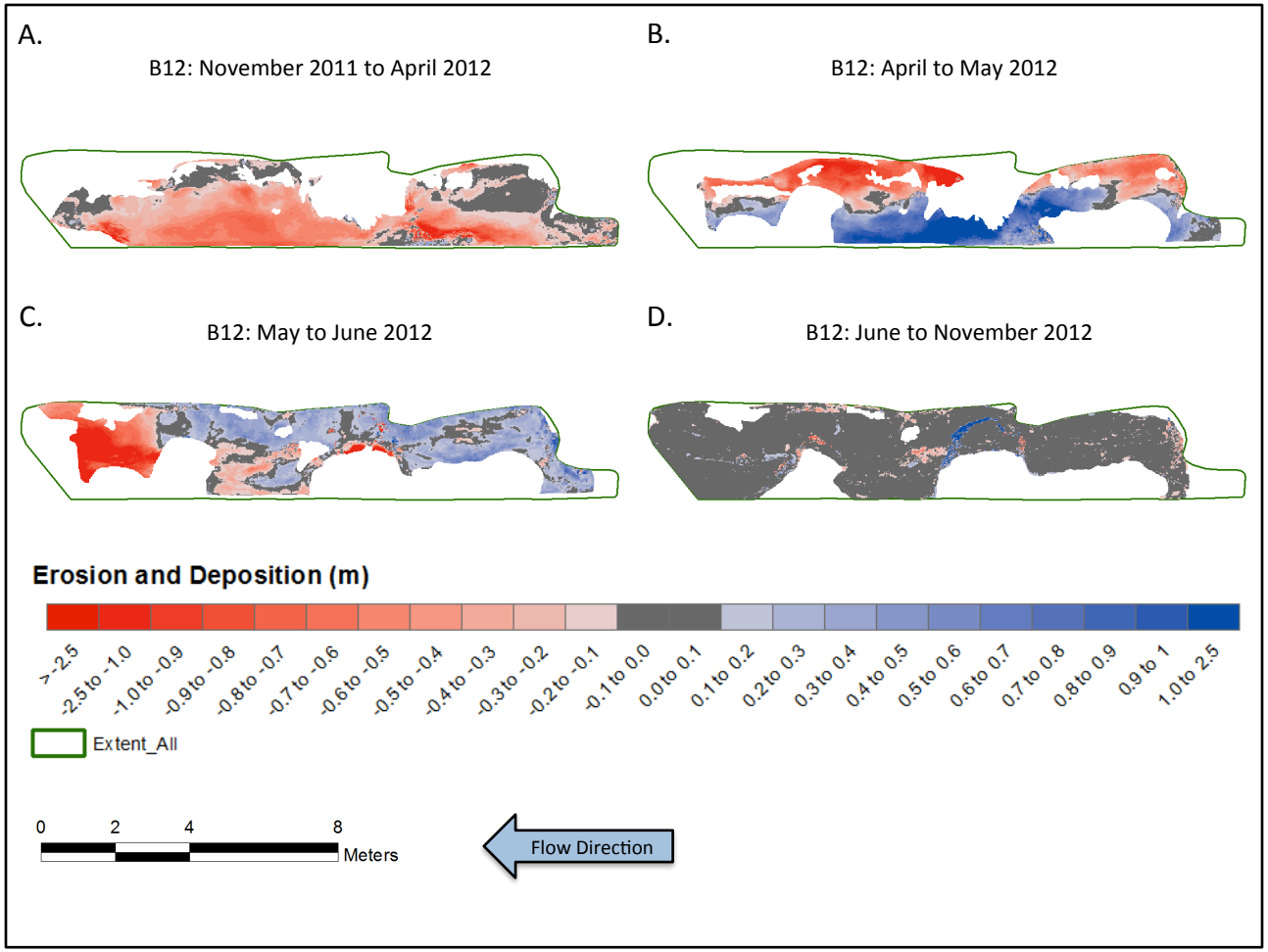

Figure 9.1: Event-scale net change at site B12 (lower East Branch Amity); flow from R to L. (A) November 2011 to April 2012; slumping observed post-melt; fluvial erosion observed along base of bluff. (B) April to May 2012; large slump along upper portion of bluff following heavy precipitation May 23 to 28; deposition of eroded material along base of bluff. (C) May to June 2012; significant erosion on downstream end of bluff following June flood; band of deposition from area above bluff spanning upper portion of face. (D) June to November 2012; bluff inactive.

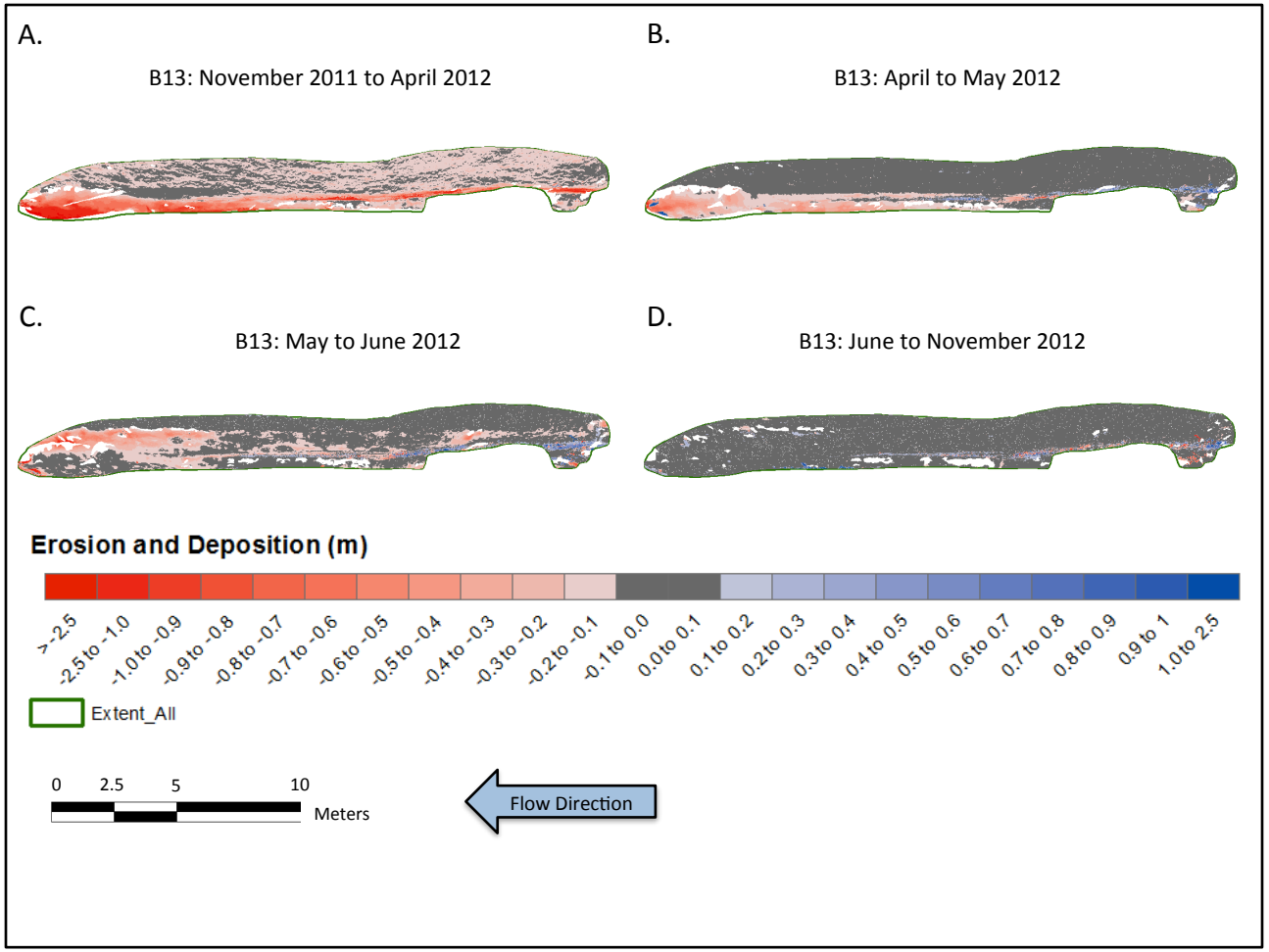

Figure 9.2: Event-scale net change at site B13 (lower East Branch Amity); flow from R to L. (A) November 2011 to April 2012; band of fluvial erosion spanning base of bluff. (B) April to May 2012; most of upper portion of lower bluff face inactive (upper bluff removed during initial post-processing due to vegetation); band of fluvial erosion along base of bluff. (C) May to June 2012; bluff fairly inactive post-flood; some erosion seen in portions of lower bluff concentrated on the downstream end. (D) June to November 2012; bluff inactive.

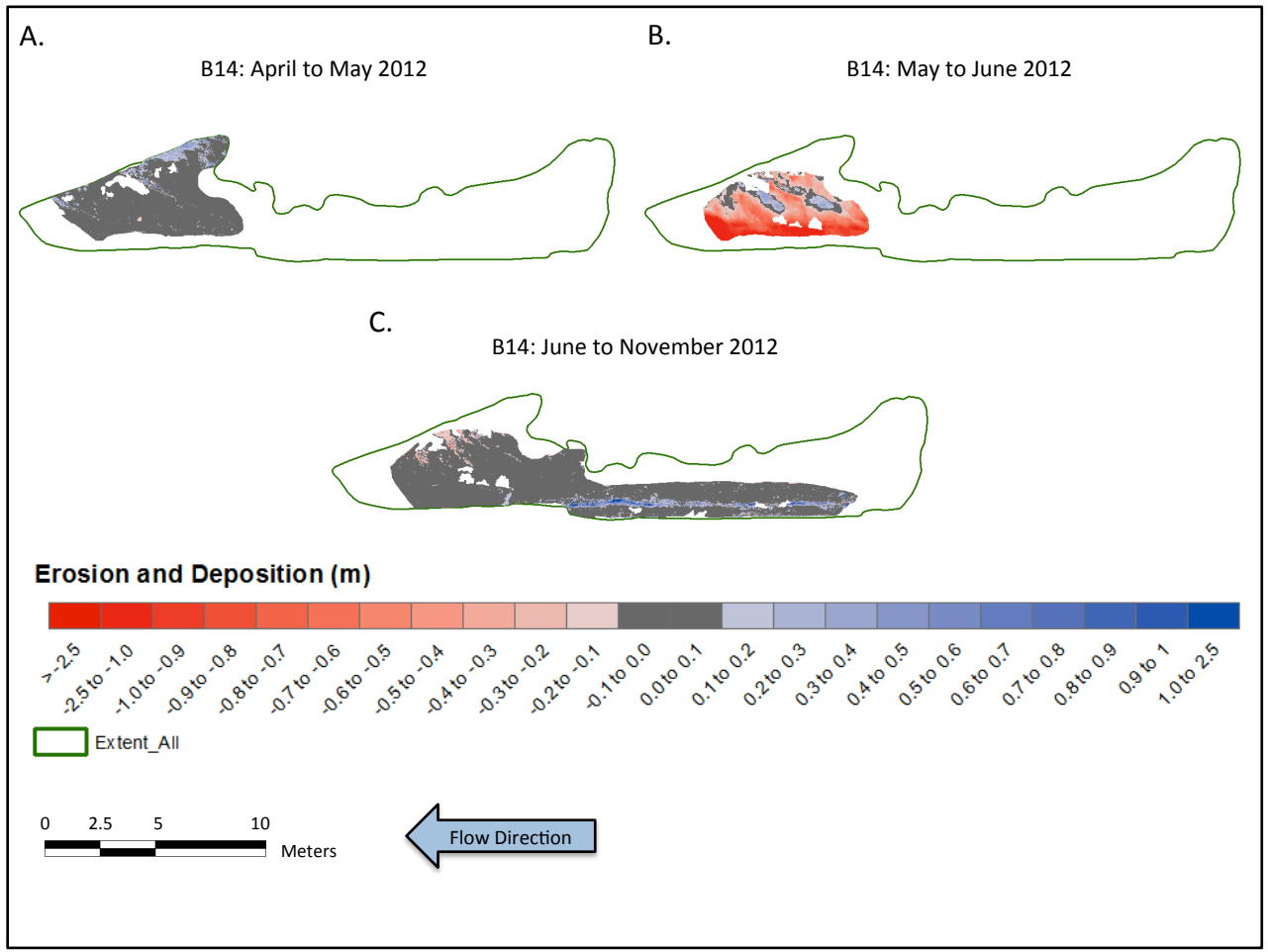

Figure 9.3: Event-scale net change at site B14 (lower East Branch Amity); flow from R to L. (A) April to May 2012; bluff inactive; bluff heavily vegetated in May and not practical for change detection. (B) May to June 2012; heavy erosion in downstream end of bluff following June flood; bluff heavily vegetated in May and June and not practical for change detection. (C) June to November 2012; bluff mostly inactive; band of deposition spanning base of bluff; signal possibly caused by vegetation.

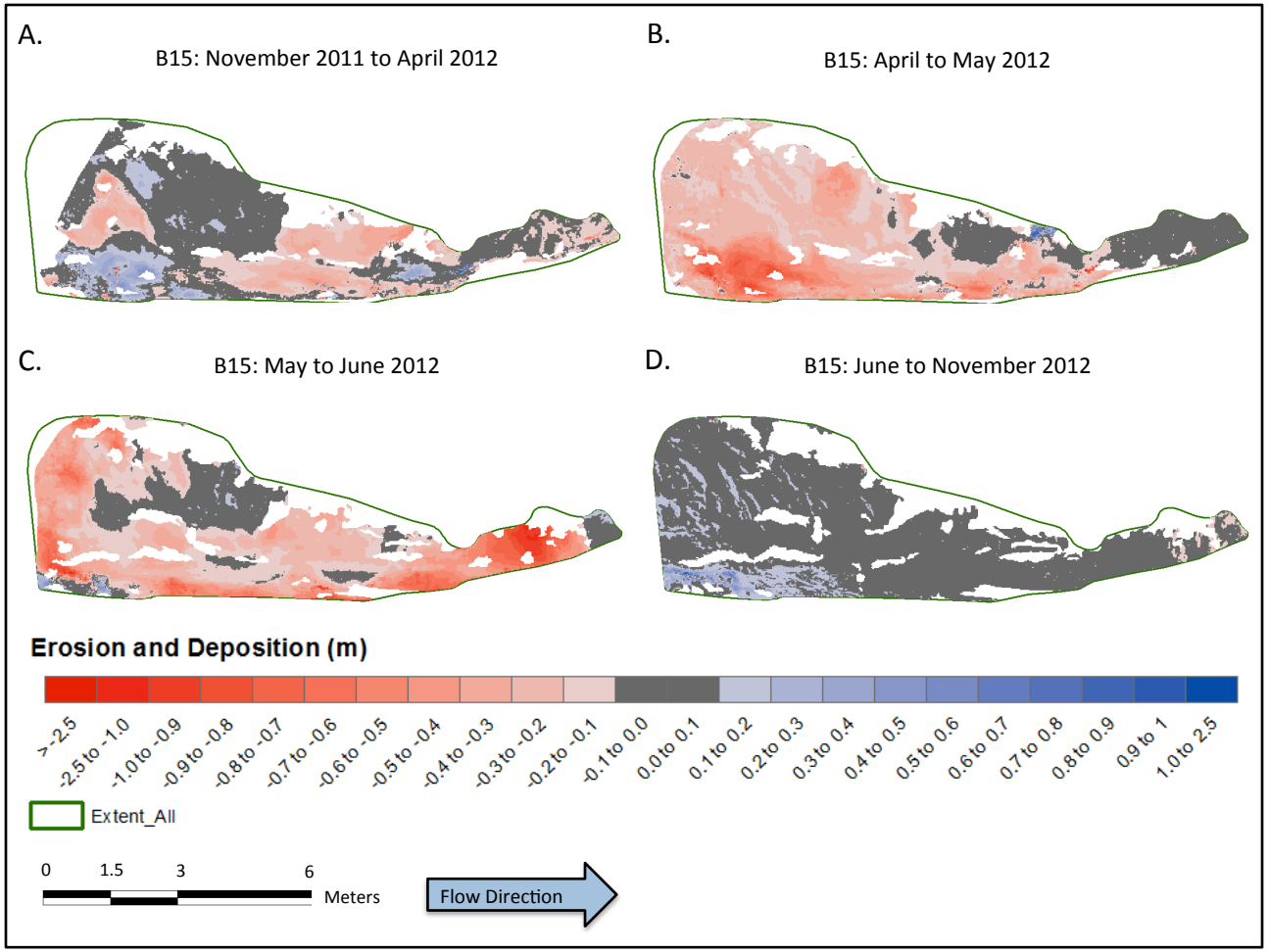

Figure 9.4: Event-scale net change at site B15 (lower West Branch Amity); flow from L to R. (A) November 2011 to April 2012; mainly erosion on bluff face; eroded material on left side of face deposited below. (B) April to May 2012; significant erosion following heavy precipitation May 23 to 28 (6m^3 net loss; see Table 6.3). (C) May to June 2012; significant erosion following June flood (6m^3 net loss; see Table 6.3); fluvial erosion along base of bluff. (D) June to November 2012; bluff inactive.

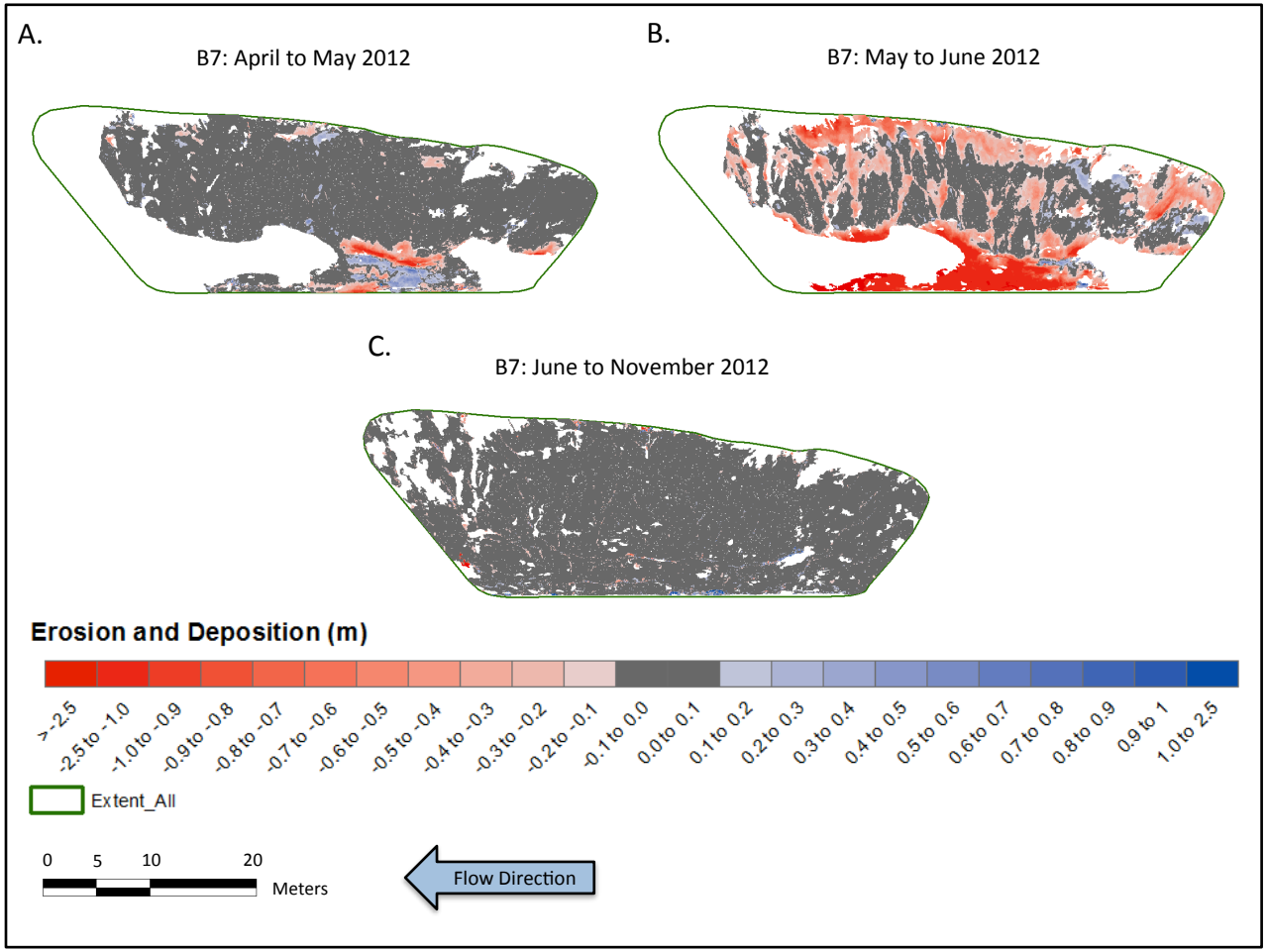

Figure 9.5: Event-scale net change at site B7 (lower Lester); flow from R to L. (A) April to May 2012; slump observed in middle of lower face; erosion above, deposition below. (B) May to June 2012; significant erosion following June flood (141m^3 net loss; see Table 6.3); fluvial erosion/undercutting along base of bluff. (C) June to November 2012; bluff inactive.

9.2 Appendix B: Overall Net Change at Study Bluffs

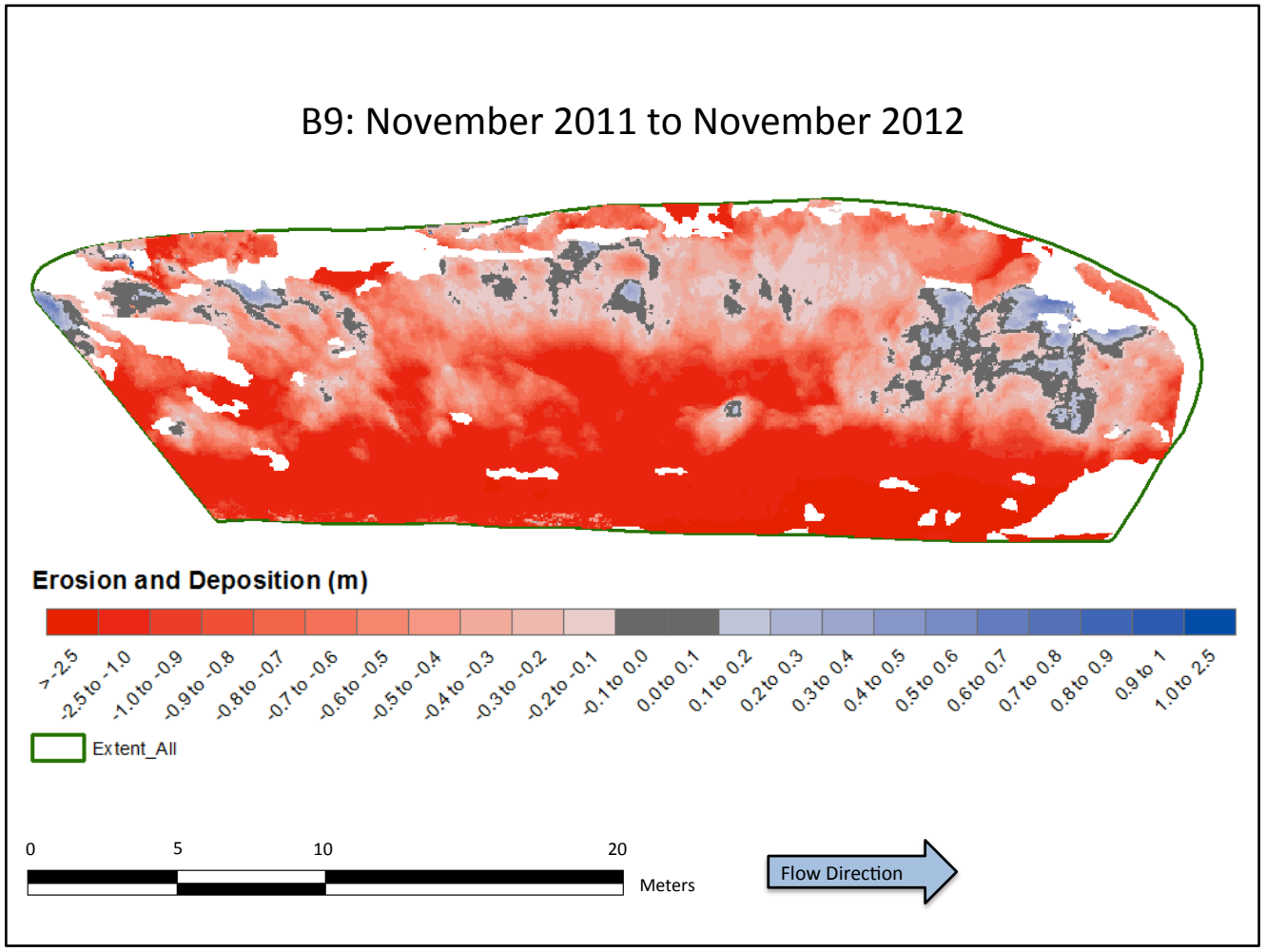

Figure 9.6: Overall Net Change at site B9 from November 2011 to November 2012.

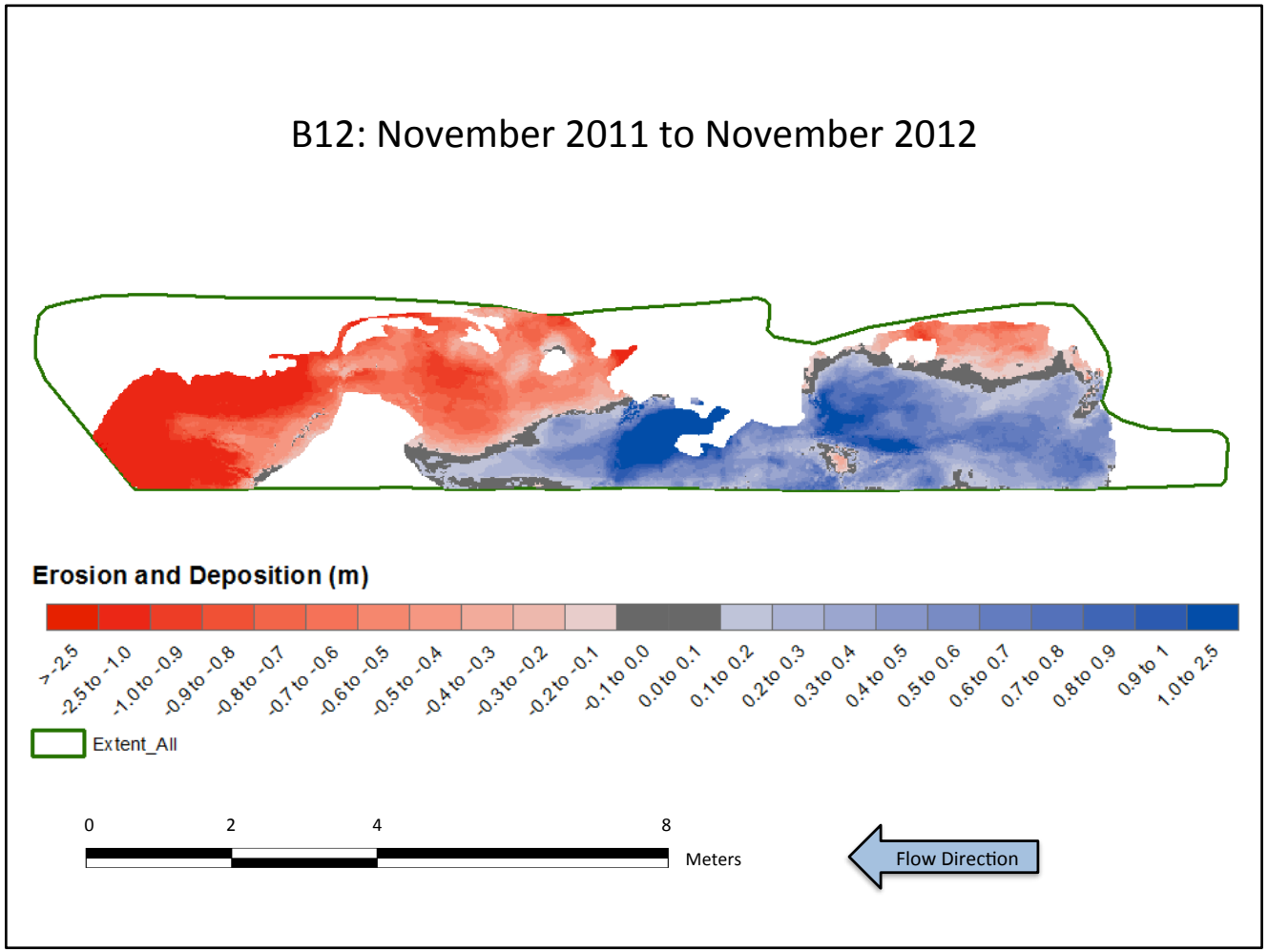

Figure 9.7: Overall Net Change at site B12 from November 2011 to November 2012.

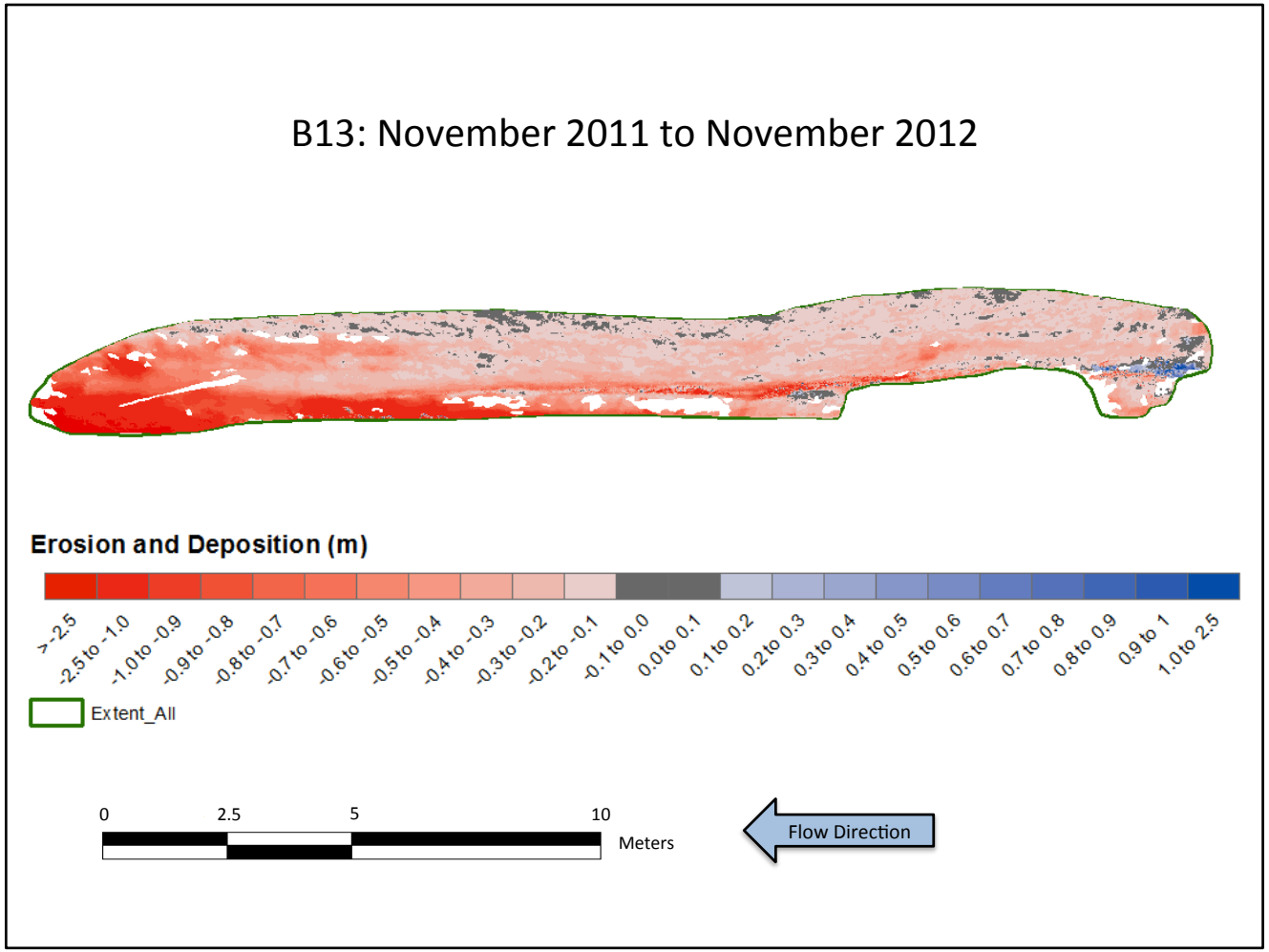

Figure 9.8: Overall Net Change at site B13 from November 2011 to November 2012.

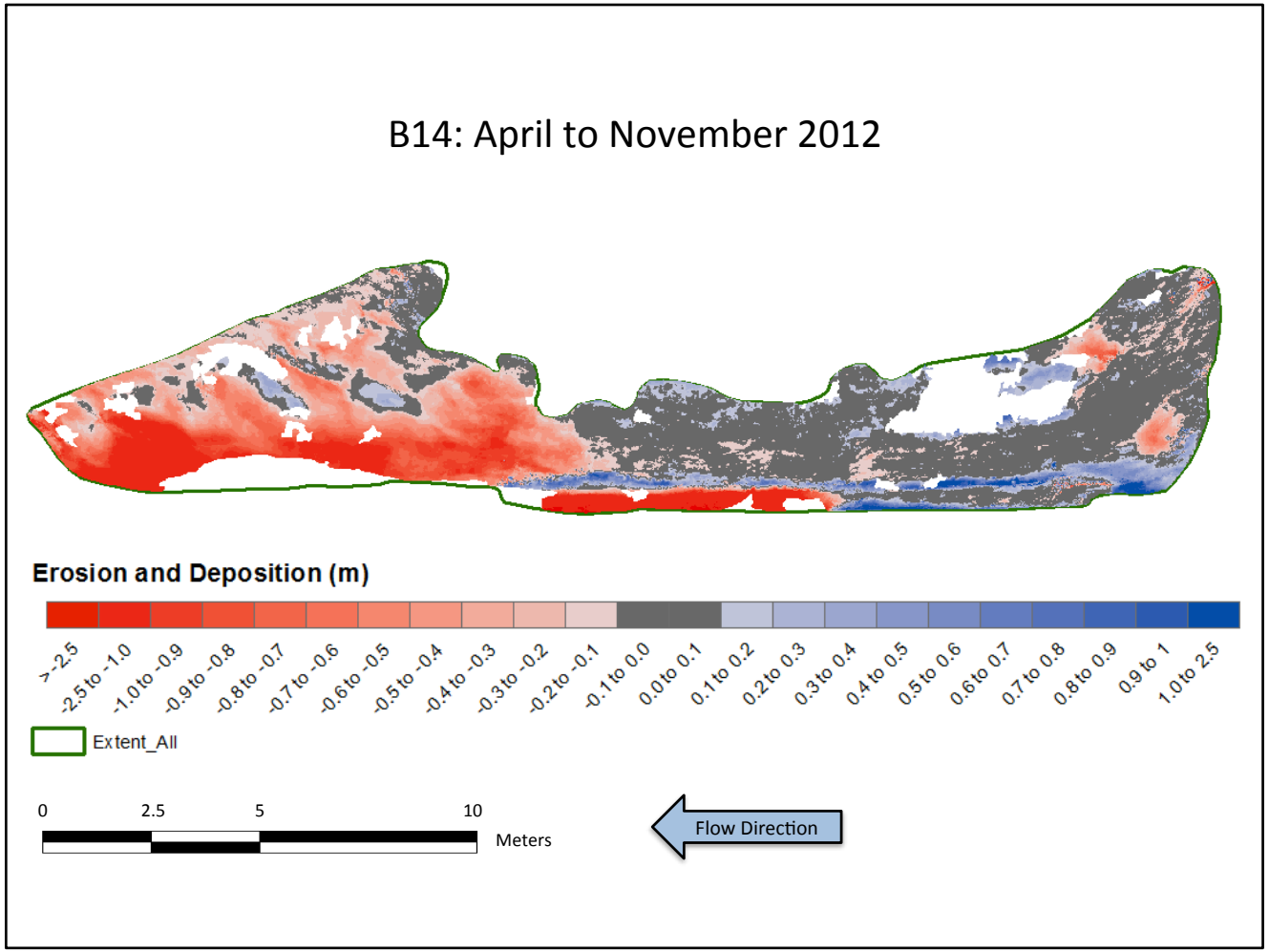

Figure 9.9: Overall Net Change at site B14 from April to November 2012.

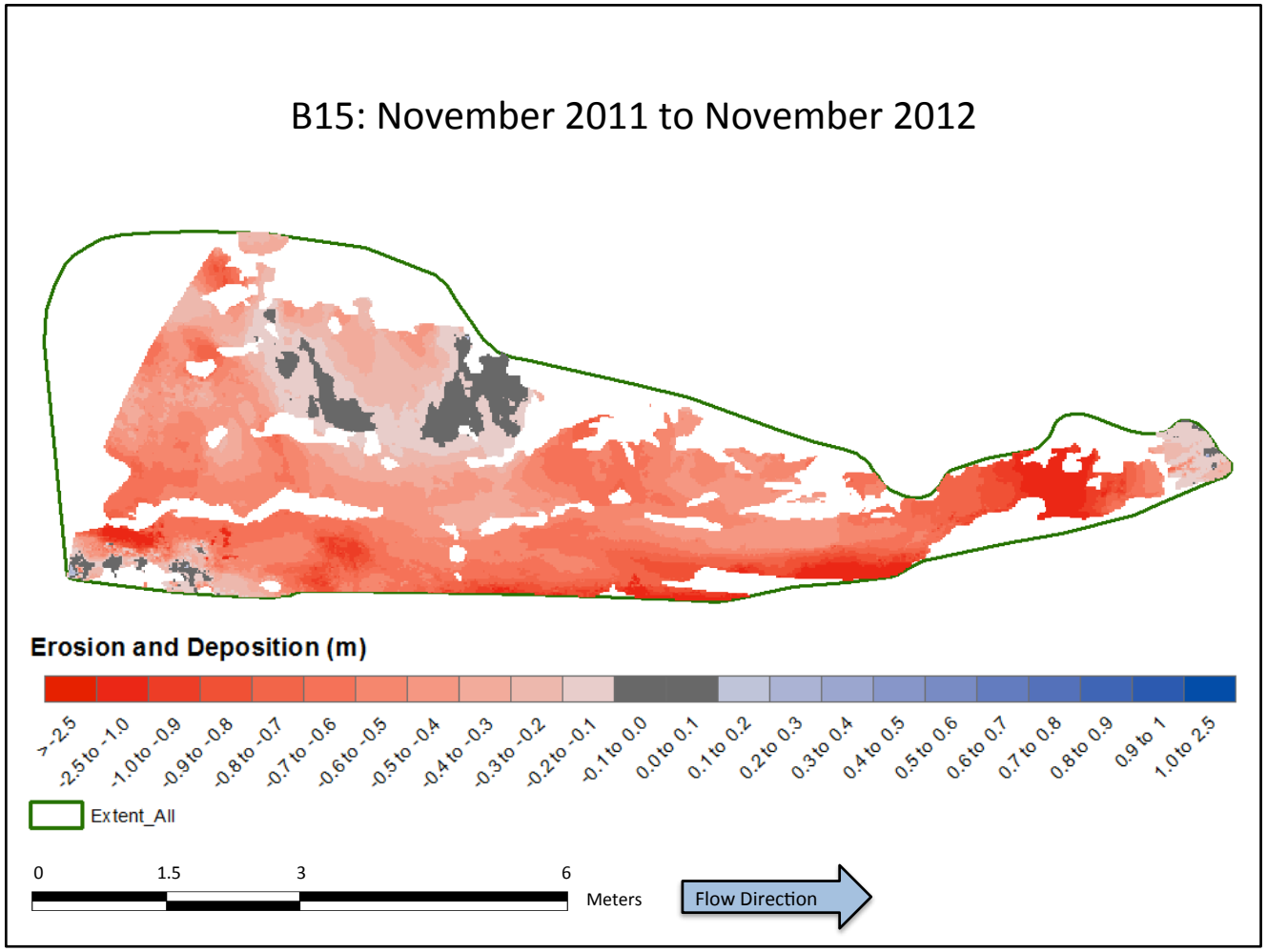

Figure 9.10: Overall Net Change at site B15 from November 2011 to November 2012.

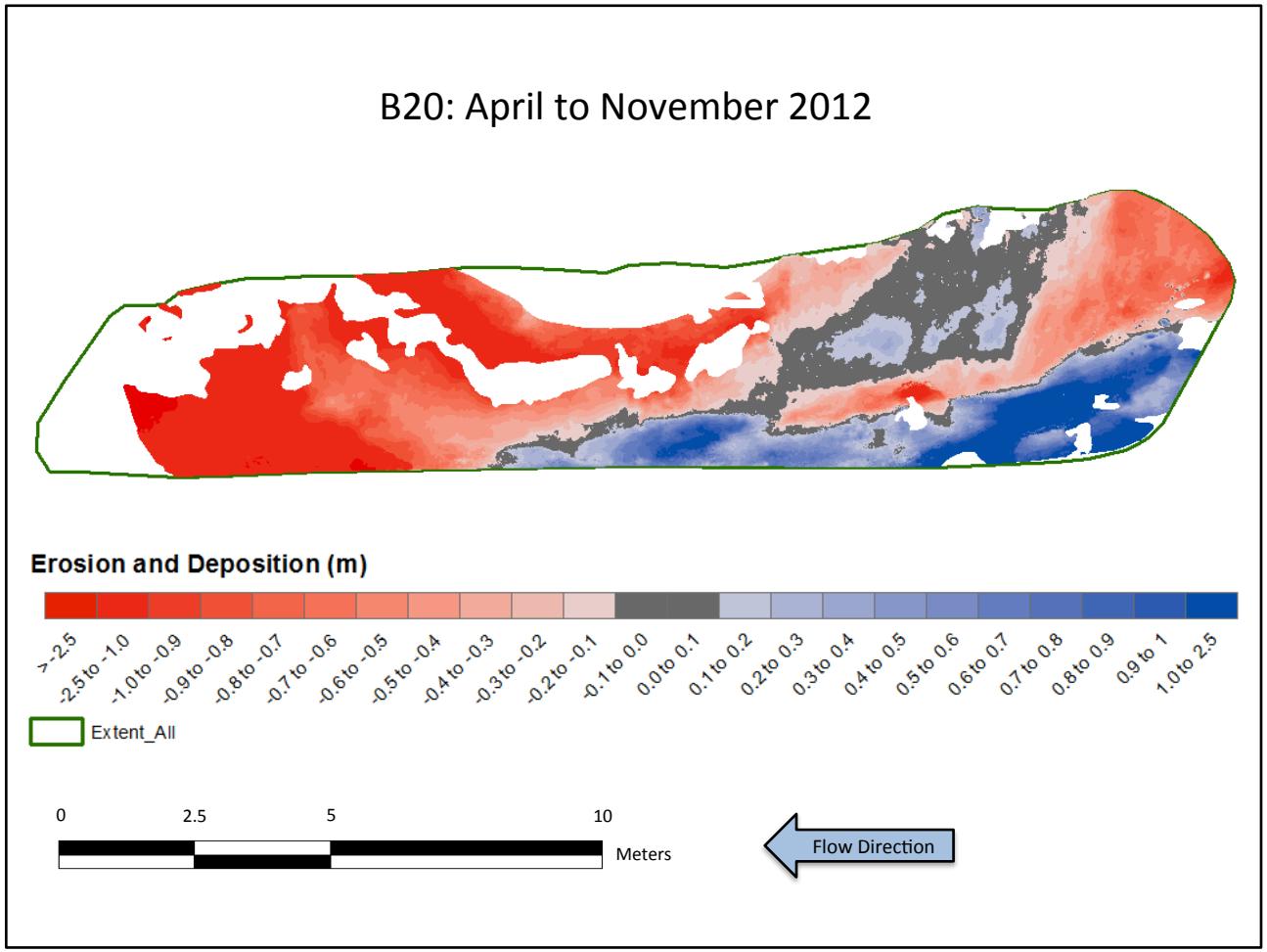

Figure 9.11: Overall Net Change at site B20 from April to November 2012.

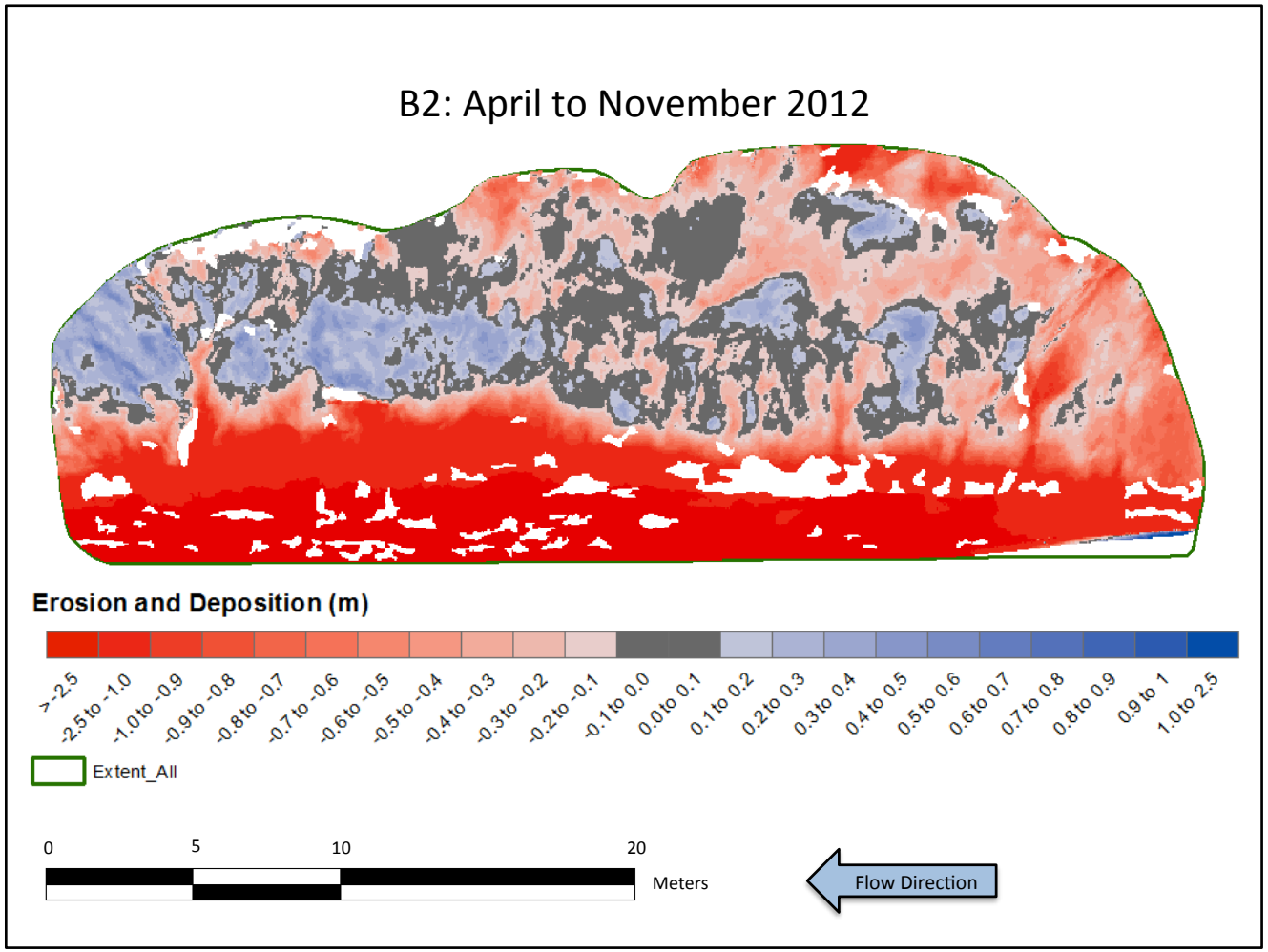

Figure 9.12: Overall Net Change at site B2 from April to November 2012.

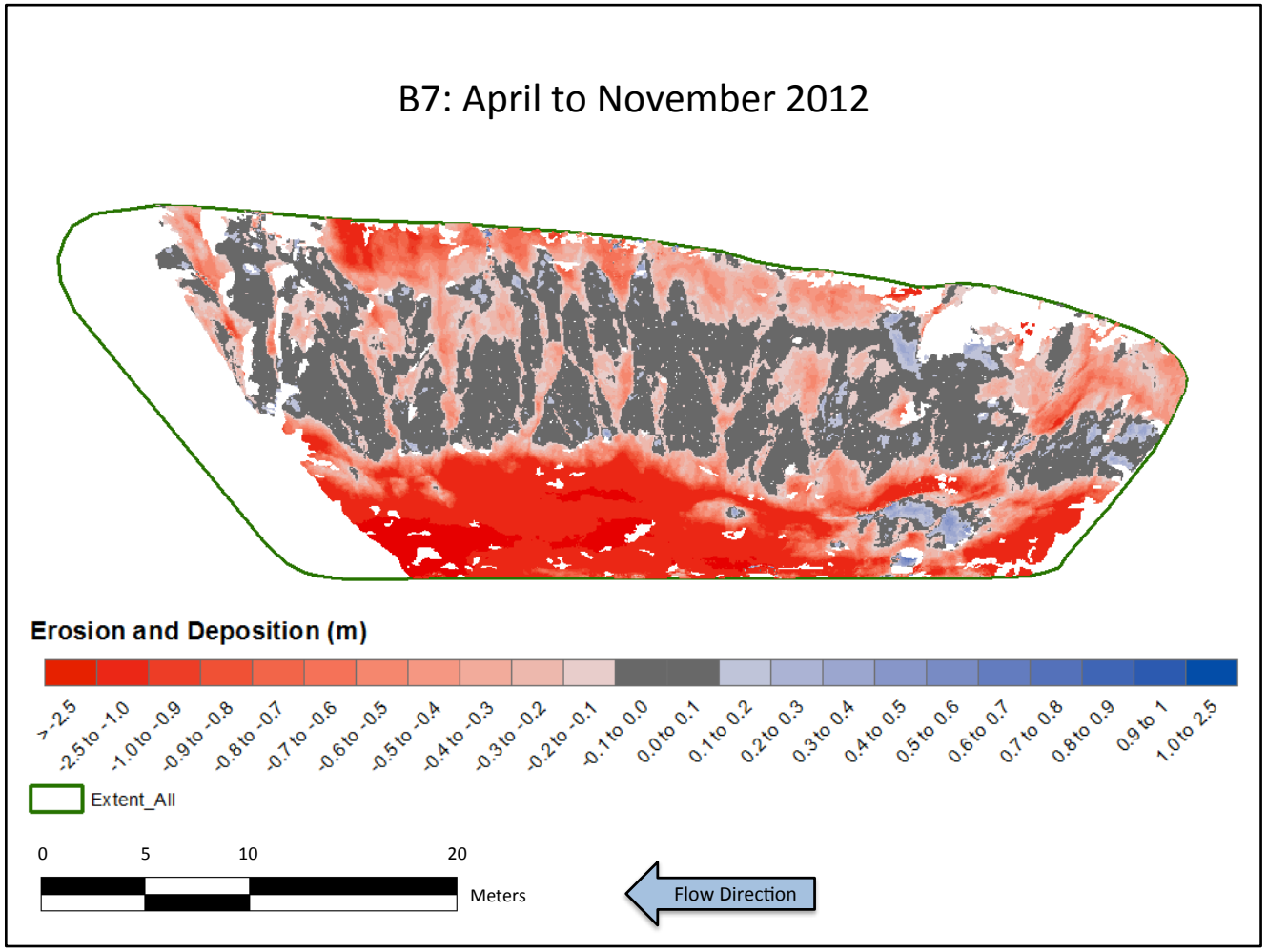

Figure 9.13: Overall Net Change at site B7 from April to November 2012.

9.3 Appendix C: GCD Summary File Results

B9: November 2011 to April 2012

Attribute	Raw	Thresholded DoD Estimate:	± Error Volume	% Error
AREAL:				
Total Area of Erosion (m²)	325.38	320.86		
Total Area of Deposition (m²)	13.66	9.86		
VOLUMETRIC:				
Total Volume of Erosion (m³)	88.10	87.98 ±	32.09	36%
Total Volume of Deposition (m³)	4.70	4.53 ±	0.99	22%
Total Net Volume Difference (m³)	-83.41	**-83.45 ± 31.10**		37%

B9: June to November 2012

Attribute	Raw	Thresholded DoD Estimate:	± Error Volume	% Error
AREAL:				
Total Area of Erosion (m²)	37.49	11.36		
Total Area of Deposition (m²)	272.81	91.22		
VOLUMETRIC:				
Total Volume of Erosion (m³)	2.54	2.09 ±	1.14	54%
Total Volume of Deposition (m³)	22.03	12.52 ±	9.12	73%
Total Net Volume Difference (m³)	19.49	**10.43 ± 7.99**		77%

B9: April to May 2012

Attribute	Raw	Thresholded DoD Estimate:	± Error Volume	% Error
AREAL:				
Total Area of Erosion (m²)	52.11	40.32		
Total Area of Deposition (m²)	266.13	184.80		
VOLUMETRIC:				
Total Volume of Erosion (m³)	9.67	9.41 ±	4.03	43%
Total Volume of Deposition (m³)	46.45	41.59 ±	18.48	44%
Total Net Volume Difference (m³)	36.78	**32.18 ± 14.45**		45%

B9: November 2011 to November 2012

Attribute	Raw	Thresholded DoD Estimate:	± Error Volume	% Error
AREAL:				
Total Area of Erosion (m²)	302.22	302.22		
Total Area of Deposition (m²)	15.73	8.95		
VOLUMETRIC:				
Total Volume of Erosion (m³)	290.86	290.86 ±	30.22	10%
Total Volume of Deposition (m³)	2.45	2.14 ±	0.90	42%
Total Net Volume Difference (m³)	-288.42	**-288.73 ± 29.33**		10%

B9: May to June 2012

Attribute	Raw	Thresholded DoD Estimate:	± Error Volume	% Error
AREAL:				
Total Area of Erosion (m²)	269.92	269.92		
Total Area of Deposition (m²)	16.95	10.36		
VOLUMETRIC:				
Total Volume of Erosion (m³)	250.36	250.36 ±	26.99	11%
Total Volume of Deposition (m³)	3.25	2.96 ±	1.04	35%
Total Net Volume Difference (m³)	-247.11	**-247.40 ± 25.96**		10%

Table 9.1: B9 GCD summary files for individual time periods examined.

B12: November 2011 to April 2012

Attribute	Raw	Thresholded DoD Estimate:	± Error Volume	% Error
AREAL:				
Total Area of Erosion (m^2)	20.96	18.73		
Total Area of Deposition (m^2)	1.61	0.30		
VOLUMETRIC:				
Total Volume of Erosion (m^3)	7.25	7.19 ±	1.87	26%
Total Volume of Deposition (m^3)	0.10	0.06 ±	0.03	52%
Total Net Volume Difference (m^3)	-7.15	**-7.13 ±**	**1.84**	26%

B12: June to November 2012

Attribute	Raw	Thresholded DoD Estimate:	± Error Volume	% Error
AREAL:				
Total Area of Erosion (m^2)	16.79	3.84		
Total Area of Deposition (m^2)	8.55	0.93		
VOLUMETRIC:				
Total Volume of Erosion (m^3)	0.74	0.47 ±	0.38	82%
Total Volume of Deposition (m^3)	0.63	0.45 ±	0.09	21%
Total Net Volume Difference (m^3)	-0.11	**-0.02 ±**	**0.29**	1456%

B12: April to May 2012

Attribute	Raw	Thresholded DoD Estimate:	± Error Volume	% Error
AREAL:				
Total Area of Erosion (m^2)	7.91	7.50		
Total Area of Deposition (m^2)	8.91	8.01		
VOLUMETRIC:				
Total Volume of Erosion (m^3)	4.12	4.11 ±	0.75	18%
Total Volume of Deposition (m^3)	5.67	5.63 ±	0.80	14%
Total Net Volume Difference (m^3)	1.55	**1.52 ±**	**0.05**	3%

B12: November 2011 to November 2012

Attribute	Raw	Thresholded DoD Estimate:	± Error Volume	% Error
AREAL:				
Total Area of Erosion (m^2)	11.39	11.07		
Total Area of Deposition (m^2)	10.89	10.09		
VOLUMETRIC:				
Total Volume of Erosion (m^3)	8.61	8.60 ±	1.11	13%
Total Volume of Deposition (m^3)	5.73	5.69 ±	1.01	18%
Total Net Volume Difference (m^3)	-2.88	**-2.91 ±**	**0.10**	3%

B12: May to June 2012

Attribute	Raw	Thresholded DoD Estimate:	± Error Volume	% Error
AREAL:				
Total Area of Erosion (m^2)	7.93	7.02		
Total Area of Deposition (m^2)	12.68	10.27		
VOLUMETRIC:				
Total Volume of Erosion (m^3)	4.07	4.04 ±	0.70	17%
Total Volume of Deposition (m^3)	3.14	3.01 ±	1.03	34%
Total Net Volume Difference (m^3)	-0.93	**-1.03 ±**	**0.33**	31%

Table 9.2: B12 GCD summary files for individual time periods examined.

B13: November 2011 to April 2012

Attribute	Raw	Thresholded DoD Estimate:	± Error Volume	% Error
AREAL:				
Total Area of Erosion (m^2)	42.46	40.28		
Total Area of Deposition (m^2)	0.12	0.03		
VOLUMETRIC:				
Total Volume of Erosion (m^3)	10.59	10.52 ±	4.03	38%
Total Volume of Deposition (m^3)	0.01	0.01 ±	0.00	39%
Total Net Volume Difference (m^3)	-10.59	**-10.51 ±**	**4.03**	38%

B13: June to November 2012

Attribute	Raw	Thresholded DoD Estimate:	± Error Volume	% Error
AREAL:				
Total Area of Erosion (m^2)	22.67	1.09		
Total Area of Deposition (m^2)	20.35	0.75		
VOLUMETRIC:				
Total Volume of Erosion (m^3)	0.73	0.35 ±	0.11	31%
Total Volume of Deposition (m^3)	0.89	0.39 ±	0.08	19%
Total Net Volume Difference (m^3)	0.16	**0.04 ±**	**0.03**	80%

B13: April to May 2012

Attribute	Raw	Thresholded DoD Estimate:	± Error Volume	% Error
AREAL:				
Total Area of Erosion (m^2)	38.77	13.61		
Total Area of Deposition (m^2)	3.42	1.12		
VOLUMETRIC:				
Total Volume of Erosion (m^3)	3.23	2.60 ±	1.36	52%
Total Volume of Deposition (m^3)	0.49	0.43 ±	0.11	26%
Total Net Volume Difference (m^3)	-2.74	**-2.17 ±**	**1.25**	58%

B13: November 2011 to November 2012

Attribute	Raw	Thresholded DoD Estimate:	± Error Volume	% Error
AREAL:				
Total Area of Erosion (m^2)	42.02	42.02		
Total Area of Deposition (m^2)	0.58	0.35		
VOLUMETRIC:				
Total Volume of Erosion (m^3)	17.85	17.85 ±	4.20	24%
Total Volume of Deposition (m^3)	0.17	0.16 ±	0.03	22%
Total Net Volume Difference (m^3)	-17.68	**-17.69 ±**	**4.17**	24%

B13: May to June 2012

Attribute	Raw	Thresholded DoD Estimate:	± Error Volume	% Error
AREAL:				
Total Area of Erosion (m^2)	34.16	34.16		
Total Area of Deposition (m^2)	8.32	1.45		
VOLUMETRIC:				
Total Volume of Erosion (m^3)	4.02	4.02 ±	3.42	85%
Total Volume of Deposition (m^3)	0.66	0.53 ±	0.15	27%
Total Net Volume Difference (m^3)	-3.36	**-3.49 ±**	**3.27**	94%

Table 9.3: B13 GCD summary files for individual time periods examined.

B14: April to May 2012

Attribute	Raw	Thresholded DoD Estimate:	± Error Volume	% Error
AREAL:				
Total Area of Erosion (m²)	13.31	2.03		
Total Area of Deposition (m²)	9.96	2.17		
VOLUMETRIC:				
Total Volume of Erosion (m³)	0.41	0.15 ± 0.20		134%
Total Volume of Deposition (m³)	0.71	0.46 ± 0.22		47%
Total Net Volume Difference (m³)	0.30	**0.31 ± 0.01**		4%

B14: June to November 2012

Attribute	Raw	Thresholded DoD Estimate:	± Error Volume	% Error
AREAL:				
Total Area of Erosion (m²)	13.95	3.50		
Total Area of Deposition (m²)	28.32	3.71		
VOLUMETRIC:				
Total Volume of Erosion (m³)	0.60	0.42 ± 0.35		83%
Total Volume of Deposition (m³)	1.81	1.21 ± 0.37		31%
Total Net Volume Difference (m³)	1.22	**0.78 ± 0.02**		3%

B14: May to June 2012

Attribute	Raw	Thresholded DoD Estimate:	± Error Volume	% Error
AREAL:				
Total Area of Erosion (m²)	14.41	13.77		
Total Area of Deposition (m²)	1.88	1.04		
VOLUMETRIC:				
Total Volume of Erosion (m³)	7.95	7.94 ± 1.38		17%
Total Volume of Deposition (m³)	0.26	0.22 ± 0.10		46%
Total Net Volume Difference (m³)	-7.69	**-7.71 ± 1.27**		17%

B14: April to November 2012

Attribute	Raw	Thresholded DoD Estimate:	± Error Volume	% Error
AREAL:				
Total Area of Erosion (m²)	54.74	44.22		
Total Area of Deposition (m²)	23.71	10.23		
VOLUMETRIC:				
Total Volume of Erosion (m³)	23.26	23.01 ± 4.42		19%
Total Volume of Deposition (m³)	4.10	3.58 ± 1.02		29%
Total Net Volume Difference (m³)	-19.16	**-19.43 ± 3.40**		17%

Table 9.4: B14 GCD summary files for individual time periods examined.

B15: November 2011 to April 2012

Attribute	Raw	Thresholded DoD Estimate:	± Error Volume	% Error
AREAL:				
Total Area of Erosion (m^2)	13.12	11.05		
Total Area of Deposition (m^2)	9.77	3.02		
VOLUMETRIC:				
Total Volume of Erosion (m^3)	2.09	2.04 ±	1.11	54%
Total Volume of Deposition (m^3)	0.93	0.59 ±	0.30	51%
Total Net Volume Difference (m^3)	-1.16	**-1.45 ±**	**0.80**	56%

B15: June to November 2012

Attribute	Raw	Thresholded DoD Estimate:	± Error Volume	% Error
AREAL:				
Total Area of Erosion (m^2)	4.50	1.21		
Total Area of Deposition (m^2)	20.11	2.82		
VOLUMETRIC:				
Total Volume of Erosion (m^3)	0.18	0.11 ±	0.12	107%
Total Volume of Deposition (m^3)	1.34	0.46 ±	0.28	61%
Total Net Volume Difference (m^3)	1.16	**0.35 ±**	**0.16**	46%

B15: April to May 2012

Attribute	Raw	Thresholded DoD Estimate:	± Error Volume	% Error
AREAL:				
Total Area of Erosion (m^2)	24.56	22.68		
Total Area of Deposition (m^2)	1.26	0.14		
VOLUMETRIC:				
Total Volume of Erosion (m^3)	6.28	6.23 ±	2.27	36%
Total Volume of Deposition (m^3)	0.08	0.06 ±	0.01	24%
Total Net Volume Difference (m^3)	-6.20	**-6.18 ±**	**2.25**	37%

B15: November 2011 to November 2012

Attribute	Raw	Thresholded DoD Estimate:	± Error Volume	% Error
AREAL:				
Total Area of Erosion (m^2)	20.49	20.18		
Total Area of Deposition (m^2)	0.12	0.01		
VOLUMETRIC:				
Total Volume of Erosion (m^3)	10.33	10.32 ±	2.02	20%
Total Volume of Deposition (m^3)	0.01	0.00 ±	0.00	43%
Total Net Volume Difference (m^3)	-10.33	**-10.32 ±**	**2.02**	20%

B15: May to June 2012

Attribute	Raw	Thresholded DoD Estimate:	± Error Volume	% Error
AREAL:				
Total Area of Erosion (m^2)	21.44	20.10		
Total Area of Deposition (m^2)	2.83	0.36		
VOLUMETRIC:				
Total Volume of Erosion (m^3)	6.53	6.50 ±	2.01	31%
Total Volume of Deposition (m^3)	0.18	0.07 ±	0.04	53%
Total Net Volume Difference (m^3)	-6.36	**-6.43 ±**	**1.97**	31%

Table 9.5: B15 GCD summary files for individual time periods examined.

B20: April to May 2012

Attribute	Raw	Thresholded DoD Estimate:	± Error Volume	% Error
AREAL:				
Total Area of Erosion (m^2)	39.57	33.13		
Total Area of Deposition (m^2)	24.30	18.04		
VOLUMETRIC:				
Total Volume of Erosion (m^3)	12.44	12.28 ±	3.31	27%
Total Volume of Deposition (m^3)	7.98	7.69 ±	1.80	23%
Total Net Volume Difference (m^3)	-4.47	**-4.58 ± 1.51**		33%

B20: June to November 2012

Attribute	Raw	Thresholded DoD Estimate:	± Error Volume	% Error
AREAL:				
Total Area of Erosion (m^2)	38.07	3.03		
Total Area of Deposition (m^2)	27.61	2.92		
VOLUMETRIC:				
Total Volume of Erosion (m^3)	0.88	0.38 ±	0.30	80%
Total Volume of Deposition (m^3)	1.18	0.62 ±	0.29	47%
Total Net Volume Difference (m^3)	0.30	**0.24 ± 0.01**		4%

B20: May to June 2012

Attribute	Raw	Thresholded DoD Estimate:	± Error Volume	% Error
AREAL:				
Total Area of Erosion (m^2)	40.13	40.13		
Total Area of Deposition (m^2)	22.27	6.96		
VOLUMETRIC:				
Total Volume of Erosion (m^3)	30.42	30.42 ±	4.01	13%
Total Volume of Deposition (m^3)	3.86	3.10 ±	0.70	22%
Total Net Volume Difference (m^3)	-26.56	**-27.33 ± 3.32**		12%

B20: April to November 2012

Attribute	Raw	Thresholded DoD Estimate:	± Error Volume	% Error
AREAL:				
Total Area of Erosion (m^2)	42.58	42.58		
Total Area of Deposition (m^2)	20.08	14.81		
VOLUMETRIC:				
Total Volume of Erosion (m^3)	32.82	32.82 ±	4.26	13%
Total Volume of Deposition (m^3)	9.70	9.45 ±	1.48	16%
Total Net Volume Difference (m^3)	-23.12	**-23.37 ± 2.78**		12%

Table 9.6: B20 GCD summary files for individual time periods examined.

B2: April to May 2012

Attribute	Raw	Thresholded DoD Estimate:		
AREAL:				
Total Area of Erosion (m²)	242.02	166.19		
Total Area of Deposition (m²)	204.98	39.73		
VOLUMETRIC:			± Error Volume	% Error
Total Volume of Erosion (m³)	31.87	30.35	± 16.62	55%
Total Volume of Deposition (m³)	12.29	7.06	± 3.97	56%
Total Net Volume Difference (m³)	-19.59	**-23.28**	**± 12.65**	54%

B2: June to November 2012

Attribute	Raw	Thresholded DoD Estimate:		
AREAL:				
Total Area of Erosion (m²)	58.02	12.86		
Total Area of Deposition (m²)	359.00	4.63		
VOLUMETRIC:			± Error Volume	% Error
Total Volume of Erosion (m³)	2.32	1.62	± 1.29	80%
Total Volume of Deposition (m³)	11.86	0.73	± 0.46	63%
Total Net Volume Difference (m³)	9.54	**-0.89**	**± 0.82**	93%

B2: May to June 2012

Attribute	Raw	Thresholded DoD Estimate:		
AREAL:				
Total Area of Erosion (m²)	311.39	260.99		
Total Area of Deposition (m²)	100.64	26.36		
VOLUMETRIC:			± Error Volume	% Error
Total Volume of Erosion (m³)	357.99	355.49	± 26.10	7%
Total Volume of Deposition (m³)	14.70	8.03	± 2.64	33%
Total Net Volume Difference (m³)	-343.29	**-347.46**	**± 23.46**	7%

B2: April to November 2012

Attribute	Raw	Thresholded DoD Estimate:		
AREAL:				
Total Area of Erosion (m²)	339.61	339.61		
Total Area of Deposition (m²)	91.87	55.76		
VOLUMETRIC:			± Error Volume	% Error
Total Volume of Erosion (m³)	395.69	395.69	± 33.96	9%
Total Volume of Deposition (m³)	15.16	13.49	± 5.58	41%
Total Net Volume Difference (m³)	-380.53	**-382.20**	**± 28.38**	7%

Table 9.7: B2 GCD summary files for individual time periods examined.

B7: April to May 2012

Attribute	Raw	Thresholded DoD Estimate:	± Error Volume	% Error
AREAL:				
Total Area of Erosion (m^2)	265.63	62.22		
Total Area of Deposition (m^2)	222.42	21.64		
VOLUMETRIC:				
Total Volume of Erosion (m^3)	18.29	15.02 ±	6.22	41%
Total Volume of Deposition (m^3)	9.13	4.99 ±	2.16	43%
Total Net Volume Difference (m^3)	-9.16	**-10.03 ±**	**4.06**	40%

B7: June to November 2012

Attribute	Raw	Thresholded DoD Estimate:	± Error Volume	% Error
AREAL:				
Total Area of Erosion (m^2)	355.26	355.26		
Total Area of Deposition (m^2)	271.20	8.63		
VOLUMETRIC:				
Total Volume of Erosion (m^3)	10.58	10.58 ±	35.53	336%
Total Volume of Deposition (m^3)	6.67	2.66 ±	0.86	32%
Total Net Volume Difference (m^3)	-3.92	**-7.92 ±**	**34.66**	438%

B7: May to June 2012

Attribute	Raw	Thresholded DoD Estimate:	± Error Volume	% Error
AREAL:				
Total Area of Erosion (m^2)	359.78	238.34		
Total Area of Deposition (m^2)	101.68	5.94		
VOLUMETRIC:				
Total Volume of Erosion (m^3)	146.76	142.40 ±	23.83	17%
Total Volume of Deposition (m^3)	5.68	1.85 ±	0.59	32%
Total Net Volume Difference (m^3)	-141.08	**-140.55 ±**	**23.24**	17%

B7: April to November 2012

Attribute	Raw	Thresholded DoD Estimate:	± Error Volume	% Error
AREAL:				
Total Area of Erosion (m^2)	478.62	478.62		
Total Area of Deposition (m^2)	106.15	19.03		
VOLUMETRIC:				
Total Volume of Erosion (m^3)	300.90	300.90 ±	47.86	16%
Total Volume of Deposition (m^3)	6.56	3.68 ±	1.90	52%
Total Net Volume Difference (m^3)	-294.34	**-297.22 ±**	**45.96**	15%

Table 9.8: B7 GCD summary files for individual time periods examined.

10.0 APPENDIX OF POST-PROCESSING PROCEDURES

10.1 Faro Scene

1) Add all .fls scan files (folders) from a given campaign to Scene.

2) Pre-Process scan files. Right click on the scans folder in the structure tree on the left. Operations → Preprocessing → Preprocess Scans; select "spheres" in the detection features and "place scans".

3) In 3D view, remove unnecessary objects from point cloud that can be easily deleted without disturbing the surface of interest (fine-tuning of vegetation removal will be completed in the next step in planar view). Right click on the scans folder: View → 3D view; use polygon selector to select points to be deleted. Right click: delete inside/outside selection.

4) To remove vegetation from portions of the surface that are inaccessible when viewing the entire bluff in 3-D view, you must do so in each scan file (i.e. from each scan setup): Right click on the individual scan in the Faro Workspace tree: View → Planar view. In planar view, use rectangular selector to delineate "vertical slices" of the bluff. Right click on selection to view in 3-D. To remove troublesome vegetation such as small shrubs and sticks protruding from the surface of interest, rotate 3-D slice of bluff and view laterally; use polygon selector to select points to be deleted. Right click: delete inside/outside selection. Complete this process for each scan file within a given campaign folder (removing vegetation from one scan file does not remove it in another). Note: as vegetation is deleted from the surface of interest in 3-D, it appears "blacked-out" in planar view.

5) Follow steps 1-4 for successive campaigns at a given site. Right click on scans folder: New → Scan Folder. Rename folder with campaign date and import .fls files from the corresponding campaign. Note: Faro Workspace tree structure should have one "master" scan folder. Inside the master folder should be a scan folder for each campaign (i.e. date in time) conducted at a site. The individual campaign folders should contain all the .fls files from a given date/campaign.

6) After processing each point cloud as described above, preprocess all the campaigns from the master folder to register all the campaigns together (i.e. place in common coordinate system). If this process does not result in proper scan registration/placement, see Notes 1 and 2 below.

7) To export points for decimation, right click on scans folder (at campaign level): Import/Export → Export Scan Points; specify ".pts" file format.

NOTES:

A) To create manual objects in cases of a lost control point(s) or need for additional point(s): in planar view, use polygon selector to delineate object or portion of object being created. Right click: Create Objects → Mean Point; rename point in data tree on left. Complete same procedure for other scans within that campaign folder to link it to scans from that same data/campaign. Complete the procedure for scans within other campaign folders to link it with other dates/campaigns.

B) When preprocessing does not result in common reference objects (control points) being in the same coordinate system: right click on scans folder (individual campaign or master folder): Operations → Registration → Place Scans (Force By Manual Target Names) Note: this procedure works well when merging campaigns containing manually-generated reference objects such as rocks.

C) To verify accuracy of scan registration: right click on scan manager: Properties.

10.2 ToPCAT (PCTools)

1) Create a separate Windows file folder for each .pts (points) file exported from Faro Scene.

2) Place ToPCAT application file (.exe) and batch file (.bat) in same folder as points file is located.

3) Edit batch file using Notepad ++ by right clicking on file: enter desired "xres" and "yres" you want to use to decimate the point cloud (e.g. 0.05 for 5 cm); enter points file name (make sure the points file name in the batch file code exactly matches that of the name of the points file in the folder); save batch file and close.

4) Navigate to points file location using Command Prompt; enter "run" to run batch file.

5) Import resulting zmin .txt (text) file into ArcMap; continue process to generate zmin text file for each scan campaign.

10.3 ArcMap/GCD

1) Import zmin text file into Arc (Add Data → navigate to file).

2) Right click on file in Layers and select "Display XY Data". In the drop-down boxes, specify the Y field as "zmin" and the Z field as "y" to swap axes.

3) Export data as point shapefile. Right click on file in Layers: Data → Export Data

4) Complete this same process for all text files imported into Arc for a given site.

5) Create "common extent" shapefile (or feature class), which will later be used as processing extent in DEM creation. Use Arc Editor to create polygon shapefile that best represents the boundary of all the individual point clouds/campaigns. Make sure all point shapefile layers are turned on when generating the common extents. Note: it helps to assign bright, contrasting colors to the point shapefiles to make this step easier.

6) Next, create "TIN shapefile" to be used in generating a TIN for an individual campaign. Again, use Arc Editor to create polygon shapefile, making sure that the extents exceed those of the common extent shapefile. Next, using the Geoprocessing dropdown menu, use the clip tool to clip the TIN shapefile to the same extents as those of the common extent shapefile. Repeat this process so that you have a TIN polygon shapefile for each campaign at a given site, each matching the extents of the common extent shapefile.

7) To avoid interpolation/extrapolating to areas with no data when generating the TINs, overlay point shapefile representing a given campaign on corresponding TIN shapefile for the same date. Use Editor to delineate regions in TIN shapefile with no data by drawing polygons. After delineating a hole in the data with a closed polygon, in the editor drop-down select "clip" and specify "discard the area that intersects". Under the Edit drop-down (main Arc ribbon) select "Delete". Continue process for entire TIN shapefile; save edits and close.

8) Continue process for each point shapefile and corresponding TIN shapefile for a given site.

9) Create TIN: 3D Analyst → Data Management → TIN → Create TIN. Use the point shapefile as your first input feature class; specify the Y coordinate as the height field, "mass points" as the SF_type, and "none" for the tag field. Use the TIN shapefile for the second input feature class; specify "none" for the height field, "hardclip" as the SF_type, and "none" for the tag field.

10) Continue process for each point shapefile and corresponding TIN shapefile to generate a TIN for each campaign.

11) Create DEM: 3D Analyst → Conversion → From TIN → Tin to Raster. Specify "Float" and "Natural Neighbors" options. To define DEM resolution, manually enter the same resolution as used in decimation of point cloud in ToPCAT/PCTools. Under "Environments" (within Tin to Raster tool), define the "processing extent" as the common extent shapefile. Next, round the top extent up to nearest whole number (or a number evenly divisible by cell resolution specified previously). Round the right extent up, and the bottom and left down using the same rule.

12) Use the Tin to Raster tool to create a DEM for each campaign. However, specify the processing extent to be the first DEM created (no rounding of extents needed). Use the original DEM as the processing extent for each successive DEM generated. This process should result in a series of DEMs that are orthogonal and concurrent.

13) Create GCD project (create GCD folder within folder containing ArcMap .mxd file; save GCD project to this location.)

14) In the Data Preparation drop-down menu, select the Survey Library. Add each DEM to GCD Survey Library. Specify the single method survey as TLS. In the GCD Analysis drop-down menu, select the Change Detection tool to difference DEMs. Within the Change Detection tool, select the older DEM (chronologically) as the new survey, and the newer DEM as the old survey. Under the Uncertainty Analysis Method, select "simple minimum level of detection". Calculate. After DoD is calculated, set threshold using the slider bar (0.10 m for our research). Save to generate a DoD with the specified threshold. Note: DoD files are automatically saved to the folder containing the GCD project.